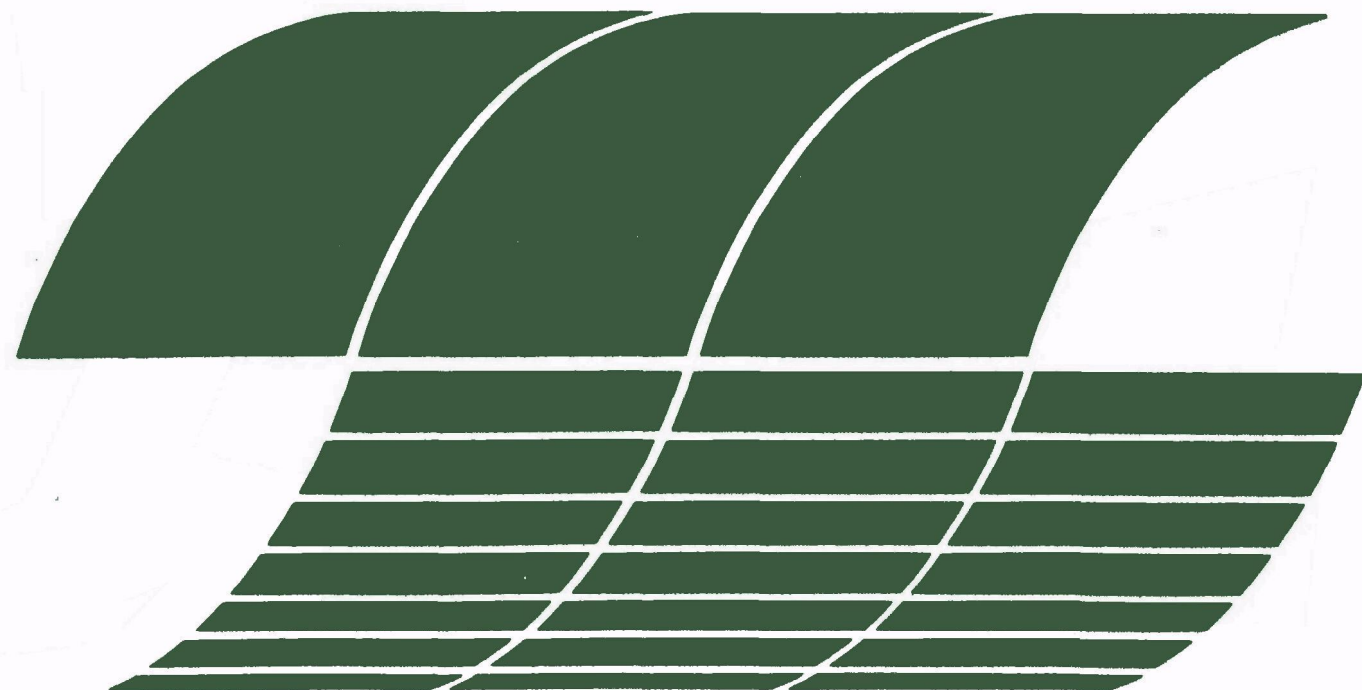


# **Support Studies in Fluidized-bed Combustion 1978 Annual Report**

**Interagency  
Energy/Environment  
R&D Program Report**



## **RESEARCH REPORTING SERIES**

Research reports of the Office of Research and Development, U.S. Environmental Protection Agency, have been grouped into nine series. These nine broad categories were established to facilitate further development and application of environmental technology. Elimination of traditional grouping was consciously planned to foster technology transfer and a maximum interface in related fields. The nine series are:

1. Environmental Health Effects Research
2. Environmental Protection Technology
3. Ecological Research
4. Environmental Monitoring
5. Socioeconomic Environmental Studies
6. Scientific and Technical Assessment Reports (STAR)
7. Interagency Energy-Environment Research and Development
8. "Special" Reports
9. Miscellaneous Reports

This report has been assigned to the INTERAGENCY ENERGY-ENVIRONMENT RESEARCH AND DEVELOPMENT series. Reports in this series result from the effort funded under the 17-agency Federal Energy/Environment Research and Development Program. These studies relate to EPA's mission to protect the public health and welfare from adverse effects of pollutants associated with energy systems. The goal of the Program is to assure the rapid development of domestic energy supplies in an environmentally-compatible manner by providing the necessary environmental data and control technology. Investigations include analyses of the transport of energy-related pollutants and their health and ecological effects; assessments of, and development of, control technologies for energy systems; and integrated assessments of a wide range of energy-related environmental issues.

## **EPA REVIEW NOTICE**

This report has been reviewed by the participating Federal Agencies, and approved for publication. Approval does not signify that the contents necessarily reflect the views and policies of the Government, nor does mention of trade names or commercial products constitute endorsement or recommendation for use.

This document is available to the public through the National Technical Information Service, Springfield, Virginia 22161.

**August 1979**

# **Support Studies in Fluidized-bed Combustion 1978 Annual Report**

by

I. Johnson, G.J. Vogel, S.H.D. Lee, D.S. Moulton,  
F.F. Nunes, J.A. Shearer, G.W. Smith, E.B. Smyk,  
R.B. Snyder, W.M. Swift, F.G. Teats, C.B. Turner,  
W.I. Wilson, and A.A. Jonke

Argonne National Laboratory  
9700 South Cass Avenue  
Argonne, Illinois 60439

EPA No. IAG-D5-E681  
DoE No. W-31-109-Eng-38  
Program Element No. INE825

Project Officers:

David A. Kirchgessner  
EPA/Industrial Environmental  
Research Laboratory  
Research Triangle Park, NC 27711

John F. Geffken  
DoE/Fossil Fuel Utilization  
Washington, DC 20540

Prepared for

U.S. ENVIRONMENTAL PROTECTION AGENCY  
Office of Research and Development  
Washington, DC 20460

U.S. DEPARTMENT OF ENERGY  
Fossil Fuel Utilization  
Washington, DC 20540

## TABLE OF CONTENTS

	<u>Page</u>
ABSTRACT . . . . .	1
SUMMARY . . . . .	1
TASK A. GASEOUS POLLUTANT EMISSION CONTROL IN FBCs . . . . .	10
1. Enhancement of Limestone Sulfation . . . . .	10
a. Introduction . . . . .	10
b. Effects of $\text{CaCl}_2$ Additive on Limestone Sulfation . . . . .	11
c. Effects of $\text{MgCl}_2$ and Other Salts on Limestone Sulfation . . . . .	17
2. Investigation of Sulfation Reactions during Fluidized-Bed Combustion of Coal. . . . .	23
3. Evaluation of Coal Pyrolysis Char as a Feedstock for FBC . . . . .	30
a. Material . . . . .	30
b. PDU Combustion System . . . . .	30
c. Test Plan and Experimental Procedure . . . . .	32
d. Results and Conclusions . . . . .	33
4. The Use of Oil Shale for $\text{SO}_2$ Emission Control in Atmospheric Pressure Fluidized-Bed Coal Combustors . . . . .	36
a. Materials . . . . .	37
b. Experimental . . . . .	37
c. Sulfation Results . . . . .	37
d. Prediction of $\text{SO}_2$ Retention for Oil Shales . . . . .	40
e. Evaluation of Oil Shale Sorbent for AFBC Sulfur-Removal Systems . . . . .	40
f. Evaluation of Oil Shale Use in a Fluidized- Bed Combustion Plant Employing a Carbon. . . Burnup Cell . . . . .	40
g. Attrition Results . . . . .	41
h. Conclusions . . . . .	42
5. Comparison of Limestone Calcium Utilization in an AFBC with TGA Projections . . . . .	42
6. Prediction of Limestone Requirements for an FBC-CBC Combustor . . . . .	46

# TABLE OF CONTENTS (Cont'd.)

	<u>Page</u>
7. Estimation of Limestone Requirements for AFBC . .	48
8. Petrographic Examination of Limestones . . . . .	53
9. Effect of Water on SO <sub>2</sub> Reactivity . . . . .	53
10. Limestone Attrition in a Fluidized Bed . . . . .	53
TASK B. TURBINE CORRODENT STUDIES . . . . .	55
1. Emission of Alkali Metals during the Combustion of Coal . . . . .	55
2. Effect of Additives on the Retention of Alkali Metals in the Bed during the Combustion of Coal . .	56
3. Removal of Alkali Metal Compounds from the Hot Combustion Gas of Coal . . . . .	58
a. Screening Tests . . . . .	59
b. Parametric Tests . . . . .	64
TASK C. TRACE POLLUTANT CONTROL IN FBC . . . . .	72
1. Trace Element Behavior in Sorbent during Cyclic Utilization . . . . .	72
a. Analytical . . . . .	72
b. Experimental . . . . .	73
c. Results . . . . .	73
TASK D. PARTICULATE CONTROL STUDIES	
1. Evaluation of On-Line Light-Scattering Particle Analyzers . . . . .	79
a. Introduction . . . . .	79
b. System and Procedure for Flue-Gas Particle Measurements . . . . .	80
c. Experimental Evaluation of the Multi- particle Analyzer . . . . .	80
d. Conclusions . . . . .	83
2. Particle Removal from Flue Gas . . . . .	84
a. Granular-Bed Filters . . . . .	84
b. Acoustic Dust Conditioning . . . . .	88
c. High Efficiency Cyclone . . . . .	91

## TABLE OF CONTENTS (Cont'd.)

	<u>Page</u>
MISCELLANEOUS STUDIES . . . . .	91
1. Pulsed L-Valve Tests . . . . .	91
a. Introduction . . . . .	91
b. Equipment and Procedure . . . . .	92
c. Test Results . . . . .	93
APPENDIX A. Compositions (wt %) of Limestones and Dolomites . .	95
APPENDIX B. Limestone Designations and Suppliers . . . . .	97
REFERENCES . . . . .	99

## LIST OF FIGURES

<u>No.</u>	<u>Title</u>	<u>Page</u>
1.	Effect of $\text{CaCl}_2$ Addition on Limestone Sulfation at $850^\circ\text{C}$ for 6 h in 0.3% $\text{SO}_2$ , 20% $\text{CO}_2$ , 5% $\text{O}_2$ , Balance $\text{N}_2$ . . . . .	13
2.	Percent Conversion to Sulfate <u>vs.</u> Average Pore Diameter for Limestones Treated with $\text{CaCl}_2$ at $850^\circ\text{C}$ and Sulfated 6 h in 0.3% $\text{SO}_2$ , 5% $\text{O}_2$ , 20% $\text{CO}_2$ , and the Balance $\text{N}_2$ . . . . .	16
3.	Changes in Porosity Curves with 0.5 mol % $\text{NaCl}$ Addition to Limestones Calcined at $850^\circ\text{C}$ for 1 h in 5% $\text{O}_2$ , 20% $\text{CO}_2$ , and the Balance $\text{N}_2$ . . . . .	19
4.	Effect of 0.5 mol % $\text{CaCl}_2$ Addition on Porosity of Limestones Calcined at $850^\circ\text{C}$ for 1 h in 5% $\text{O}_2$ , 20% $\text{CO}_2$ , and the Balance $\text{N}_2$ . . . . .	20
5.	Changes in Porosity Curves with 0.5 mol % $\text{MgCl}_2$ Addition to Limestones Calcined at $850^\circ\text{C}$ for 1 h in 5% $\text{O}_2$ , 20% $\text{CO}_2$ , and the Balance $\text{N}_2$ . . . . .	21
6.	Porosity Curves of ANL-9701 Comparing Combustor-Sulfated Samples (C) and Samples Sulfated in a Laboratory Tube Furnace (A and B) . . . . .	24
7.	Porosity Curves Showing the Effect of Calcining on Limestone ANL-9701 in a Laboratory Tube Furnace . . . . .	26
8.	Porosity Curves of ANL-9501 Comparing Combustor-Sulfated Samples (C) with Samples Sulfated in a Laboratory Tube Furnace (A and B) . . . . .	27
9.	Porosity Curves for (A) Heat-Treated ANL-9501 and (B) $\text{CaCl}_2$ -Treated ANL-9501 Sulfated in a Laboratory Tube Furnace . . . . .	29
10.	Simplified Equipment Flowsheet of PDU Fluidized-Bed Combustor and Associated Equipment . . . . .	32
11.	Combustion Efficiency of Coal Char as a Function of Bed Temperature, Combustor Pressure, and Fluidizing-Gas Velocity . . . . .	35
12.	Conversion (Measured with a TGA) of $\text{CaO}$ to $\text{CaSO}_4$ in Precalcined Spent Green River Oil Shale at 700 to $1050^\circ\text{C}$ . . . . .	38

# LIST OF FIGURES (Cont'd.)

<u>No.</u>	<u>Title</u>	<u>Page</u>
13.	Conversion (Measured with a TGA) of CaO to CaSO <sub>4</sub> in Spent Oil Shale, Tymochtee Dolomite, Greer Limestone, and Germany Valley Limestone, Using 0.3% SO <sub>2</sub> -5% O <sub>2</sub> in N <sub>2</sub> at 900°C . . . . .	39
14.	Calcium Utilization in Seven Precalcined Limestones at 900°C as a Function of Time . . . . .	44
15.	Experimental and Calculated Calcium Utilizations . . . . .	47
16.	TGA Reactivity Curves for ANL-9901 and ANL-9902 Limestones . . . . .	51
17.	Calcium Utilization of Limestone versus their CaCO <sub>3</sub> Concentrations . . . . .	52
18.	Calcium Utilization as a Function of Pore Size for Calcined Stones . . . . .	52
19.	Effect of Sorbent Bed Temperature on Sorption Capacity as a Function of Experiment Duration . . . . .	64
20.	Effect of Superficial Gas Velocity on Sorption Capacity at 800°C . . . . .	68
21.	Effect of the Contact Time of Flue Gas with Sorbent on NaCl Vapor Capture . . . . .	71
22.	Typical Pulse Jet Tested in the Pulse-Jet Development Program . . . . .	89
23.	Schematic of the Pulse Jet/Resonant Manifold System . . . . .	90



## LIST OF TABLES

<u>No.</u>	<u>Title</u>	<u>Page</u>
1.	Effects of $\text{CaCl}_2$ and $\text{NaCl}$ upon Six-Hour Sulfation of Limestones at $850^\circ\text{C}$ in 0.3% $\text{SO}_2$ , 5% $\text{O}_2$ , 20% $\text{CO}_2$ , and the Balance $\text{N}_2$ . . . . .	12
2.	Average Pore Diameter and Percent Conversion to Sulfated State at $850^\circ\text{C}$ for Limestones Treated with $\text{CaCl}_2$ . . . . .	15
3.	Percent Conversion to Sulfate after 6 h with 0.3% $\text{SO}_2$ at $850^\circ\text{C}$ for Limestones Precalcined with $\text{MgCl}_2$ Additive at $850^\circ\text{C}$ 1 h in 5% $\text{O}_2$ , 20% $\text{CO}_2$ , Balance $\text{N}_2$ . . . . .	18
4.	Percent Conversion to Sulfate after 6 h with 0.3% $\text{SO}_2$ at $850^\circ\text{C}$ for Limestones Precalcined with Inorganic Additives at $850^\circ\text{C}$ 1 h in 5% $\text{O}_2$ , 20% $\text{CO}_2$ , and the Balance $\text{N}_2$ . . . . .	22
5.	Sulfation Conversions and Average Pore Diameters for ANL-9701 Stone Under Various Reaction Conditions . . . . .	25
6.	Percent Conversion to Sulfate and Average Pore Diameters for ANL-9501 Stone Under Various Reaction Conditions . . . . .	28
7.	Average Particle Size and Chemical Properties of Occidental Research Corporation's Flash-Pyrolysis Coal Char . . . . .	31
8.	Combustion Efficiency of Flash-Pyrolysis Coal Char in Fluidized-Bed Combustion Process Development Unit . . . . .	34
9.	Concentrations (in wt %) of Major Constituents of Calcareous Materials . . . . .	37
10.	Requirements for Green River Oil Shale, Germany Valley Limestone, Greer Limestone, and Tymochtee Dolomite to Meet $\text{SO}_2$ -Emission Standard . . . . .	41
11.	Comparison of Predicted and Pilot-Plant Calcium Utilization . . . . .	45
12.	Projected Limestone Requirements, kg Stone/kg of Coal, to Meet 0.5 g $\text{SO}_2$ /MJ Standard for AFBC . . . . .	49
13.	Material Balances of Sodium and Potassium from Combustion of 0.5 wt % $\text{NaCl}$ -Impregnated Activated Coconut Charcoal Mixed with 5 wt % Additive . . . . .	57

# LIST OF TABLES (Cont'd.)

<u>No.</u>	<u>Title</u>	<u>Page</u>
14.	Experimental Conditions for Testing Diatomaceous Earth and Activated Bauxite Sorbents for $K_2SO_4$ Vapor Capture . . . .	61
15.	Material Balances of $K_2SO_4$ from Tests of $K_2SO_4$ Vapor Capture by Diatomaceous Earth and Activated Bauxite . . . . .	62
16.	Distribution of Potassium Ion in the Sorbents . . . . .	63
17.	Sodium Chloride Distributions from Tests of NaCl-Vapor Capture by Diatomaceous Earth as a Function of Superficial Gas Velocity of Flue Gas . . . . .	66
18.	Sodium Chloride Distributions from Tests of NaCl-Vapor Capture by Activated Bauxite as a Function of Superficial Gas Velocity of Flue Gas . . . . .	67
19.	Sodium Chloride Distributions from Tests of NaCl-Vapor Capture by Diatomaceous Earth as a Function of Gas Hourly Space Velocity . . . . .	70
20.	Sodium Chloride Distributions from Tests of NaCl-Vapor Capture by Activated Bauxite as a Function of Gas Hourly Space Velocity . . . . .	71
21.	Samples Analyzed in the Trace Element Study . . . . .	74
22.	Trace-Element Analyses for Tymochtee Dolomite Samples from the First and Tenth Combustion Cycles . . . . .	75
23.	Concentrations and Material Balances for Trace Elements in Steady-State Samples of Solids Entering and Leaving the Regeneration Reactor during the Tenth Regeneration Cycle . . .	78
24.	Particle Sizes and Loadings Obtained with the Multi-particle Analyzer, the Andersen Impactor, and the Membrane Filter in Coal Combustion and Cold Elutriation Experiments . . . . .	81

SUPPORTIVE STUDIES IN  
FLUIDIZED BED COMBUSTION

Annual Report

July 1977 - September 1978

by

Irving Johnson, G. J. Vogel, S. H. D. Lee, D. S. Moulton, F. F. Nunes,  
J. A. Shearer, G. W. Smith, E. B. Smyk, R. B. Snyder, W. M. Swift,  
F. G. Teats, C. B. Turner, W. I. Wilson, and A. A. Jonke

ABSTRACT

These laboratory and process development-scale studies support the Fossil Energy development program for atmospheric and pressurized fluidized-bed coal combustion. The specific objectives of the current program are (1) to establish the basic understanding needed to optimize the use of limestones for the control of SO<sub>2</sub> emission from FBCs and (2) to develop the technical basis for processes for the treatment of high-temperature, high-pressure gases from PFBCs so that these gases can be used to operate gas turbines.

This report presents information on the enhancement of limestone sulfation by the use of chemical additives, the evaluation of coal char as a fuel for FBCs, the use of oil shale in place of limestone for SO<sub>2</sub> emission control, development of a model for the prediction of the performance of limestones in FBCs from laboratory-data, studies of the emission of alkali metal compounds from coal combustion systems, development of sorbents for the removal of gaseous KCl and NaCl from hot gas streams, studies of the fate of trace elements in a FBC combustion-regeneration system, evaluation of two laser instruments for the in situ measurement of particle size and concentration in a hot gas stream, evaluation of a high efficiency cyclone, the development of a granular bed filter for particulate removal, the development of a high-intensity sound source to enhance particulate agglomeration and the development of a pulsed L valve for the metering of the flow of solids.

SUMMARY

Task A. Gaseous Pollutant Emission Control in Fluidized-Bed Combustors (FBCs)

Enhancement of Limestone Sulfation. The use of various salts (NaCl, CaCl<sub>2</sub>, etc.) to increase the rate and the extent of sulfation of limestones

is being investigated on a laboratory scale, using a horizontal tube furnace. The results of studies using NaCl, CaCl<sub>2</sub>, MgCl<sub>2</sub>, and other inorganic salts are reported.

Detailed studies have been made of the mechanism by which NaCl additive changes the sulfation characteristics of limestones. Earlier work showed that the addition of NaCl increases the size of the pores in the calcined limestone. Therefore the gaseous SO<sub>2</sub>/O<sub>2</sub> mixture can more readily penetrate the limestone particle and react with the CaO to form CaSO<sub>4</sub>. As stated previously, the NaCl is believed to form a liquid film on the surface of the CaO grains which facilitates the growing together of these grains and their recrystallization. This process leads to larger pores. The large pores permit a greater extent of reaction before they are closed off by CaSO<sub>4</sub>, which has a larger volume than does CaO. The presence of the NaCl in the system appears to lead to the recrystallization of CaO and CaSO<sub>4</sub> which allows the gaseous SO<sub>2</sub>/O<sub>2</sub> mixture to more easily diffuse through the layer of CaSO<sub>4</sub> that forms on the CaO grains.

The pore size of the calcined limestone was earlier found to increase as the amount of NaCl added was increased. In current work, the extent of sulfation was observed to pass through a maximum value when the average pore diameter was in the range, 0.3 to 0.4  $\mu\text{m}$ . The decrease in the extent of sulfation for average pore diameters larger than this maximum is believed due to a decrease in internal surface area. For some limestones, an increase in the extent of limestone sulfation similar to that obtained by NaCl treatment can be achieved by heating the calcined limestone at elevated temperatures or by calcination in an atmosphere of CO<sub>2</sub> at high pressure. Both of these treatments also increase the average pore diameter.

The addition of CaCl<sub>2</sub> is more effective than the addition of NaCl in increasing the extent of sulfation of limestones. The average pore diameter of the calcined limestone is increased by the addition of  $\leq 0.5$  mol % CaCl<sub>2</sub> to give a maximum sulfation and hence the mechanism of the process is the same as for NaCl. Large ( $>1$  mol %) additions of CaCl<sub>2</sub> produce a second maximum in the plot of extent of sulfation vs. average pore diameter. This second maximum (which has not been observed for NaCl) is believed due to the formation of a liquid CaCl<sub>2</sub>-CaO phase (CaO is soluble in liquid CaCl<sub>2</sub>) which facilitates the SO<sub>2</sub>-O<sub>2</sub>-CaO reaction. The effect of 0.1 and 0.5 mol % CaCl<sub>2</sub> additions on approximately thirty different limestones was determined. In 60% of the cases a larger extent of sulfation was obtained for the 0.1 mol % addition. The amount of CaCl<sub>2</sub> needed for optimum extent of sulfation of a specific limestone depends on the amount and type of impurities present in the limestone.

The effect of MgCl<sub>2</sub> additive on (1) the pore size of the calcined limestone and (2) the extent of sulfation was very similar to that observed for CaCl<sub>2</sub>. Also, the effects of NaOH, Na<sub>2</sub>CO<sub>3</sub>, Na<sub>2</sub>SO<sub>4</sub>, Na<sub>2</sub>SiO<sub>3</sub>, Na<sub>2</sub>SiO<sub>3</sub>·9H<sub>2</sub>O, Ca(OH)<sub>2</sub>, CaF<sub>2</sub>, CaSO<sub>4</sub>, and H<sub>3</sub>BO<sub>3</sub> on the extent of sulfation of four different limestones were tested. Most of these substances had a positive effective on the extent of sulfation. The extent of sulfation was strongly influenced by the impurity content of the stone.

Investigation of Sulfation Reaction during Fluidized-Bed Coal Combustion. Studies of the sulfation process which occurs in fluidized bed coal combustion are under way. In these studies, samples of limestones which had undergone

sulfation in an FBC have been compared with samples which had been sulfated in a small laboratory tube furnace using similar sulfation conditions. In a set of comparisons for one limestone type, the extents of sulfation of the limestone in the FBC and in the laboratory-scale apparatus were very similar; furthermore, the porosities of the samples were nearly identical. However, for a second limestone type and a different FBC, the extent of sulfation of samples from the FBC was significantly greater than for a sample of the same limestone sulfated in a laboratory-scale tube furnace. In the latter comparison, the average pore diameter of the sulfated material from the FBC was larger than that obtained in the laboratory-scale sulfator. The greater extent of sulfation obtained in the FBC is due to the average pore diameter being closer to optimum. The cause of this additional pore growth in the combustor has not been determined.

Evaluation of Coal-Pyrolysis Char as a Feedstock for FBC. As part of a program to evaluate flash pyrolysis coal char for power generation, a series of combustion tests was performed to measure the effects of bed temperature, combustor pressure, and fluidizing-gas velocity on the combustion efficiency of the char and to determine whether the char would be an acceptable feedstock for FBC units. The char used in the study was the product of the flash pyrolysis of a Wyoming subbituminous coal at a pyrolysis temperature of  $\sim 650^{\circ}\text{C}$ . The combustion tests were performed in a 15.2-cm-ID fluidized-bed combustion process development unit at the following nominal conditions of the three independent variables: bed temperatures of 800 and  $900^{\circ}\text{C}$ , combustor pressures of 405 and 810 kPa, and fluidizing-gas velocities of 0.76 and 1.1 m/s. In all experiments, excess air was held to 3% oxygen ( $\sim 17\%$  excess air) in the dry flue gas.

Feeding of the extremely fine particle size char proved to be a significant problem in testing. Attempts to blend the char with sorbent and to feed both materials from the same hopper were not successful in eliminating the problem. However, the data obtained are considered to be sufficiently accurate to assess the combustibility of the char in an FBC and to observe the effects of the changes made in operating conditions.

Combustion efficiency of the char, based on the rates of unburned carbon leaving the combustor and of fresh carbon fed to the combustor, was measured and found to range from  $\sim 94$  to 99%. Combustion efficiencies of 99% have been measured for coal combustion in FBCs, but only at much higher excess air levels, i.e.,  $\sim 95\%$ .

Of the three independent variables, only temperature was observed to affect the combustion efficiency of the char. Combustion efficiency increased from an average of  $\sim 95$  at  $800^{\circ}\text{C}$  to 98% at  $900^{\circ}\text{C}$ .

The potential of the char as a fuel for FBCs has been demonstrated. The two factors most likely to be responsible for the high combustion efficiencies measured were (1) the extremely fine particle size of the char, and (2) the fact that the char originated from a subbituminous coal. It should not be concluded that all coal chars would be equally attractive for FBC applications.

Use of Oil Shales for  $\text{SO}_2$ -Emission Control in AFBCs. The use of oil shales for the control of  $\text{SO}_2$  emission in atmospheric-pressure fluidized-bed coal combustors has been studied by measuring the rate and extent of sulfation of oil

shale, using a thermogravimetric analyzer (TGA). From these TGA data and similar data on various limestones, it was estimated that to meet the Federal SO<sub>2</sub>-emission standards for a coal containing 3% sulfur, 0.6 and 1.4 kg of spent oil shale and virgin oil shale, respectively, per kilogram of coal would be needed. For the same coal, 0.4 kg of a limestone or 0.2 kg of a dolomite per kilogram of coal would be needed. Greater quantities of oil shale are required due to its lower CaO content. The attrition rate of Green River oil shale was found to be similar to the attrition rates for typical limestones.

Comparison of Calcium Utilization in an AFBC with Predictions from TGA Data. A method has been developed to predict the utilization of calcium in limestones used for SO<sub>2</sub>-emission control in AFBCs. Rate constants for the reaction of bed materials with SO<sub>2</sub> were measured, using a thermogravimetric analyzer. These constants, as well as specific values of the Ca/S feed ratio, superficial gas velocity, fluidized bed height, and bed voidage are used in the Keairns equation to predict calcium utilization. Predicted values of calcium utilization differed from observed PDU values by about +4%. This method can be used to determine what Ca/S in the feed will give the SO<sub>2</sub> retention required by Federal SO<sub>2</sub> emission standards.

Prediction of Limestone Requirements for AFBC-CBC Systems. To improve the combustion efficiency of AFBCs, the carbon-rich material removed from the flue-gas stream by cyclones may be burned in a high-temperature (1100°C), low-gas-velocity (1.8 m/s) fluidized-bed carbon burnup cell (CBC). The method previously developed to predict the calcium utilizations in AFBCs from TGA data (see above section) has been used to predict the overall limestone requirements of an AFBC having a CBC. These computations indicate that about 60% of the sulfur in the elutriated material can be retained in the CBC if fresh limestone or partially sulfated stone is added to the cell. The actual SO<sub>2</sub> retentions obtained in a CBC depend on the particular limestone used and the CBC temperature.

Estimation of Limestone Requirements in AFBCs. Sixty-one different limestones have been tested for their reactivity with SO<sub>2</sub> in a TGA, and the performance of each stone in an AFBC predicted. The predictions were made for 0.9-m deep beds at 2.4 and 3.6 m/s linear gas velocity. The coal contained 4.3% sulfur and required an 83% sulfur retention. For the dolomitic limestones tested, between 0.27 and 1.2 kg of stone per kg of coal was required at 2.4 m/s (8 ft/s) gas velocity and between 0.36 and 2.4 kg stone/kg coal at 3.6 m/s (12 ft/s) gas velocity. For the calcitic limestones tested, the estimates were 0.37 to 1.5 kg stone/kg coal and 0.37 to 2.0 kg stone/kg coal at 2.4 and 3.6 m/s gas velocities, respectively. These studies point out the large variations in limestone requirements which can exist, depending on the nature of the limestone. The average pore size of about 40 of the calcined stones was measured. Although there was a general trend showing the extent of sulfation increasing with increasing average pore diameter, there was a large scatter in the data which indicated that one or more additional factors are also important.

Petrographic Examination of Limestone. Previous studies revealed that limestones from various quarries vary greatly in SO<sub>2</sub>-scavenging capacity. Five stones have been examined using petrographic techniques. Results have been

obtained on too few stones to allow the morphology of the stone to be correlated with the  $\text{SO}_2$  reactivity. However, in the case of two dolomitic stones examined, the less reactive stone had very coarse grains. The grains from one stone which is a "popper" (*i.e.*, explodes upon calcination) contain a large number of inclusions; however, another stone (not one of the five studied here) which is not a popper also has a large number of inclusions. This suggests that the type of inclusions as well as their number may be important in determining whether popping occurs.

### Task B. Turbine-Corrosion Studies

The objective of these studies is to understand the factors which influence the emission of alkali-metal compounds from coal combustion systems and to develop methods for reducing the alkali-metal compound content of hot combustion gases. These studies are in support of the development of a pressurized fluidized-bed coal combustion system utilizing a gas turbine. The transport of alkali-metal compounds from a combustor to a gas turbine is expected to be the major cause of hot corrosion of turbine blades.

Emission of Alkali Metals during Coal Combustion. The emission of alkali-metal compounds during the combustion of various coals, charcoal, and lignite has been previously studied. Additional studies have now been made on emissions during the combustion of lignite. These studies show that during the combustion of lignite, potassium is more volatile than sodium. When NaCl was added to a lignite sample prior to combustion, emission of potassium (as KCl) was enhanced.

Effect of Additives on the Retention of Alkali Metals in the Bed during Coal Combustion. Studies of the emission of alkali metals from coal during combustion indicate that the fraction of the alkali in the coal that is emitted is inversely proportional to the ash content of the coal. A series of different additives was added to charcoal which had been impregnated with 0.5% NaCl, and the quantity of sodium and potassium retained in the residue after combustion was measured. (Charcoal contains a large amount of potassium.) The retention of sodium ranged from 76 to 10%, and that of potassium from 71 to 5%. The order of effectiveness of these mineral additives in retaining sodium is as follows: silica gel, montmorillonite, kaolinite, bauxite, Greer limestone, Tymochee dolomite, alumina powder, Dolowite (a dolomite), no additive, and pure alumina. The order for effectiveness of potassium retention was about the same. The clay minerals were very effective in retaining alkali metals.

Removal of Gaseous Alkali Metal Compounds from the Hot Combustion Gases of Coal. Solid granular sorbents are under investigation for the removal of gaseous alkali-metal compounds (*viz.*, NaCl or KCl) from hot combustion gases. In these studies, a hot (850°C) simulated flue gas is loaded with gaseous NaCl or KCl and then passed through a hot packed bed of the granular substance being tested to determine its effectiveness for removing the alkali-metal compound. After screening tests with gaseous NaCl using alundum, diatomaceous earth, silica gel, kaolinite, attapulgus clay and activated bauxite, systematic studies with NaCl, KCl, and  $\text{K}_2\text{SO}_4$  continued. Tests with diatomaceous earth and activated bauxite are continuing and have thus far shown that both of these substances are effective in removing gaseous NaCl, KCl, and  $\text{K}_2\text{SO}_4$  from hot gases.

Tests have been made to determine the effect of bed temperature, linear gas velocity, and gas contact time on the retention of gaseous NaCl by diatomaceous earth and activated bauxite. Increasing the temperature from 800 to 880°C increased the amount of gaseous NaCl sorbed by diatomaceous earth and decreased the amount sorbed by activated bauxite. This difference is believed to be due to an endothermic chemical reaction occurring between the diatomaceous earth and the gaseous NaCl contrasted with physical adsorption of gaseous NaCl on the activated bauxite.

For linear gas velocities of 25, 66, and 155 cm/s and constant gas contact time, the amount of gaseous NaCl sorbed was found to be the same for both sorbents. Thus, at the test conditions, the rate of the sorption reaction is not controlled by the mass transfer of gas from the bulk to the external surface of the granular sorbent. In tests with activated bauxite, increasing the gas contact time from 0.05 to 0.19 s increased the removal of gaseous NaCl from the gas stream from about 80% to 98%. These results suggest that gas contact times of 0.2 s will be practical.

#### Task C. Trace-Pollutant Control in FBCs

Trace-Element Behavior in Sorbent During Cyclic (Sulfation-Regeneration) Utilization. The objectives of the work reported here were (1) to measure the level of selected trace elements in the sorbent over several cycles of sulfation and regeneration and to determine the tendency of trace elements to be enriched or depleted in the sorbent in several utilization cycles and (2) to make a material balance (of particulate samples only) for a single regeneration experiment, assessing changes in the trace-element concentrations in the sorbent for evidence of trace-element losses by volatilization.

Samples of (1) particulate sulfated Tymochtee dolomite from the first and tenth combustion cycles of a 10-cycle combustion-regeneration experiment and (2) particulate sulfated and regenerated sorbent, coal, and recovered fly ash from the tenth regeneration cycle of the same cyclic experiment have been analyzed for trace elements by spark-source mass spectrometry.

Based on the analyses of sulfated dolomite sorbent from the first and tenth combustion cycles, the concentrations of at least 9 of 31 elements appear to have increased. This enrichment was probably due to the buildup of coal ash on the surface of the sorbent particles during the ten combustion-regeneration cycles. During the ten cycles, none of the 31 elements appear to have been depleted.

Trace element concentrations in sulfated sorbent feed and in regenerated sorbent product from the tenth regeneration cycle were compared. Of 31 elements, only nickel showed any evidence of being depleted during regeneration.

For the tenth regeneration half-cycle, material balances were taken around the regeneration reactor for 27 of the 31 elements studied. There was a large scatter in the material balances of the various elements, making the behavior of the elements during regeneration difficult to assess.



## Task D. Particulate Control Studies

Evaluation of On-Line Light-Scattering Particle Analyzers. Two light-scattering particle-size analyzers have been tested at ANL in the process development unit (PDU) fluidized-bed combustion system. The analyzers are (1) a single-particle analyzer developed by Spectron Development Laboratory and (2) a multiparticle analyzer developed by Leeds and Northrup. Particle-size distributions and mass loadings determined at various flue-gas duct locations with the Spectron and the Leeds and Northrup instruments were compared with those obtained with (1) an Andersen cascade impactor, (2) a Coulter counter, and (3) positive filters. These comparisons were used to evaluate the two instruments at their present stage of development.

Based on the experimental work performed, the multiparticle analyzer developed by Leeds and Northrup is at a stage of development allowing it to be used with little operator training. Operation of the single-particle analyzer developed by Spectron Development Laboratory requires much more care, and data reduction is presently very time-consuming. The single-particle analyzer is a first-generation instrument and has much potential. On the other hand, the multiparticle analyzer is a more advanced instrument and with some refinement can be useful now in the development of PFBC technology.

Particulate Removal From Flue Gas. An experimental program is under way at ANL to test and evaluate promising high temperature/pressure flue-gas cleaning methods in the off-gas system of the 15.2-cm-dia (i.e., process development unit or PDU) fluidized-bed combustor. Techniques identified for investigation are granular-bed filtration (using beds of limestone sorbent from the FBC), high-efficiency controlled-vortex cyclones, and acoustic agglomeration.

Filtration experiments have been performed using small (7.8 or 15.4-cm-ID), horizontal fixed beds of limestone material and a downward flow of flue gas through the granular-bed filter.

The effects of bed depth, bed-particle size, and filtration velocity on filtration efficiency have been studied. For a -6 +14 mesh bed, filtration efficiency increased from ~91% at a 5.1-cm bed depth to ~98% at a 40.6-cm bed depth. Over the range of bed depths studied, using a -14 +30 mesh bed material rather than the coarse material decreased the penetration of particles through the filter by 35 to 40%.

In experiments using a shallow (5.1-cm) bed of -6 +14 mesh virgin dolomite, no effect of gas velocity on filtration efficiency was observed over the range of 15 to 60 cm/s. However, at a bed depth of 20.4 cm with the -6 +14 mesh virgin dolomite and at a bed depth of 5.1 cm with a sulfated limestone (mean particle diameter of ~700  $\mu\text{m}$ ), filtration efficiency was observed to increase with decreasing gas velocity, increasing from ~94% at 60 cm/s to ~99% at 15 cm/s for the sulfated limestone.

Particle loadings in the flue gas leaving the granular-bed filter generally ranged from 0.01 to 0.07 g/m<sup>3</sup>. There was little change in mass mean diameter of the dust as a result of passing through the granular-bed filter, and differences in filtration efficiency were not significant over the range of dust-particle sizes entering the filter.

For a 200-MWe PFBC, the rates of limestone usage and flue-gas volumetric flow were used to assess the permissible range of parameters such as bed depth, face velocity, and bed-replacement rate for the granular bed filter. The results indicated that at the filtration conditions of the PDU tests, the limestone requirements of the granular-bed filter would exceed the quantity available from a PFBC. The PDU tests were performed, however, with very high particulate loadings to the granular-bed filter, resulting in very short filtration times and high limestone requirements. Further testing of the granular bed filter with more typical inlet dust loadings is planned.

Acoustic dust conditioning is a technique to enhance the natural tendency of polydispersed particulates to impact upon each other and to agglomerate. Thus, acoustic dust conditioning is designed to increase the efficiency of downstream dust collectors.

Work is currently being carried out under a subcontract with the University of Toronto to develop and fabricate a pulse-jet sound generator, a resonant manifold, and acoustic treatment sections for subsequent installation and testing in the flue-gas system of the ANL PDU combustor.

Prototype pulse jets have been fabricated and tested at ambient conditions to finalize the design of the pulse jet for operation at elevated pressure. A sound intensity of 155 to 160 dB at a frequency of  $\sim 280$  Hz has been achieved.

Design of the resonant manifold has been completed, and testing of the unit at ambient pressure is being performed. Installation of the pneumatic control system for testing both the pulse jet and the resonant manifold at elevated pressures is nearly complete.

A high-efficiency, controlled-vortex cyclone.(TAN-JET) has been obtained from the Donaldson Co. and installed in the flue gas system of the ANL combustor as a secondary cyclone. Experiments to establish the performance of the unit as a particulate-removal device are being initiated. The cyclone's performance will be tested, and its use will also permit testing of the granular-bed filter at lower loadings than those used in earlier granular-bed experiments. In addition, the cyclone will be used in evaluating the ability of the pulse-jet acoustic agglomeration system to increase the particle-removal efficiency of mechanical collectors.

### Miscellaneous Studies

Pulsed L-Valve Tests. The L-valve, a type of nonmechanical valve, is a device which can be used to control the flow of solids into either dense-phase or lean-phase media, such as fluidized beds and pneumatic transport lines.

A small test program was initiated to develop an intermittently aerated L-valve feeder capable of feeding solids at very low rates. The L-valve tested was a standard 9.52-mm (3/8-in.) stainless steel tube cross fitting. Solids flowed by gravity from a hopper into the top of the L-valve. By use of a timer and a solenoid valve, pulsed aeration gas was supplied at right angles to the solids downward flow. The gas transported the solids horizontally in dense-phase flow to a point where the solids were discharged into a pneumatic transport line.

Test results demonstrated the ability of the valve to feed both coal and coal-limestone mixtures at low feed rates and within rigid specifications for feed-rate variance. With refinement of the timer used in the tests, the L-valve could be easily adapted for on-line control of solids feed rates.

## TASK A. GASEOUS POLLUTANT EMISSION CONTROL IN FBCs

1. Enhancement of Limestone Sulfation  
(J. Shearer and C. Turner)a. Introduction

We have studied the effects of adding NaCl to a fluidized-bed coal combustion system in order to enhance SO<sub>2</sub> capture by a limestone sorbent to form CaSO<sub>4</sub>. The proposed mechanism of interaction between NaCl and limestones is based on structural changes in the stone induced by the presence of trace amounts of liquid phase. Eutectic mixtures of salt and CaO form locally at temperatures greater than 700°C, and the increased ionic mobility enhances structural rearrangement and recrystallization which, in turn, affects the porosity of the lime produced. The resulting increase in average pore diameter causes increased permeability to SO<sub>2</sub>/O<sub>2</sub> mixtures. The larger pore sizes also permit further reaction to form CaSO<sub>4</sub> which has a larger molar volume than the original CaCO<sub>3</sub>. The buildup of an impervious layer of CaSO<sub>4</sub> is prevented by these dynamic structural changes occurring throughout the reaction. As pore size increases, total surface area decreases and, at some point, loss of surface area available for reaction causes a decrease in sulfation despite the increasing permeability. Thus, in a plot of percent conversion of CaO to CaSO<sub>4</sub> versus average pore diameter, the curve at first rises to a maximum conversion at an optimum pore diameter and then decreases as the average pore size increases further. Laboratory data show that for natural limestones average pore diameters for calcines formed at 850°C in 20% CO<sub>2</sub>,\* 5% O<sub>2</sub> and the balance N<sub>2</sub> are generally below this optimum value of 0.3-0.4 μm.

Thus, slight increases in average pore diameter will maximize the potential for capture of SO<sub>2</sub>. Data given below for 29 limestones show that in most cases, 1 mol % NaCl or less is needed to achieve this increase. Sulfations were carried out in a synthetic flue gas with the intention of applying the results to actual coal combustion systems.

A similar situation occurs for dolomites. However, upon calcination, of large amounts of MgCO<sub>3</sub> species, which are unreactive to SO<sub>2</sub>/O<sub>2</sub> mixtures, extensive porosity is produced. Thus, in natural dolomites a greater percentage of the CaO component is converted to CaSO<sub>4</sub> since the inert MgO prevents the CaSO<sub>4</sub> from forming a shell that blocks access to internal pores. For this reason, maximum conversion occurs at a somewhat smaller average pore diameter than for limestones and smaller amounts of salt additive are required to increase the average to this optimum.

Changes produced by the addition of NaCl then lead to enhanced sulfation in both limestones and dolomites. Laboratory studies indicate that any phenomenon that affects porosity can be used to enhance sulfation. Thus, high-temperature sintering, high CO<sub>2</sub> pressure, and the addition of other inorganic salts will all have a beneficial effect on limestone sulfation if the extent of pore growth can be controlled and optimized.

A more detailed presentation of the experimental results and conclusions can be found in Ref. 1.

---

\*All gas concentrations are given in vol %.

b. Effects of  $\text{CaCl}_2$  Additive on Limestone Sulfation

Earlier work in this area (ANL/CEN/FE-77-3) suggests that  $\text{CaCl}_2$  enhances  $\text{SO}_2$  capture by limestones. (It has since been pointed out that substantial amounts of  $\text{CaCl}_2$  are routinely added to coal storage piles to prevent freezing during the winter in colder areas.) A more complete study was initiated to demonstrate the effectiveness of  $\text{CaCl}_2$  as a sulfation enhancer and to compare the mode of interaction with that of  $\text{NaCl}$ . Experiments were performed in a horizontal tube furnace capable of achieving  $1100^\circ\text{C}$  and with a gas-mixing system capable of producing appropriate combinations of  $\text{O}_2$ ,  $\text{CO}_2$ ,  $\text{SO}_2$ , and  $\text{N}_2$ . Limestone samples (18-20 mesh) were contained in quartz boats in the furnace. The source of salt on the treated limestones was evaporated aqueous slurry.

Table 1 presents data on sulfation of calcite spar, ANL-9501, ANL-8903, and ANL-8001 limestones in the  $\text{CaCl}_2$ -treated and  $\text{NaCl}$ -treated states. These four stones represent a fairly broad range of impurity levels, as noted in the table. (Data for  $\text{NaCl}$ -treated stones were obtained earlier.) The results are given as percent conversion of  $\text{CaO}$  to  $\text{CaSO}_4$ . Figure 1 is a bar graph showing the effect of  $\text{CaCl}_2$ .

The effectiveness of  $\text{CaCl}_2$  is apparent from Table 1 and Figure 1 and is comparable to the effectiveness of  $\text{NaCl}$ . However, in contrast to  $\text{NaCl}$ , there are apparently two concentration regions of  $\text{CaCl}_2$  where sulfation of limestones is enhanced (Fig. 1). The first is at very low concentrations of  $\text{CaCl}_2$  ( $<0.5$  mol %).

The low melting point of  $\text{CaCl}_2$  and its capability of forming low-melting eutectics with  $\text{CaO}^2$  and  $\text{CaSO}_4$  support the mechanism proposed for  $\text{NaCl}$  effectiveness (reported earlier in ANL/CEN/FE-77-3) which results in changing the pore diameters and increasing the stone permeability. Porosity measurements given below show that with small additions of salt, "average" pore diameters of  $\text{CaCl}_2$ -treated stones shift to a much greater extent than does the pore diameter of stones treated with the same percent  $\text{NaCl}$ . Therefore, an optimum porosity structure will be reached with only trace amounts of  $\text{CaCl}_2$  additive, as shown in Fig. 1. The stone with the greatest impurity content, ANL-8001 (Greer limestone), achieves maximum sulfation with a slightly higher concentration of  $\text{CaCl}_2$  than gives maximum sulfation in the other stones. The  $\text{Ca}^{2+}$  in the additive can react with silica in the Greer limestone, effectively reducing the interaction of  $\text{CaCl}_2$  with  $\text{CaO}$  and  $\text{CaSO}_4$  so that maximum sulfation occurs at the higher salt concentrations.

The second concentration region where sulfation is enhanced (Fig. 1) is at higher  $\text{CaCl}_2$  concentrations ( $>1$  mol %). For  $\text{NaCl}$  in the range of concentrations investigated, this phenomenon has not been observed. Apparently, for all  $\text{CaCl}_2$ -treated stones studied, sufficiently large amounts of  $\text{CaCl}_2$  would cause the entire  $\text{CaO}$  content of the limestone to be sulfated. It is believed that complete sulfation would be due to the formation in this system of a substantial amount of liquid containing a large amount of dissolved  $\text{CaO}$ . The phase diagram for  $\text{CaO}$ - $\text{CaCl}_2$  shows that a liquid containing up to 20%  $\text{CaO}$  can be formed at these temperatures with locally high salt concentrations.<sup>2a</sup> The presence of  $\text{CaSO}_4$  may even enhance this effect. With so much  $\text{CaO}$  in a "liquid" form, sulfation can proceed rapidly by dissolution and crystallization

Table 1. Effects of  $\text{CaCl}_2$  and  $\text{NaCl}$  upon Six-Hour Sulfation of Limestones at  $850^\circ\text{C}$  in 0.3%  $\text{SO}_2$ , 5%  $\text{O}_2$ , 20%  $\text{CO}_2$ , and the Balance  $\text{N}_2$

Limestone	Quantity of Salt Added, mol %	% Conversion of $\text{CaO}$ to $\text{CaSO}_4$ with $\text{CaCl}_2$ Addition	% Conversion of $\text{CaO}$ to $\text{CaSO}_4$ with $\text{NaCl}$ Addition
Calcite Spar (no impurities)	0	5.2	5.2
	0.1	35.0	21.0
	0.2	33.8	27.0
	0.5	30.1	39.8
	1.0	19.2	34.0
	2.0	24.4	23.0
	3.0	33.0	--
	4.0	46.0	20.7
	5.0	73.9	--
ANL-9501 (Grove) (~3% impurities)	0	13.0	13.0
	0.1	50.0	--
	0.2	45.0	--
	0.5	28.5	52.2
	1.0	19.9	44.6
	2.0	27.1	31.6
	3.0	40.6	--
	4.0	53.8	19.8
	5.0	71.1	--
ANL-8903 (~9% impurities)	0	43.0	43.0
	0.1	55.4	--
	0.5	30.0	47.5
	1.0	31.1	--
	2.0	48.2	--
	3.0	53.0	--
	4.0	65.2	27.9
	5.0	69.0	--
ANL-8001 (Greer) (~20% impurities)	0	38.0	38.0
	0.1	49.3	--
	0.5	52.8	43.9
	1.0	50.6	45.5
	2.0	40.2	55.0
	3.0	43.6	--
	4.0	52.9	55.5
	5.0	55.0	--

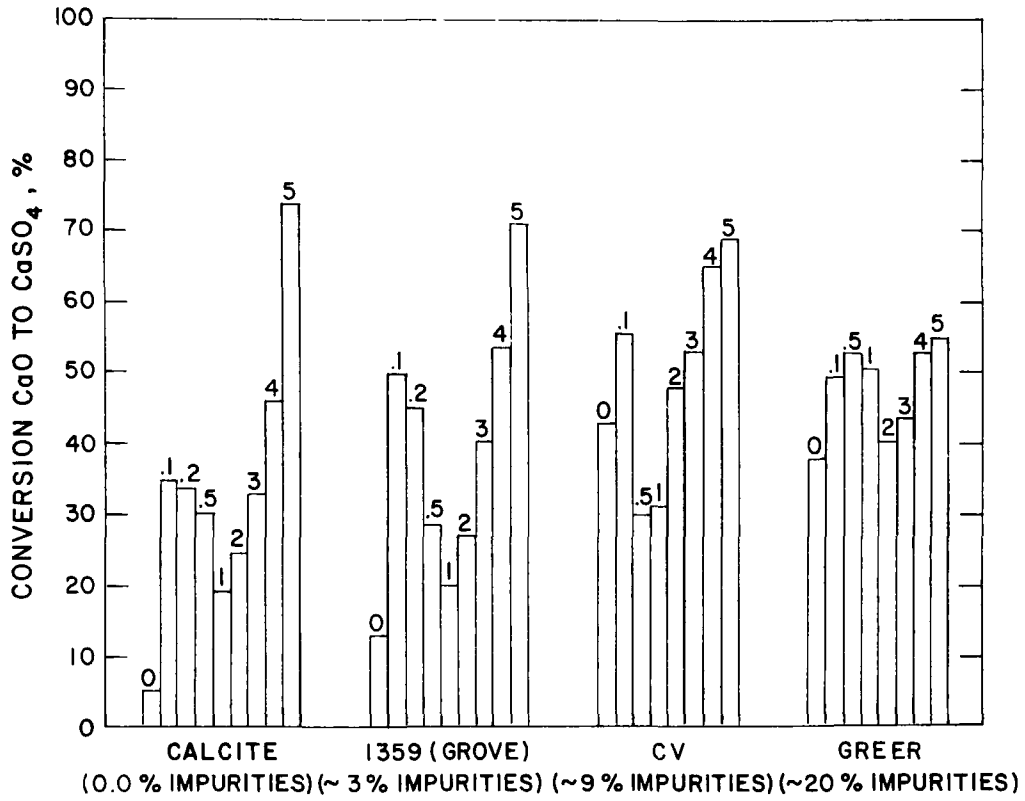


Fig. 1. Effect of  $\text{CaCl}_2$  Addition on Limestone Sulfation at  $850^\circ\text{C}$  for 6 h in 0.3%  $\text{SO}_2$ , 20%  $\text{CO}_2$ , 5%  $\text{O}_2$ , Balance  $\text{N}_2$ . (All stones precalcined without  $\text{SO}_2$  present.) Numbers above bars each refer to mol %  $\text{CaCl}_2$  added.

and can progress through entire particles as long as enough liquid is present. In terms of practical application in a fluidized bed, the large amounts of  $\text{CaCl}_2$  required plus the possibility of agglomeration would seem to prohibit the application of this liquid formation for sulfation enhancement. However, as shown, the use of even small amounts of  $\text{CaCl}_2$  has major effects and deserves further attention.

In order to clearly define the effect of  $\text{CaCl}_2$ , a larger number of limestones (with added  $\text{CaCl}_2$ ) representing large variations in composition and morphology were reacted in a simulated flue gas. The flue gas consisted of 0.3%  $\text{SO}_2$ , 5%  $\text{O}_2$ , 20%  $\text{CO}_2$ , and the balance  $\text{N}_2$ . Reaction was carried out at 850°C for 6 h using both untreated stones and stones treated by evaporating  $\text{CaCl}_2$  from an aqueous solution. Chemical analyses for these stones are listed in Appendix A. Results of sulfation experiments carried out with these limestones are presented in Table 2 as percent conversions of  $\text{CaO}$  to  $\text{CaSO}_4$ . Data are presented for untreated stones, limestones treated with a 0.1 mol %  $\text{CaCl}_2$ , and stones treated with 0.5 mol %  $\text{CaCl}_2$ . As suggested earlier in this report, one range of  $\text{CaCl}_2$  additions at which maximum conversions to sulfate are achieved is  $<0.5$  mol %; larger quantities of salt are generally required for stones with the greatest impurity content. In 60% of the cases a larger extent of sulfation was obtained for the 0.1 mol % addition. In most cases, except for some very pure limestones, the maximum conversion to sulfate approaches 50-60%. Even in these pure stones, the increase in reactivity relative to the reactivity of untreated stones is substantial.

For an FBC in which introduction of a major amount of corrosive species is to be avoided the effectiveness of such small amounts of  $\text{CaCl}_2$  for sulfation enhancement makes this salt appear more promising than  $\text{NaCl}$  (which required  $>1.0$  mol %). Moreover, when  $\text{CaCl}_2$  is used routinely as a freeze-proofing material for coal storage piles, the quantities used are comparable to those used in this work, with no apparent major corrosive effects. In work in a PDU-scale unit paralleling this sulfation-enhancement work,<sup>3</sup> a series of metal corrosion specimens is being exposed to flue gas in the presence of limestone containing  $\text{CaCl}_2$  and in the freeboard above the limestone bed. Metallographic analysis will be performed to determine corrosive effects.

The effects of  $\text{CaCl}_2$  on the calcined limestones are similar to the effects of  $\text{NaCl}$  addition. When either salt is added to the limestone during calcination, the average pore diameters of the calcines increase. Representative curves are presented in a later portion of this report. Calcium chloride is slightly more effective than is  $\text{NaCl}$  in increasing the pore diameters, smaller amounts of  $\text{CaCl}_2$  being required to produce the same magnitude of change as  $\text{NaCl}$ . The porosity reaches an optimum pore-size distribution with respect to sulfation with small amounts of  $\text{CaCl}_2$ . This distribution has a maximum sulfation reactivity occurring near  $0.3 \mu\text{m}$ , as shown in Fig 2, which plots average pore diameter versus percent conversion for stones treated with various amounts of  $\text{CaCl}_2$ . These average pore diameters were calculated from surface areas and volumes for pores  $>0.01 \mu\text{m}$  (since pores smaller than  $0.01 \mu\text{m}$  are ineffective in sulfation) and corrected for mercury compression. The range of pore-size distributions which results in optimum sulfation reactivity



Table 2. Average Pore Diameter and Percent Conversion to Sulfated State at 850°C for Limestones Treated with  $\text{CaCl}_2$ . Sulfated 6 h in 0.3%  $\text{SO}_2$ , 5%  $\text{O}_2$ , 20%  $\text{CO}_2$ , and the Balance  $\text{N}_2$ .

Stone	Untreated Limestone		0.1 mol % $\text{CaCl}_2$ Added		0.5 mol % $\text{CaCl}_2$ Added	
	Avg. Pore Dia, $\mu\text{m}$	Conver., %	Avg. Pore Dia, $\mu\text{m}$	Conver., %	Avg. Pore Dia, $\mu\text{m}$	Conver., %
ANL-5304	0.140	42.6	0.376	58.4	0.574	55.5
ANL-6702	0.187	38.4	0.549	60.9	1.84	56.6
ANL-7401	0.171	41.5	0.217	48.6	0.305	65.2
ANL-8001	0.224	38.0	0.244	49.3	0.382	52.8
ANL-8101	0.144	33.5	0.166	49.9	0.292	44.6
ANL-8301	0.096	29.3	0.122	42.7	0.253	59.9
ANL-8701	0.232	33.2	0.306	50.3	0.577	59.4
ANL-8902	0.134	29.9	0.237	49.0	0.304	47.4
ANL-8903	0.159	43.0	0.288	55.4	0.542	30.0
ANL-9201	0.094	28.1	0.143	43.9	0.521	30.5
ANL-9401	0.229	51.7	0.366	56.3	0.812	30.0
ANL-9402	0.089	17.5	0.372	36.0	1.18	34.3
ANL-9501	0.100	13.0	0.144	50.0	1.32	28.5
ANL-9502	0.205	34.9	0.280	38.6	0.753	39.2
ANL-9503	0.170	42.8	0.379	45.2	1.85	58.1
ANL-9504	0.124	25.9	0.328	44.2	0.778	35.4
ANL-9505	0.163	31.2	0.483	40.1	1.68	38.6
ANL-9601	0.090	30.0	0.232	36.7	0.884	46.0
ANL-9602	0.118	38.8	0.183	43.5	0.962	32.8
ANL-9603	0.127	16.5	0.228	43.8	0.620	36.5
ANL-9701	0.117	7.0	0.186	37.7	0.896	36.9
ANL-9702	0.074	35.8	0.105	41.0	0.966	37.6
ANL-9703	0.182	53.2	0.280	41.6	1.37	47.0
ANL-9704	0.186	33.3	0.586	37.7	1.29	36.9
ANL-9801	0.146	42.8	0.536	41.2	1.24	42.7
ANL-9802	0.198	48.4	0.524	47.2	1.64	63.9
ANL-9901	0.141	36.4	0.216	39.7	0.781	24.8
ANL-9902	0.180	43.6	0.672	50.8	1.53	51.7
Calcite	0.039	5.2	0.475	35.0	0.803	30.1

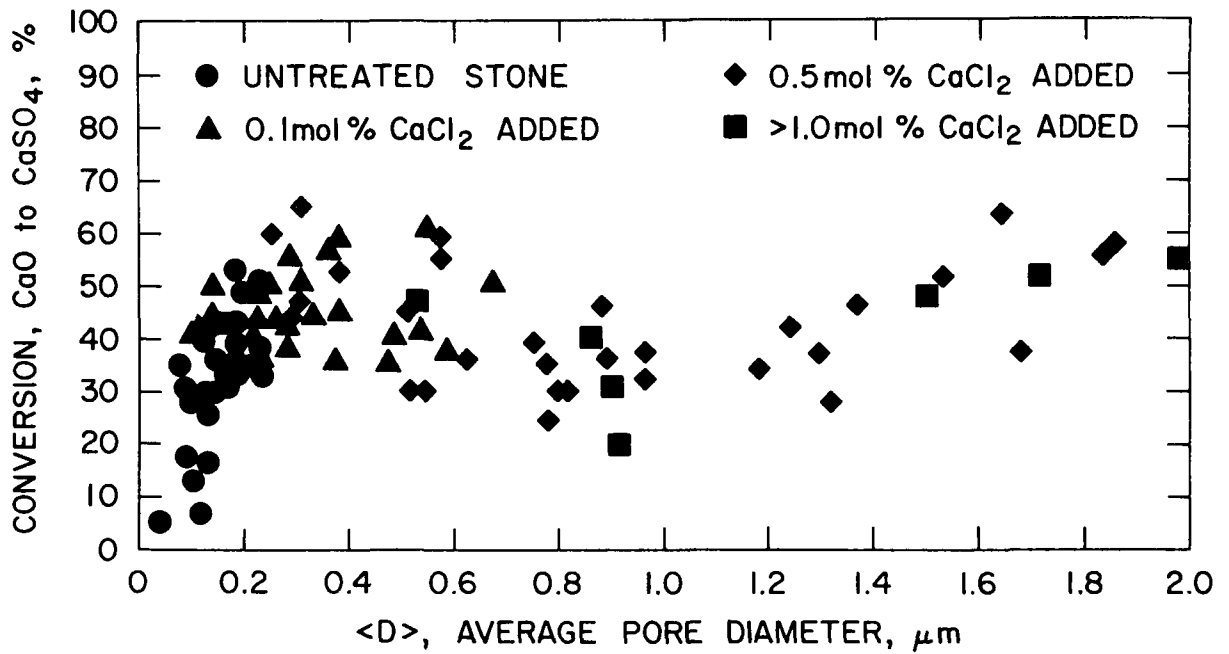


Fig. 2. Percent Conversion to Sulfate versus Average Pore Diameter for Limestones Treated with  $\text{CaCl}_2$  at  $850^\circ\text{C}$  and Sulfated for 6 h in 0.3%  $\text{SO}_2$ , 5%  $\text{O}_2$ , 20%  $\text{CO}_2$ , and the Balance  $\text{N}_2$

when the additive is  $\text{CaCl}_2$  is also the optimum range observed for  $\text{NaCl}$  addition. This correlation supports the concept that pore size and distribution are the most important factors determining the extent of sulfation of limestones in  $\text{SO}_2/\text{O}_2$  mixtures for limestone particles averaging 18-20 mesh size.

The second increase in  $\text{SO}_2$  capture with increasing  $\text{CaCl}_2$  concentrations (see Fig. 2) occurs at average pore diameters greater than  $1.0\ \mu\text{m}$ . As discussed earlier, this phenomenon is believed to be a result of the formation of large amounts of a liquid phase containing dissolved  $\text{CaO}$ . Higher concentrations of  $\text{CaCl}_2$  were also tried that resulted in pore diameters much greater than  $2.0\ \mu\text{m}$  but are not presented in this graph. The presence of a liquid phase leading to major structural rearrangement is supported by preliminary scanning electron micrographs.

### c. Effects of $\text{MgCl}_2$ and Other Salts on Limestone Sulfation

In a continuing study of the effects of various salts,  $\text{MgCl}_2$  at very low concentrations was found to be an effective enhancer of limestone sulfation. Table 3 lists the percent conversions of available  $\text{CaO}$  to  $\text{CaSO}_4$  for four limestones treated with  $\text{MgCl}_2$  (introduced via evaporation from an aqueous slurry). The same two-maximum effect observed for  $\text{CaCl}_2$  is present for  $\text{MgCl}_2$ . The low- $\text{MgCl}_2$ -concentration region ( $<0.5\ \text{mol}\%$ ) results in porosity changes favorable to sulfation via trace amounts of a liquid phase; intermediate amounts ( $1\text{-}2\ \text{mol}\%$ ) cause large amounts of a liquid phase to form with substantial amounts of dissolved  $\text{CaO}$  accelerating the formation of  $\text{CaSO}_4$ .

The magnitude of the  $\text{MgCl}_2$  effect may be compared with that of  $\text{NaCl}$  and  $\text{CaCl}_2$  by examining Figs. 3, 4, and 5, which show porosity curves measured on four limestones treated with (1)  $\text{NaCl}$ , (2)  $\text{CaCl}_2$ , and (3)  $\text{MgCl}_2$ , respectively. The horizontal bars with arrowheads mark the extent of shift in pore diameters of the majority of pores from the pore distribution of untreated stone to the pore distribution of salt-treated ( $0.5\ \text{mol}\%$ ) stone. In all three figures, the effect is greatest for the purest limestone and decreases as the impurity content increases until finally there are very small effects for ANL-8001 which contains  $\approx 20\%$  impurities. The relative effectiveness of the three salts can be represented by  $\text{MgCl}_2 > \text{CaCl}_2 > \text{NaCl}$  for the same mole percent addition of salt. In terms of weight percent addition,  $\text{MgCl}_2$  and  $\text{CaCl}_2$  have comparable effects; by weight, more of each is required than of  $\text{NaCl}$ . At this salt concentration ( $0.5\ \text{mol}\%$ ), most treated limestones have greater total porosity as well as larger average pore diameters than do the same stones when not treated.

The effects of other inorganic salts on limestone sulfation were examined concurrently with the  $\text{NaCl}$  and  $\text{CaCl}_2$  work. Table 4 lists percent conversions to  $\text{CaSO}_4$  for four limestones treated with a variety of salts at concentrations of  $1\ \text{mol}\%$ . The results for  $\text{NaCl}$ ,  $\text{CaCl}_2$ , and  $\text{MgCl}_2$  are also included to allow comparison. The data in Table 4 do show that most salts tested have some measurable positive effects and hence may be sulfation enhancers at the proper salt concentrations.

Table 3. Percent Conversion to Sulfate after 6 h with 0.3% SO<sub>2</sub> at 850°C for Limestones Precalcined with MgCl<sub>2</sub> Additive at 850°C 1 h in 5% O<sub>2</sub>, 20% CO<sub>2</sub>, Balance N<sub>2</sub>

Limestone	MgCl <sub>2</sub> Added, mol %	% Conversion of CaO to CaSO <sub>4</sub>
Calcite Spar (~0% impurities)	0.0	5.2
	0.1	24.0
	0.5	25.7
	1.0	21.0
	4.0	36.8
ANL-9501 (~3% impurities)	0.0	13.0
	0.1	28.4
	0.5	36.6
	1.0	20.9
	4.0	32.9
ANL-8903 (~9% impurities)	0.0	43.0
	0.1	57.9
	0.5	45.6
	1.0	33.9
	4.0	52.4
ANL-8001 (Greer) (~20% impurities)	0.0	38.0
	0.1	49.2
	0.5	54.7
	1.0	57.0
	4.0	41.3
	5.0	48.5

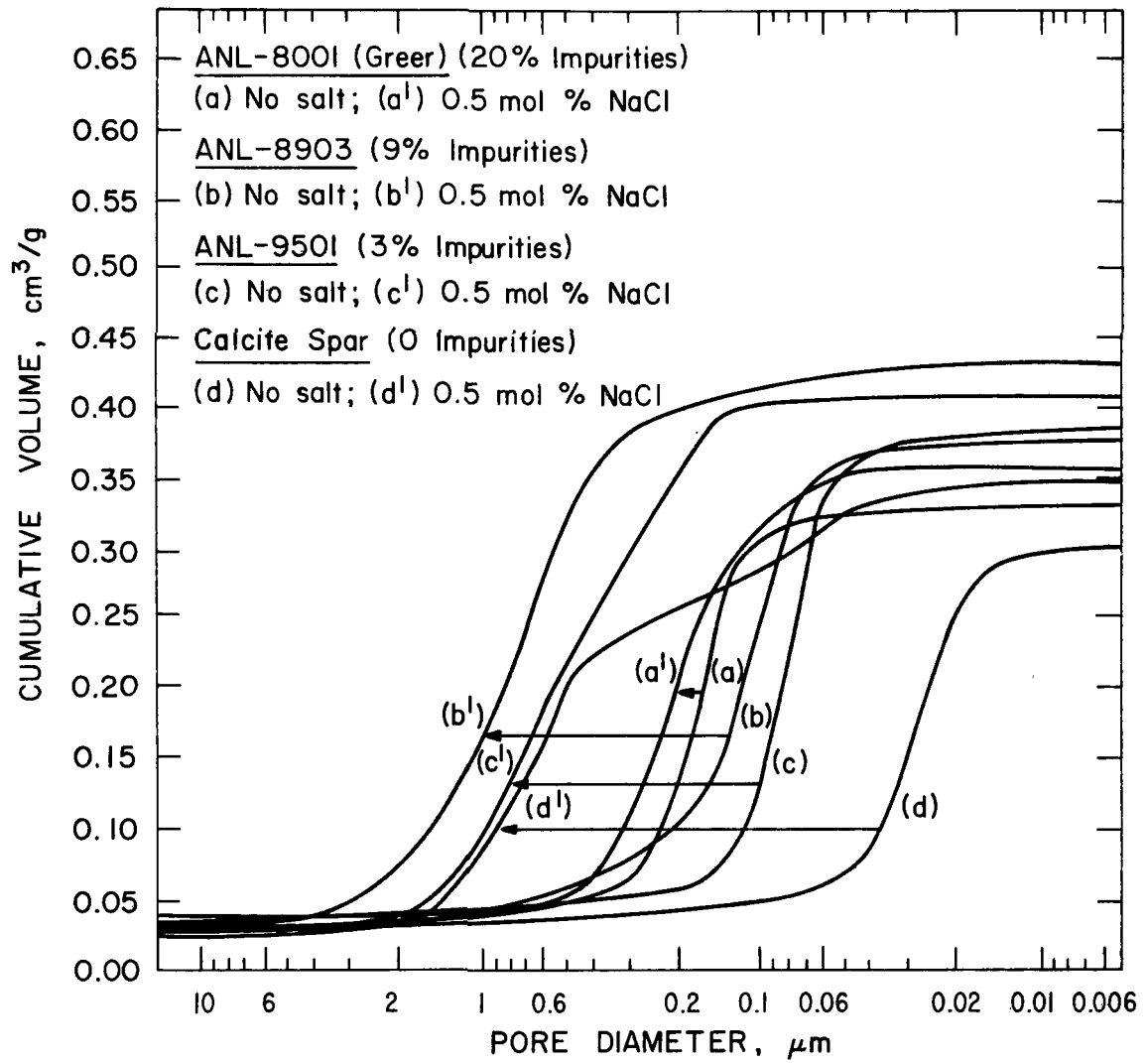


Fig. 3. Changes in Porosity Curves with 0.5 mol % NaCl Addition to Limestones Calcined at 850 °C 1 h in 5% O<sub>2</sub>, 20% CO<sub>2</sub>, and the Balance N<sub>2</sub>

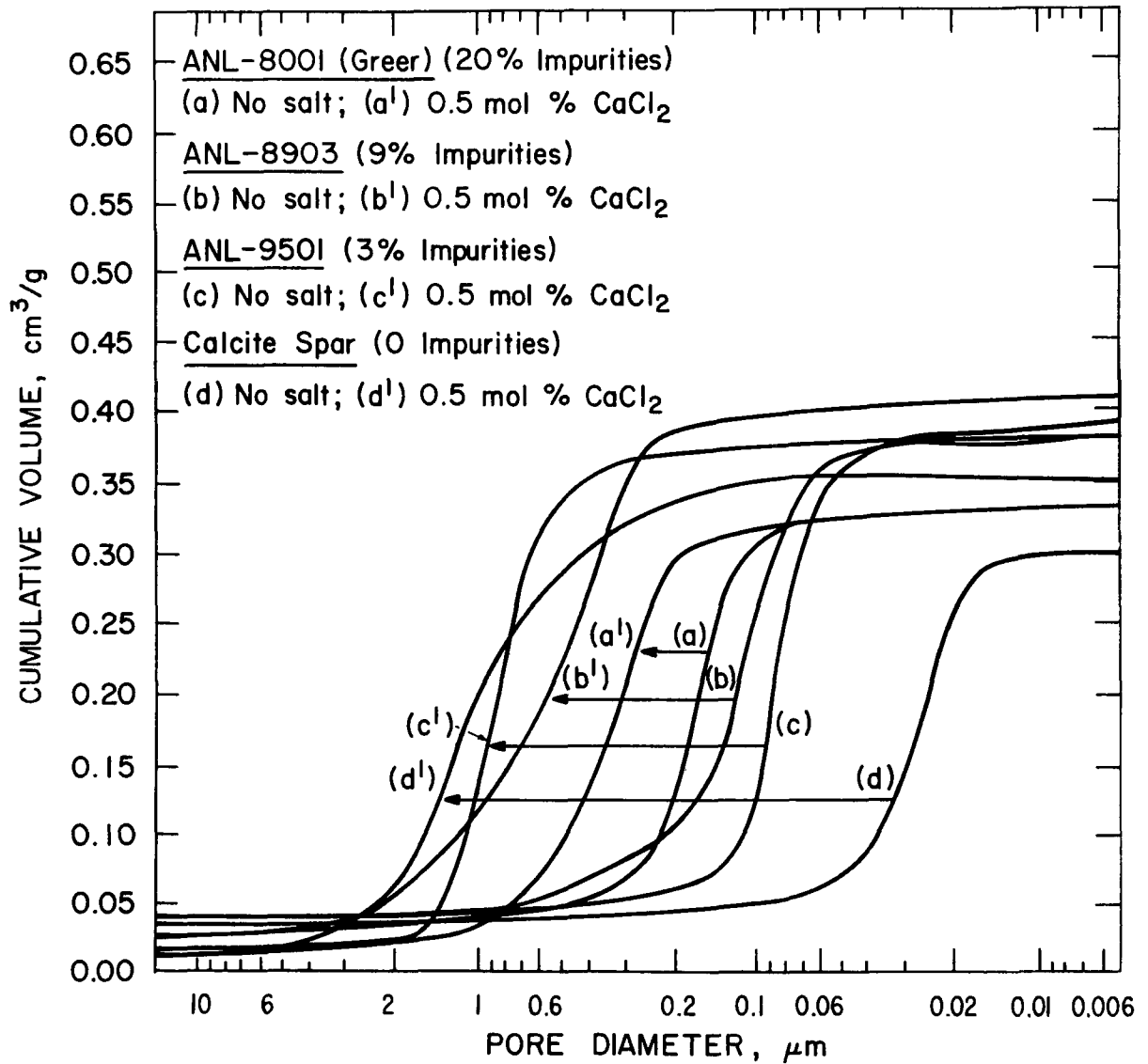


Fig 4. Effect of 0.5 mol %  $\text{CaCl}_2$  Addition on Porosity of Limestones Calcined at  $850^\circ\text{C}$  for 1 h in 5%  $\text{O}_2$ , 20%  $\text{CO}_2$ , and the Balance  $\text{N}_2$

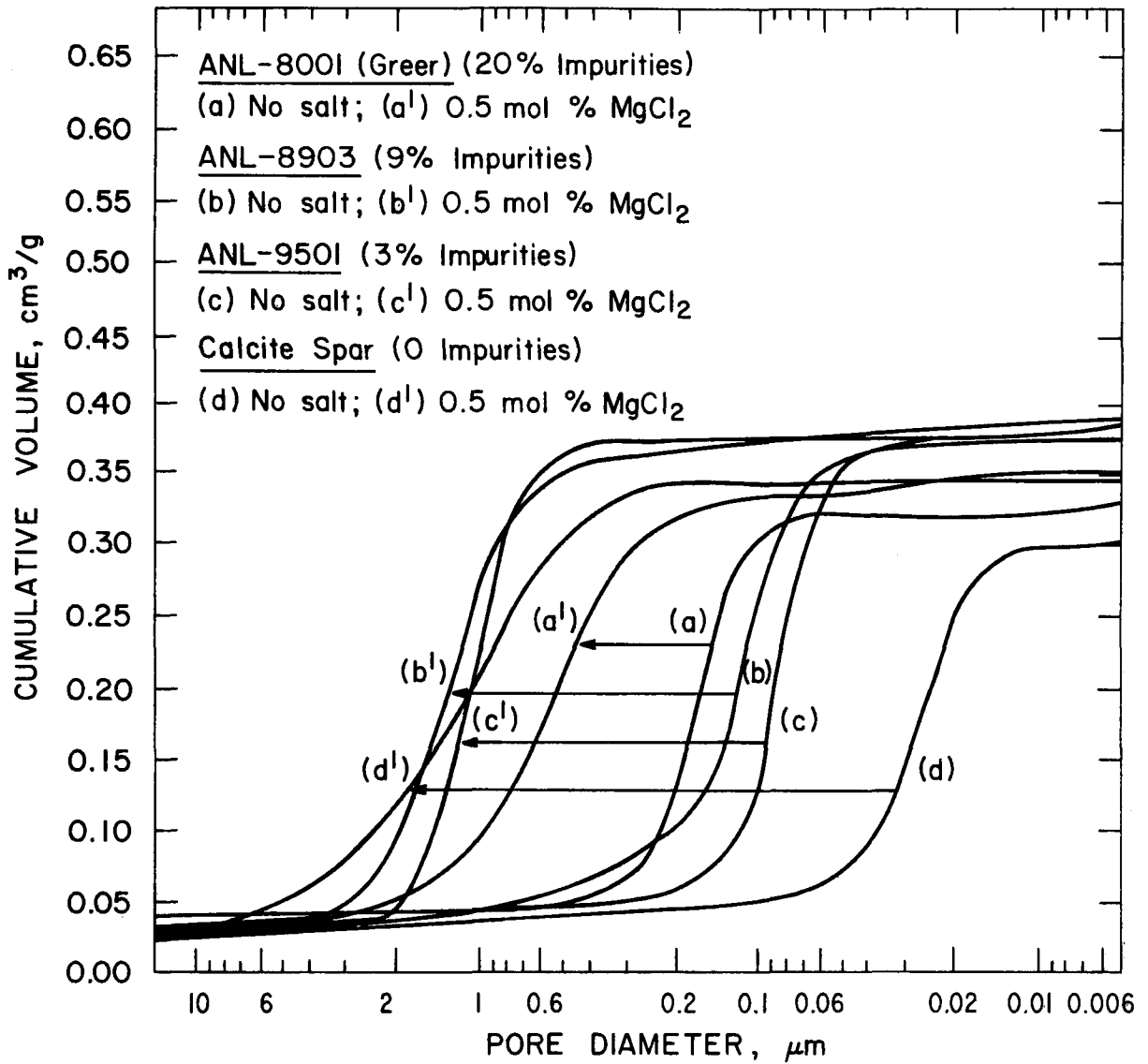


Fig. 5. Changes in Porosity Curves with 0.5 mol %  $\text{MgCl}_2$  Addition to Limestones Calcined at  $850^\circ\text{C}$  1 h in 5%  $\text{O}_2$ , 20%  $\text{CO}_2$ , and the Balance  $\text{N}_2$

Table 4. Percent Conversion to Sulfate of Limestones after 6 h with 0.3% SO<sub>2</sub> at 850°C for Limestones Precalcined with Inorganic Additives at 850°C 1 h in 5% O<sub>2</sub>, 20% CO<sub>2</sub>, and the Balance N<sub>2</sub>

Salt Added (1 mol %)	Calcite Spar (~0% Impurities)	ANL-9501 (Grove) (~3% Impurities)	ANL-8903 (~9% Impurities)	ANL-8001 (Greer) (~20% Impurities)
Untreated Stones	5.2	13.0	43.0	38.0
NaCl	33.3	44.4	47.5	43.9
NaOH	20.2	27.6	43.5	41.0
Na <sub>2</sub> CO <sub>3</sub>	23.6	43.6	41.0	40.0
Na <sub>2</sub> SO <sub>4</sub>	23.8	41.5	43.2	46.8
Na <sub>2</sub> SiO <sub>3</sub>	5.2	12.3	48.4	40.3
Na <sub>2</sub> SiO <sub>3</sub> ·9H <sub>2</sub> O	21.4	36.8	39.8	44.9
CaCl <sub>2</sub>	19.2	19.9	34.7	50.6
MgCl <sub>2</sub>	21.0	20.9	33.0	54.7
Ca(OH) <sub>2</sub>	10.4	12.4	47.5	49.0
CaF <sub>2</sub>	20.6	26.3	53.6	45.8
CaSO <sub>4</sub>	8.0	13.6	44.4	46.1
H <sub>3</sub> BO <sub>3</sub>	5.1	17.3	43.9	46.8



We know from our understanding of the effects of NaCl and CaCl<sub>2</sub> that maximum sulfation enhancement cannot be found by using only one concentration of salt in a single sulfation experiment. Porosity curves at several salt concentrations should be used to locate the salt concentration most likely to give maximum reactivity with SO<sub>2</sub>/O<sub>2</sub>, assuming that an optimum pore distribution for limestone sulfation can be reached despite differing limestone compositions. Once this salt concentration is found, a series of bracketing sulfation experiments should serve to indicate maximum sulfations achievable for the particular stone and salt used.

## 2. Investigation of Sulfation Reactions during Fluidized-Bed Combustion of Coal

(J. Shearer, R. Snyder, J. Lenc, and C. Turner)

To understand the effects of salt addition in a real combustor system, the basic reaction of limestone with SO<sub>2</sub>/O<sub>2</sub> must be understood first. Comparisons were made between sulfations carried out in horizontal tube furnaces and in actual small-scale-combustor runs under similar conditions.

Limestone ANL-9701 (Germany Valley) was reacted for ~6 h in a PDU fluidized-bed coal combustor at 850°C with steady-state SO<sub>2</sub> levels in the exhaust gas. Bed material was continually added to and removed from the combustor. For comparison, 6-h runs were performed in the tube furnace assemblies, using a synthetic flue gas of 0.3% SO<sub>2</sub>, 5% O<sub>2</sub>, 20% CO<sub>2</sub>, and the balance N<sub>2</sub>. Gas concentrations in the combustor (except O<sub>2</sub> which was 12%) were estimated to be similar. Figure 6 (A, B, and C) shows porosity curves for time fractions of various sulfation systems. Plot A shows curves for tube furnace samples of limestone ANL-9701 precalcined and sulfated for various intervals as shown. Plot B shows a similar set of porosity curves for ANL-9701 stone simultaneously calcined and sulfated in tube furnaces. Plot C is a series of porosity curves measured on an over-flow sample from the coal combustor. The sample was separated by color into fractions representing increased length of exposure to the combustor gases from (a) to (e).

A basic similarity of all three graphs is the shifting of the average pore diameter to larger pore sizes during the course of reaction. The extents of shift for both of the tube-furnace samples and the combustor samples are similar. Table 5 lists conversions to sulfate and average pore diameters for the three cases, as well as average pore diameters for a sample that was calcined (without SO<sub>2</sub> present) at 850°C in 5% O<sub>2</sub>, 20% CO<sub>2</sub>, and the balance N<sub>2</sub> (for which porosity curves are shown in Fig. 7). From these data (Table 5), one can see that similar average pore diameters correspond to similar extents of sulfation in all three systems; the last experiment (with no SO<sub>2</sub>) shows that the apparent gradual increase in pore sizes can be accounted for by long-term (6-h) heating under these conditions. On the basis of the above data, the results obtained in (1) the tube furnace assembly and (2) this particular combustor system appeared to be in excellent agreement.

In contrast to the above results, the data from a study done on another limestone (ANL-9501) in another PDU fluidized-bed coal combustor and in our tube furnaces were not in such good agreement. Figure 8 (A, B, C) shows

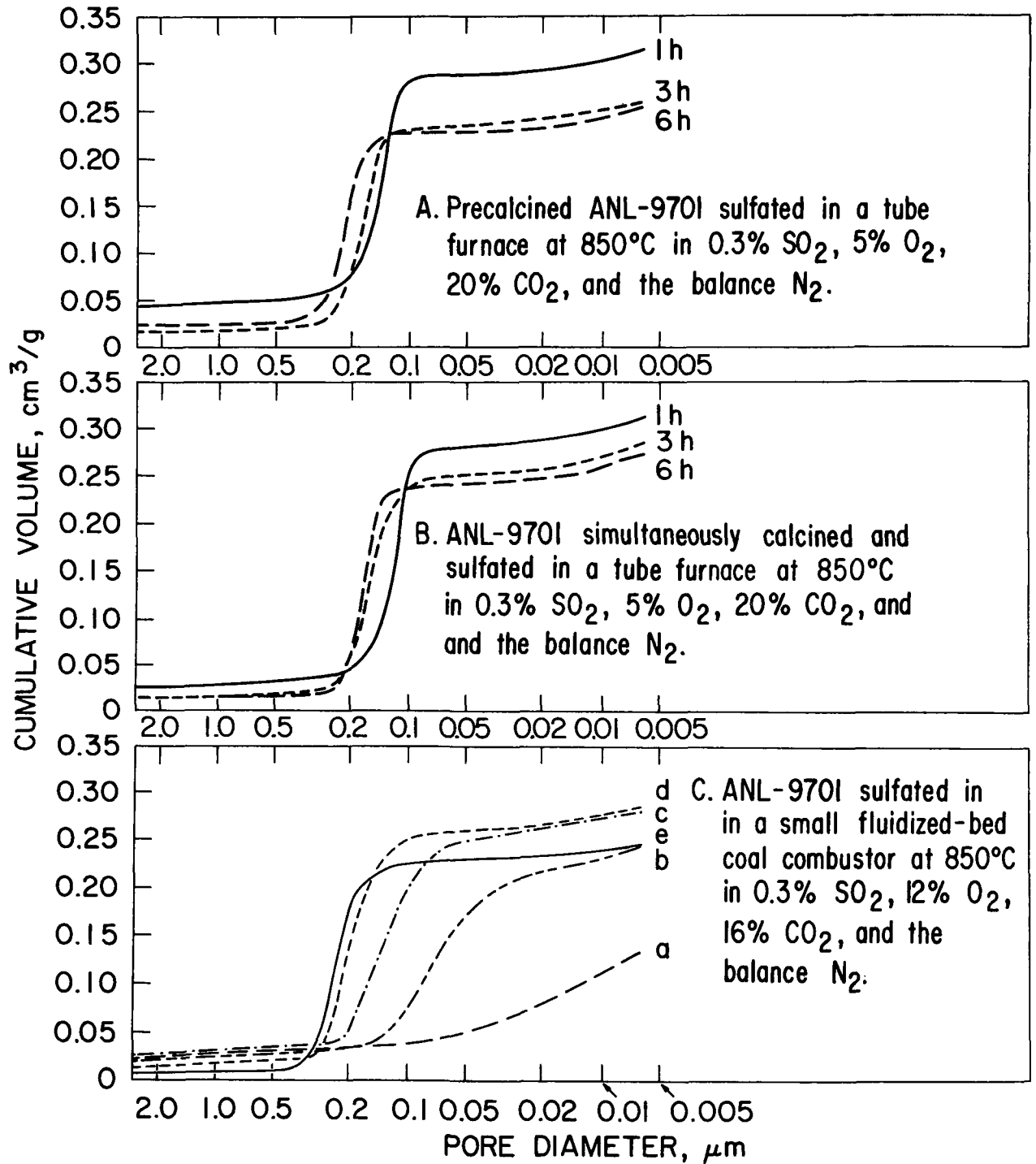


Fig. 6. Porosity Curves of ANL-9701 Comparing Combustor-Sulfated Samples (C) and Samples Sulfated in a Laboratory Tube Furnace (A and B)

Table 5. Sulfation Conversions and Average Pore Diameters  
for ANL-9701 Stone Under Various Reaction Conditions

Reaction Conditions at 850 °C	Average Pore Diameter $\mu\text{m}$	Conversion CaO to $\text{CaSO}_4$ , %
Precalcined 1 h without $\text{SO}_2$ Present and then Sulfated in 0.3% $\text{SO}_2$ , 5% $\text{O}_2$ , 20% $\text{CO}_2$ and the balance $\text{N}_2$ for:		
1 h	0.144	8.0
3 h	0.162	10.0
6 h	0.199	11.0
Simultaneously Calcined and Sulfated in 0.3% $\text{SO}_2$ , 5% $\text{O}_2$ , 20% $\text{CO}_2$ , and the balance $\text{N}_2$ for:		
1 h	0.124	6.4
3 h	0.153	8.0
6 h	0.163	10.8
Sulfated Samples from Fluidized-Bed Coal Combustor: <sup>a</sup>		
a	partially calcined	undefined
b	0.065	4.6
c	0.121	7.5
d	0.173	9.1
e	0.203	11.5
Calcined in 5% $\text{O}_2$ , 20% $\text{CO}_2$ , and the balance $\text{N}_2$ for:		
0.5 h	0.090	--
1 h	0.110	--
2 h	0.120	--
4 h	0.175	--
6 h	0.190	--

<sup>a</sup>Flue gas: ~0.3%  $\text{SO}_2$ , 12%  $\text{O}_2$ , 16%  $\text{CO}_2$ , and the balance  $\text{N}_2$ . Entries are  
in order of increasing length of time in the combustor.

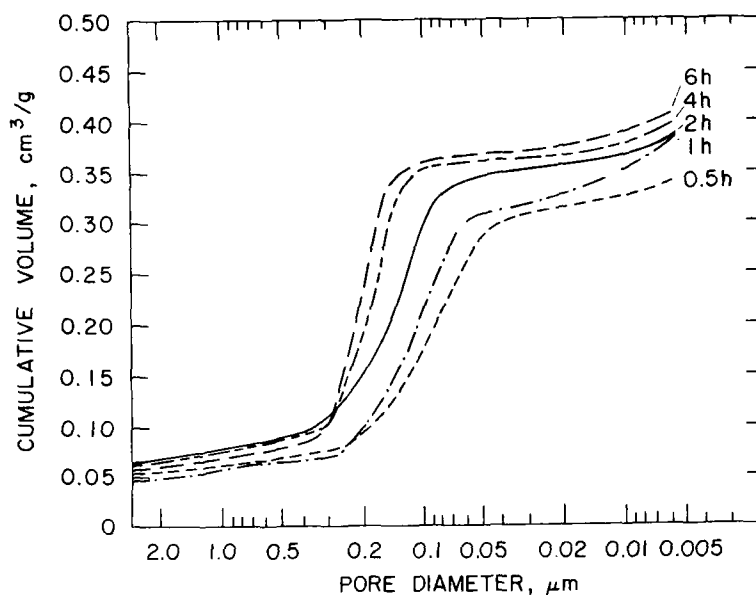


Fig. 7. Porosity Curves Showing the Effect of Calcining on Limestone ANL-9701 in a Laboratory Tube Furnace. Limestone Calcined at 850°C in 5% O<sub>2</sub>, 20% CO<sub>2</sub> and the balance N<sub>2</sub>.

porosity curves for (A) precalcined ANL-9501 sulfated in a tube furnace, (B) ANL-9501 simulatenously calcined and sulfated in a tube furnace, and (C) separated fractions of a partially sulfated limestone ANL-9501 sample from the fluidized-bed combustor test. Notable differences between results for the tube-furnace samples and the combustor samples are apparent. In particular, the extent of sulfation is much greater for the combustor samples. Table 6 lists percent conversions to sulfate and average pore diameters for the various samples.

Whereas for limestone ANL-9701 sulfated in the earlier mentioned combustor, there was excellent correlation of average pore diameter and a low extent of sulfation. In this system the much greater sulfation fills the pores to such an extent that the assumed increase in pore diameter is masked.

Figure 9A shows porosity curves for 1-h and 6-h calcined ANL-9501 limestone in a laboratory tube furnace. The average pore diameter shifted, due to ionic migration and diffusion. Figure 9B shows porosity curves for a 0.2 mol% CaCl<sub>2</sub>-treated sample of ANL-9501 undergoing calcination and then sulfation. The average pore diameter of the calcined limestone was much larger than in the absence of salt and, as sulfation progressed, the apparent average pore diameter decreased due to infilling of pore space by newly formed CaSO<sub>4</sub>. In this particular case, the average pore diameter apparently changed from >1.0 μm to <0.7 μm due to CaSO<sub>4</sub> formation. The extent of conversion after 5 h of sulfation is >40%. The difficulty in determining the average pore diameter of the limestone when only porosity curves for the end product are available is apparent.

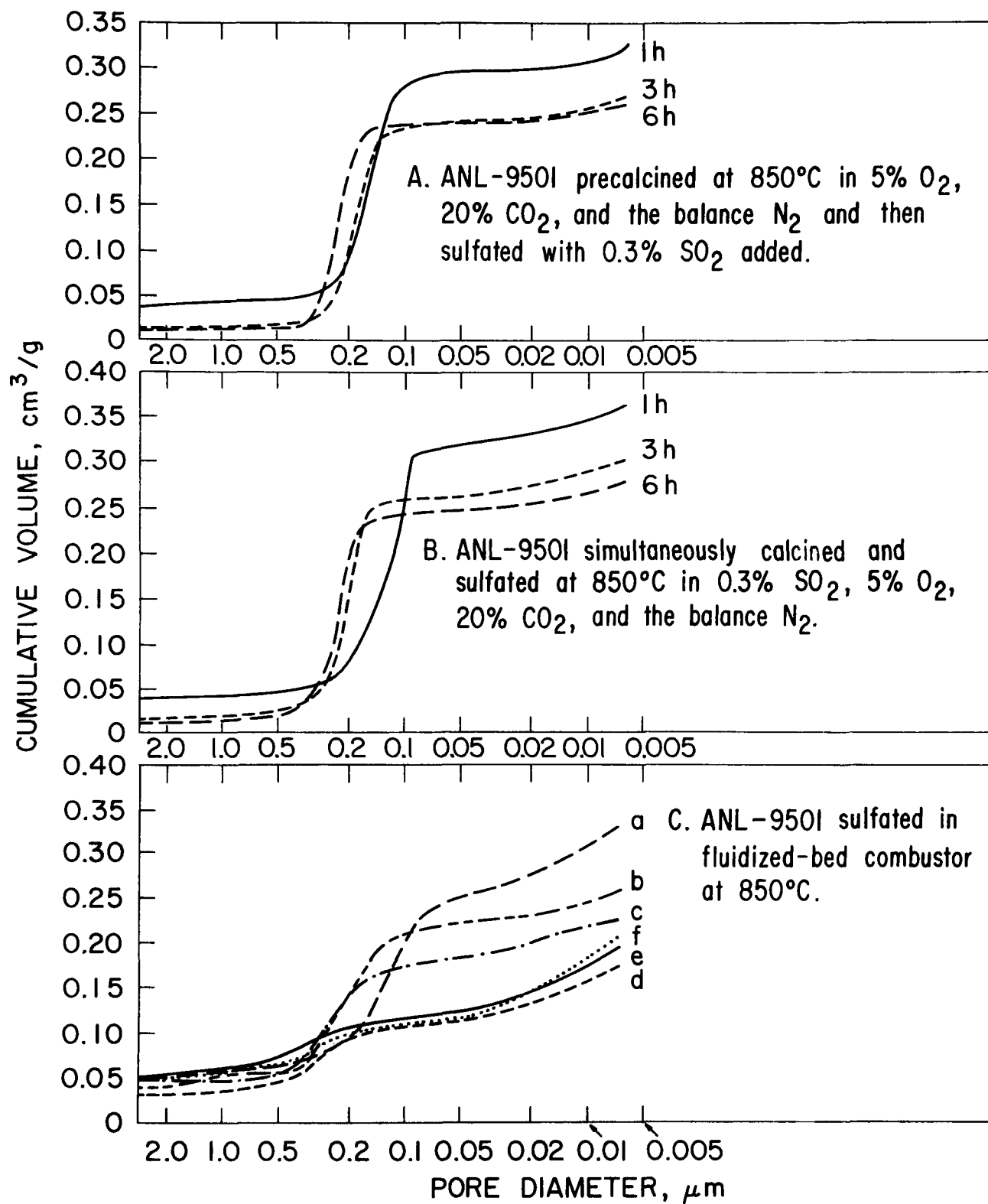


Fig. 8. Porosity Curves of ANL-9501 Comparing Combustor-Sulfated Samples (C) with Samples Sulfated in a Laboratory Tube Furnace (A and B)

Table 6. Percent Conversion to Sulfate and Average Pore Diameters for ANL-9501 Stone Under Various Reaction Conditions

Reaction Conditions at 850°C	Average Pore Diameter, μm	Conversion CaO to CaSO <sub>4</sub> , %
<b>A. Precalcined 1 h without SO<sub>2</sub> and then Sulfated in 0.3% SO<sub>2</sub>, 5% O<sub>2</sub>, 20% CO<sub>2</sub>, and the balance N<sub>2</sub> in a Tube Furnace for:</b>		
1 h	0.155	6.5
3 h	0.177	7.0
6 h	0.222	10.1
<b>B. Simultaneously Calcined and Sulfated in a Tube Furnace in 0.3% SO<sub>2</sub>, 5% O<sub>2</sub>, 20% CO<sub>2</sub>, and the balance N<sub>2</sub> for:</b>		
1 h	0.128	6.3
3 h	0.195	7.5
6 h	0.232	13.0
<b>C. Sulfated Samples from Fluidized-Bed Coal Combustor<sup>a</sup></b>		
a	0.140	17.0
b	0.211	23.5
c	0.232	27.0
d	0.269	38.5
e	0.340	50.0
f	(0.300)	(8.7% as CaSO <sub>4</sub> )
<b>D. Calcined in 5% O<sub>2</sub>, 20% CO<sub>2</sub>, and the balance N<sub>2</sub> for:</b>		
1 h	0.089	--
6 h	0.200	--

<sup>a</sup>Flue gas: ~0.3% SO<sub>2</sub>, 3% O<sub>2</sub>, 16% CO<sub>2</sub>, and the balance N<sub>2</sub>.

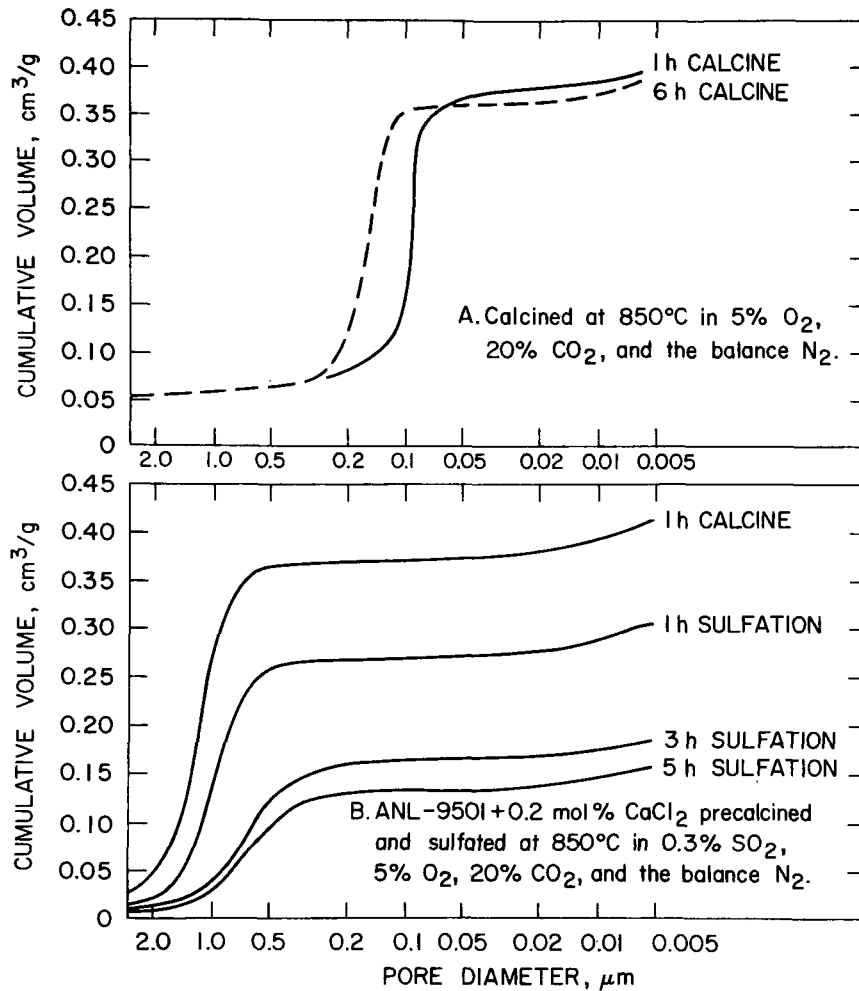


Fig. 9. Porosity Curves for (A) Heat-Treated ANL-9501 and (B) CaCl<sub>2</sub>-Treated ANL-9501 Sulfated in a Laboratory Tube Furnace

In the case of the combustor samples, growth of pores due to long-term heating and possibly other factors is masked by the apparent decrease in pore size due to infilling with CaSO<sub>4</sub>. When the extent of sulfation is low as for the aforementioned ANL-9701, the average pore diameter is not significantly affected and still correlates with the extent of sulfation. When sulfation is rapid and extensive infilling of pore space occurs, the calculated average pore diameter is lower than the extent of sulfation would suggest.

From previous work with NaCl and CaCl<sub>2</sub> on many limestones, maximum sulfation occurs when average pore diameter is in the range 0.3-0.5  $\mu\text{m}$ . At larger pore sizes, reactivity decreases. The combustor data presented here for ANL-9501 suggest that, because the extent of sulfation of some stone in the system is as high as 50%, the average pore diameters of those stones are in the optimum range of 0.3-0.4  $\mu\text{m}$  or larger. The reasons for the greater increase in average pore diameter for the combustor samples than in the tube-furnace samples are not yet fully understood. One reason may be increased reaction time due to longer turnover times in the fluidized-bed for this particular combustor. Also, lower oxygen concentrations in the combustor may increase the likelihood of reducing zones forming, which have been found to enhance sulfation in laboratory studies. Possible causes are being investigated in laboratory-scale furnaces and a small quartz fluidized-bed unit.

### 3. Evaluation of Coal-Pyrolysis Char as a Feedstock for FBC (W. M. Swift)

In many coal-conversion processes, char is produced as a by-product. One such process is Occidental Research Corporation's flash-pyrolysis process for converting coal to liquids and gases. As part of a program to evaluate flash-pyrolysis coal char for power generation via direct combustion, fluid-bed combustion, and magnetohydrodynamics, a series of combustion tests was performed in the ANL 15.2-cm-ID fluidized-bed combustion process development unit (PDU). The objectives of the tests were to measure the effects of bed temperature, combustor pressure, and fluidizing-gas velocity on the combustion efficiency of the char and to determine whether the char would be an acceptable feedstock for FBC units.

#### a. Material

The char was produced at Occidental Research Corporation's flash-pyrolysis process development unit located in LaVerne, CA. The particular char tested in the ANL combustion experiments was produced from Wyoming subbituminous coal (Big Horn) at a pyrolysis temperature of  $\sim 650^\circ\text{C}$ . A size analysis and a chemical analysis (supplied by Occidental Research Corporation) for the char used in the tests are presented in Table 7.

As indicated by the size-analysis data given in Table 7, the char was a very finely divided material. Extrapolation of the size-analysis data on log-probability graph paper indicates a mass mean particle diameter of only 30  $\mu\text{m}$  for the char. According to Occidental Research Corporation, the material tested was somewhat finer than that usually produced by the flash-pyrolysis process; typically, the char is only 70% through 200 mesh. The finely divided char had poor flow characteristics, and there were severe feeding problems in the combustion experiments.

#### b. PDU Combustion System

The experimental equipment and instrumentation of the PDU at Argonne consist of a 15.2-cm-ID fluidized-bed combustor that can be operated at pressures up to 1014 kPa; a compressor to provide fluidizing-combustion air;



Table 7. Average Particle Size and Chemical Properties of Occidental Research Corporation's Flash-Pyrolysis Coal Char<sup>a</sup>

<u>Size Analysis</u>			
Screen Mesh	Particle Size, $\mu\text{m}$	Cummulative wt % through Screen	
400	38	63.0	
270	53	80.5	
200	75	89.7	
150	106	96.3	
100	147	98.8	
60	246	99.8	

<u>Chemical Analysis</u>			
<u>Proximate Analysis</u>		<u>Ultimate Analysis</u>	
Component	wt %	Component	wt %
Moisture	Negligible	Carbon	79.6
Ash	14.7	Hydrogen	1.8
Volatile Matter	6.9	Oxygen	2.1
Fixed Carbon	78.4	Nitrogen	1.1
		Sulfur	0.7
		Ash	14.7

<sup>a</sup>Data provided by Occidental Research Corporation.

a preheater for the fluidizing-combustion air; peripherally sealed rotary feeders for metering solids into an air stream fed into the combustor; two cyclone separators and a filter in series for solids removal from the flue gas; associated heating and cooling arrangements and controls; and devices for sensing and displaying temperature and pressure. A simplified schematic flowsheet of the combustion equipment is presented in Fig. 10.

The flue gas (off-gas) is sampled continuously and is analyzed for the constituents of primary importance. Nitrogen oxide and total  $\text{NO}_x$  are analyzed using a chemiluminescent analyzer; sulfur dioxide, methane, carbon monoxide, and carbon dioxide determinations are made using infrared analyzers; oxygen is monitored using a paramagnetic analyzer; and total hydrocarbons are analyzed by flame ionization.

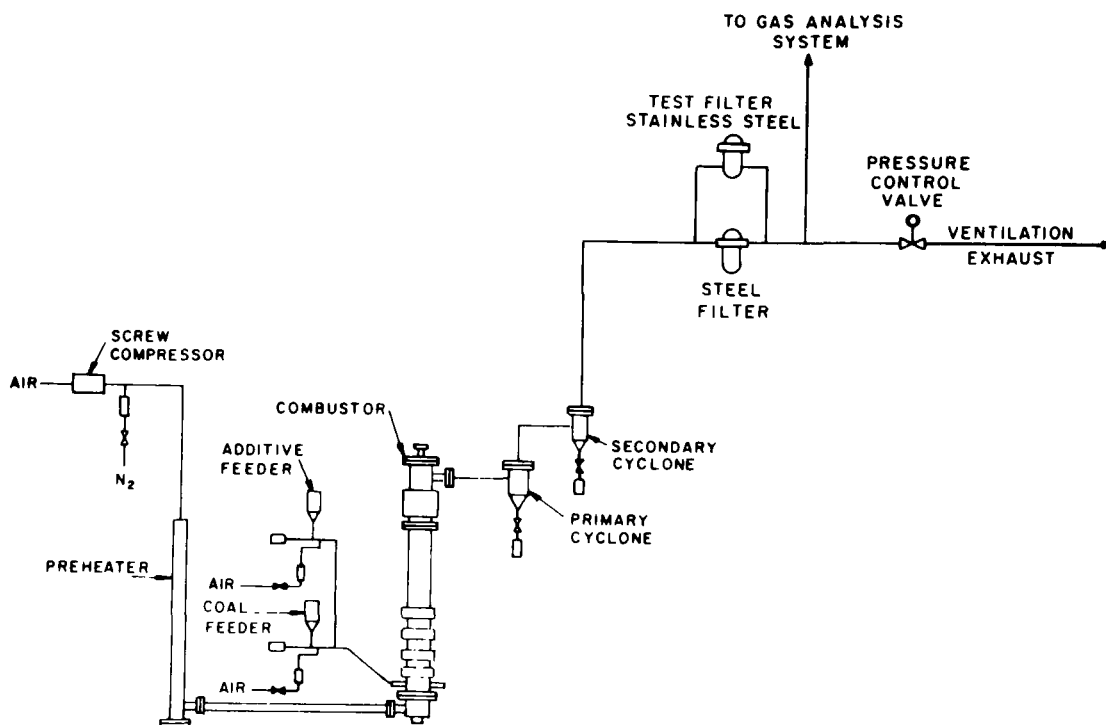


Fig. 10. Simplified Equipment Flowsheet of PDU Fluidized-Bed Combustor and Associated Equipment. The "additive feeder" is actually a "sorbent feeder."

### c. Test Plan and Experimental Procedure

To measure the effects of bed temperature, combustor pressure, and fluidizing gas velocity on combustion efficiency of the char in the ANL PDU, a complete factorial series of experiments was planned at the following nominal conditions: bed temperatures of 800 and 900°C; combustor pressures of 405 and 810 kPa; and gas velocities of 0.76 and 1.1 m/s. In all experiments, combustion was performed at the condition of 3% oxygen in the dry flue gas. When there is complete combustion, 3% oxygen in the dry flue gas corresponds to 16.5% excess air.

In an experiment, partially sulfated limestone from a previous experiment was charged to the reactor to provide an initial bed of material for start-up. The limestone used in most of the char experiments was Greer limestone (44.8 wt % CaO, 1.9 wt % MgO). In a few of the experiments, Grove limestone (53.4 wt % CaO, 0.6 wt % MgO) was used.

The starting bed temperature was raised to about 430°C by passing preheated fluidizing air through the combustor and simultaneously employing resistance heaters on the combustor wall. At this point, the system was raised to the operating pressure, and coal was pneumatically injected into the bed. Coal, rather than char, was used during start-up for safety since the combustion characteristics of the char at low temperatures were unknown.

To prevent carbon accumulation in the fluidized bed at the initially low bed temperatures, the coal was first injected intermittently until a rapidly increasing bed temperature and a changing flue-gas composition confirmed sustained combustion. Coal was then injected continuously, and the bed temperature was raised to the combustion temperature selected for the experiment.

The switchover in fuel from coal to char was accomplished by initially charging the coal feed hopper (Fig. 10) with just enough coal for startup. Sufficient char was added to the hopper on top of the coal to provide adequate operating time to acquire the necessary data for determining combustion efficiency. Once the combustor was operating on char and conditions were established, the primary and secondary cyclone hoppers in the flue-gas system were emptied, and steady-state samples of solids carried over in the flue gas were collected.

During the combustion experiments, limestone was also fed to the combustor. Sulfated sorbent was removed from the combustor by overflow into a standpipe to maintain a constant fluidized-bed level of 0.9 m.

#### d. Results and Conclusions

Char Feed Problems. The only real problem encountered in performing the char combustion experiments was in maintaining a steady feed rate of char to the combustor. As indicated above, the char was extremely fine (estimated mass mean particle diameter of  $\sim 30 \mu\text{m}$ ). The flow of char from the feed hopper via a rotary valve into the pneumatic-transport feed line was very poor. As a result, maintaining the combustion conditions at exactly the design nominal operating conditions was virtually impossible. The duration of many experiments was considerably shorter than planned due to complete stoppage of char feed.

In several experiments, the char and sorbent were premixed and fed from a single hopper in an attempt to improve the flow characteristics of the char. This operation gave only a slight improvement; there was the added complication that the two materials segregated during feeding, which made accurate determination of the char feed rate considerably more difficult.

In spite of the feeding difficulties, however, the data obtained are considered to be sufficiently accurate to assess the combustibility of the char in the PDU and to observe the effects of the gross changes in the operating conditions on combustion. Since the carbon holdup in the FBC is very low, the system can, for practical purposes, be assumed to be at steady state relative to combustion efficiency at all times. Thus, even relatively short combustion experiments of  $\sim 1$  h were sufficient for this particular assessment.

In those cases where it was necessary to make assumptions regarding char feed rate, the assumptions were based on results of experiments in which char was metered separately from the sorbent. It is also noteworthy that combustion efficiency is not particularly sensitive to the char feed rate. Errors of a factor of two in the char feed rate would alter the calculated combustion efficiencies by only about 5% of the calculated value.

Combustion Efficiency. Combustion efficiency for each experiment was calculated according to Eq. 1:

$$\text{Combustion Efficiency} = 100\% - \frac{(\text{Rate of Unburned-Carbon Carryover})}{(\text{Rate of Carbon Feed})} \quad (1)$$

Unburned carbon carryover included carbon in the limestone overflow, as well as carbon recovered in the primary and secondary cyclones. Concentrations of carbon monoxide, methane, and other gases representing incomplete combustion were sufficiently low that they did not enter into the combustion efficiency calculations.

The calculated results of the experiments are presented in Table 8. The combustion efficiencies are also plotted in Fig. 11 as a function of the three independent variables: bed temperature, combustor pressure, and gas velocity.

Table 8. Combustion Efficiency of Flash-Pyrolysis Coal Char in Fluidized-Bed Combustion Process Development Unit (Combustion experiments were performed with 3% oxygen in the dry flue gas.)

Bed Temperature, °C	Combustor Pressure, kPa	Fluidizing-Gas Velocity m/s	Combustion Efficiency, <sup>a</sup> %
800	405	0.76	95, 94 <sup>b</sup>
800	405	1.10	96
800	810	0.76	94, <sup>b</sup> 95 <sup>b</sup>
800	810	1.10	no data
900	405	0.76	97
900	405	1.10	97
900	810	0.76	99, 98 <sup>b</sup>
900	810	1.10	98 <sup>b</sup>

<sup>a</sup>More than one value indicates replicate experiments.

<sup>b</sup>Based on estimate of char feed rate when feeding char/sorbent mixture.

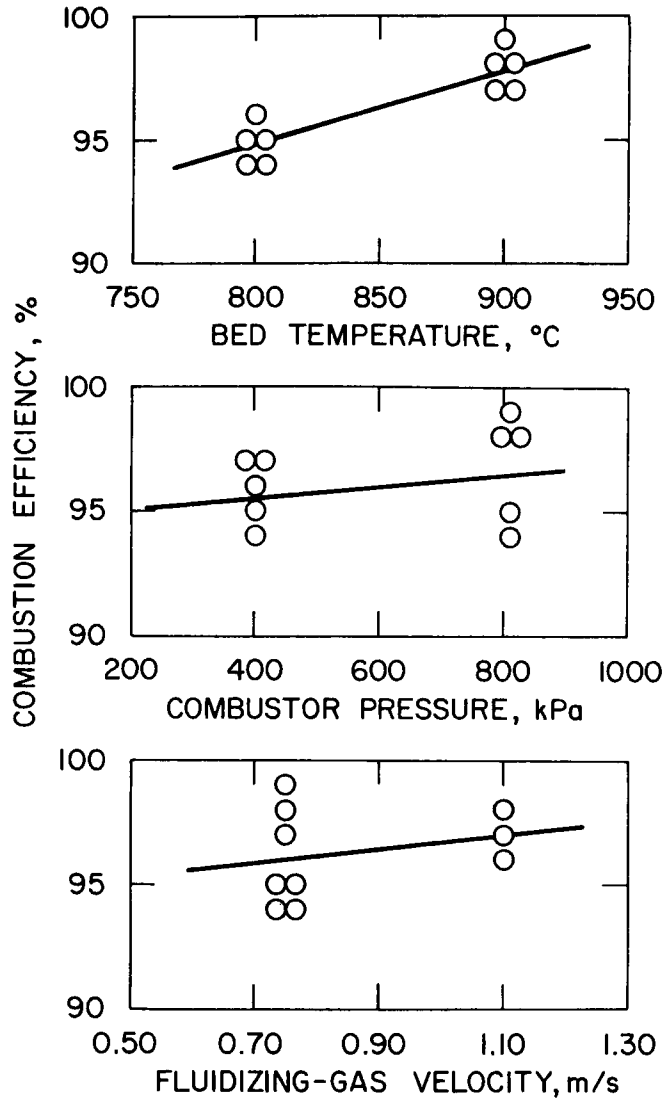


Fig. 11. Combustion Efficiency of Coal Char as a Function of Bed Temperature, Combustor Pressure, and Fluidizing-Gas Velocity

As mentioned above and as indicated in Table 8, it was necessary to estimate the char feed rate in experiments where the char and sorbent were premixed and fed to the combustor from a common feed hopper. The estimate was required because the char and sorbent tended to segregate during feeding, (evidenced by the feed rate needed to maintain 3% oxygen in the dry flue gas constantly decreasing with experiment time). For replicate experiments in which an estimate of the char feed rate was required for one of the replicates (lines 1 and 7, Table 8) there was excellent agreement of combustion efficiencies. The fact that in each case, the combustion efficiency based on the estimated char feed rate was 1% lower than the other is a reflection of an intentional bias used in estimating the char feed rate. For the five experiments in which the char feed rate was directly measured, the char/air feed ratios were determined. The highest ratio (rather than the average) was then used--the

char feed rate in those experiments using char/sorbent feed mixtures was estimated from the air feed rate. Thus, the combustion efficiencies calculated from the estimated feed rates are considered conservative, with the reported values equal to or less than the actual combustion efficiencies.

Calculated combustion efficiencies for the char varied from a low of ~94% to a high of ~99% in these experiments. These are considerably higher than the combustion efficiencies obtained from burning coal in the same PDU and under similar combustion conditions. Previous studies<sup>4</sup> have indicated combustion efficiencies of 90% or less for coal at 900°C and ~17% excess combustion air; combustion efficiencies of ~98% were obtained with coal at 900°C, but ~75% excess air was required.

The plots of the data in Fig. 11 show that temperature is the only variable which appears to have a significant effect on the combustion efficiency; combustion efficiency increasing from an average of ~95% at 800°C to ~98% at 900°C. A thorough statistical analysis of the results could not be performed due to missing data at one set of operating conditions (Table 8). Efforts to perform this experiment were repeatedly unsuccessful due to char feeding difficulties.

Conclusions. The potential of this char as fuel for FBC has been demonstrated. The two factors most likely to be responsible for the high combustion efficiency of the char are (1) its extremely fine particle size and (2) the fact that the char originated from a subbituminous coal. It cannot be concluded from these results that all coal chars would be equally suitable for FBC applications.

#### 4. The Use of Oil Shale for SO<sub>2</sub>-Emission Control in Atmospheric Pressure Fluidized-Bed Coal Combustors (AFBC) (W. I. Wilson and R. B. Snyder)

The feasibility of using oil shale, rather than limestone or dolomite, for SO<sub>2</sub> emission control in atmospheric fluidized-bed combustors (AFBCs) has been investigated. The oil shale used in this study was from the Green River formation in northwest Colorado. The Green River deposits are reported to contain total reserves equivalent to  $644 \times 10^9 \text{ m}^3$  (4050 billion barrels) of oil; of this total, the equivalent of  $99 \times 10^9 \text{ m}^3$  (620 billion barrels) of oil shale at concentrations ranging from 0.1 to 0.27 m<sup>3</sup>/Mg (25 to 65 gal/ton) is considered to be economically recoverable.<sup>5</sup> The processing of this vast energy resource by retorting will yield a substantial quantity of spent oil shale.

In our experiments, the SO<sub>2</sub> reactivity of both virgin shale and spent shale (kerogen removed) was determined by thermogravimetric analysis, and the results were used to estimate the quantities of shale required to reduce the SO<sub>2</sub> concentration in the effluent gas sufficiently for compliance with federal standards. These quantities were then compared with the required quantities of Germany Valley limestone, Greer limestone, and Tymochtee dolomite. The attrition rate of the virgin shale was also compared with those of the limestones and dolomite.

### a. Materials

The compositions of the virgin and spent oil shales studied are given in Table 9. Spent oil shale was prepared by heating virgin oil shale at 400°C in air for 3 h to remove the organic material (kerogen). The chemical compositions of Germany Valley limestone, Greer limestone, and Tymochtee dolomite are also given in Table 9.

Table 9. Concentrations (in wt %) of Major Constituents of Calcareous Materials

	CaCO <sub>3</sub>	MgCO <sub>3</sub>	Fe <sub>2</sub> O <sub>3</sub>	Al <sub>2</sub> O <sub>3</sub>	SiO <sub>2</sub>	Na <sub>2</sub> O	K <sub>2</sub> O	S
Virgin Oil Shale	27.7	13.8	2.60	4.14	30.1	2.19	1.21	0.89
Spent Oil Shale	33.5	16.7	3.14	5.0	36.4	2.64	1.46	0.66
Tymochtee (ANL-5101)	51.8	43.3	0.41	1.46	3.61	0.07	--	--
Greer (ANL-8001)	80.4	3.50	1.24	3.18	10.34	2.23	--	--
Germany Valley (ANL-9701)	97.75	0.6	0.1	1.8	0.2	0.25	--	--

### b. Experimental

A thermogravimetric analyzer (TGA) was used for the kinetic studies. The TGA apparatus has been discussed in detail in a previous paper.<sup>6</sup> The oil shale reactions with SO<sub>2</sub> were performed at temperatures of 700 to 1050°C.

The attrition tests were performed for 2 h at 870°C, using a fluidizing gas composed of 0.3% SO<sub>2</sub>-5% CO<sub>2</sub> and the balance N<sub>2</sub> at a superficial gas velocity of 1.45 m/s. The apparatus (described in detail in ANL/CEN/FE-78-4) was a 5-cm-ID externally heated fluidized-bed reactor.

### c. Sulfation Results

Spent oil shale was precalcined at 900°C in 20% CO<sub>2</sub>-N<sub>2</sub>; sulfation was for 3 h with the same gas except that 0.3% SO<sub>2</sub> and 5% O<sub>2</sub> were added. In Fig. 12, the conversion of CaO to CaSO<sub>4</sub> in spent, calcined oil shale at various temperatures

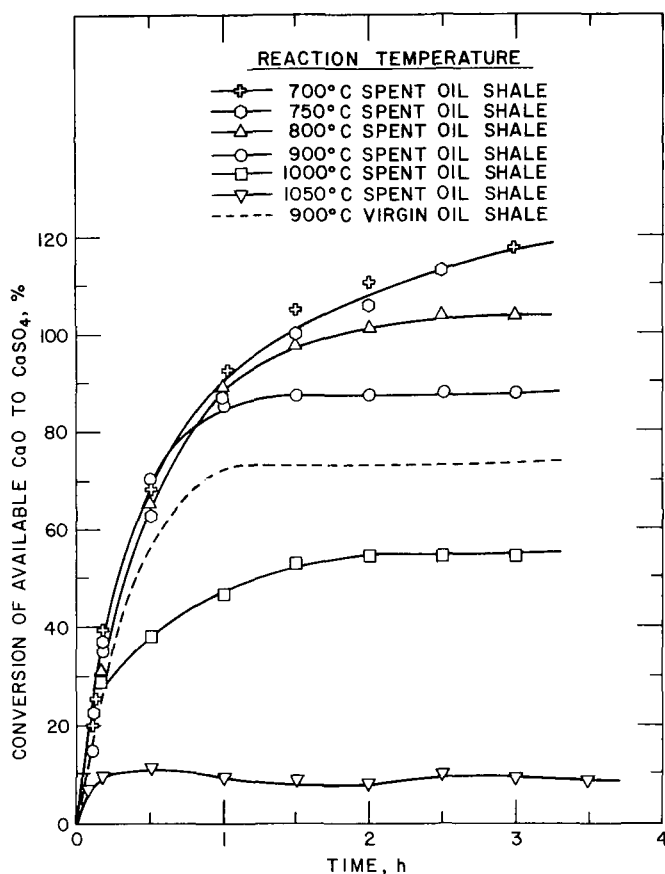


Fig. 12. Conversion (Measured with a TGA) of CaO to  $\text{CaSO}_4$  in Precalcined Spent Green River Oil Shale at 700 to 1050°C. Reaction conditions: -50 +70 mesh material precalcined in 20%  $\text{CO}_2$ -balance  $\text{N}_2$ ; sulfation gas, 0.3%  $\text{SO}_2$ -5%  $\text{O}_2$ -20%  $\text{CO}_2$  in  $\text{N}_2$ .

(700–1050°C) is given as a function of time. During the first hour of experiments performed at 700–900°C, the reaction rates were the same; however, during the remaining two hours, the reaction rates for all experiments except those at 700 and 750°C varied significantly with temperature. The reaction rates at 1000 and 1050°C were much lower than those at the lower temperatures. This inverse variation of reaction rate with temperature is believed to be due to the competing reaction of  $\text{CaSO}_4$  with  $\text{SiO}_2$  and other impurities at the higher temperatures. The latter reactions release  $\text{SO}_2$  and form the products,  $(\text{Ca}, \text{Fe}, \text{Mg})\text{SiO}_3$  and  $\text{Ca}(\text{Fe}, \text{Mg})\text{SiO}_2$ . However, the shale sulfated between 700 and 800°C contained  $\text{CaSO}_4$ , the double salt  $3\text{MgSO}_4 \cdot \text{CaSO}_4$ , silica, and silicates.



At the lower temperatures, 700 to 800°C, the weight gain determined with the TGA was larger than would be obtained if the sole reaction was 100% of the CaO being converted to  $\text{CaSO}_4$  (Fig. 12). Results from X-ray diffraction and wet chemical analyses confirmed that at these temperatures,  $3\text{MgSO}_4 \cdot \text{CaSO}_4$  forms, as mentioned above. The formation of this compound would account for the excessive weight gain.

Also, virgin oil shale was sulfated under these conditions. Conversion of calcium to  $\text{CaSO}_4$  for the virgin oil shale was slightly lower (73%) than for the spent oil shale, (86%). Both reactions were essentially complete in 1 h (Fig. 12). Spent oil shale was simultaneously calcined and sulfated at 900°C, using a synthetic combustion gas of 0.3%  $\text{SO}_2$ -5%  $\text{O}_2$ -20%  $\text{CO}_2$ -balance  $\text{N}_2$ . The reaction rate was the same as for the precalcined material.

Fig. 13 compares the reaction rate of spent oil shale with  $\text{SO}_2$  with those of Tymochtee dolomite, Greer limestone, and Germany Valley limestone.<sup>7</sup> During the first hour, the percentage of calcium converted to  $\text{CaSO}_4$  for the oil shale is higher than that for Tymochtee Dolomite (which is a highly reactive dolomite). Nevertheless, by the end of the 3-h run, 98% of the CaO in the Tymochtee dolomite was utilized to capture  $\text{SO}_2$ , compared with 83.5% for the spent oil shale. The reaction rates of Greer limestone and Germany Valley limestone are much lower than those of spent shale and Tymochtee dolomite.

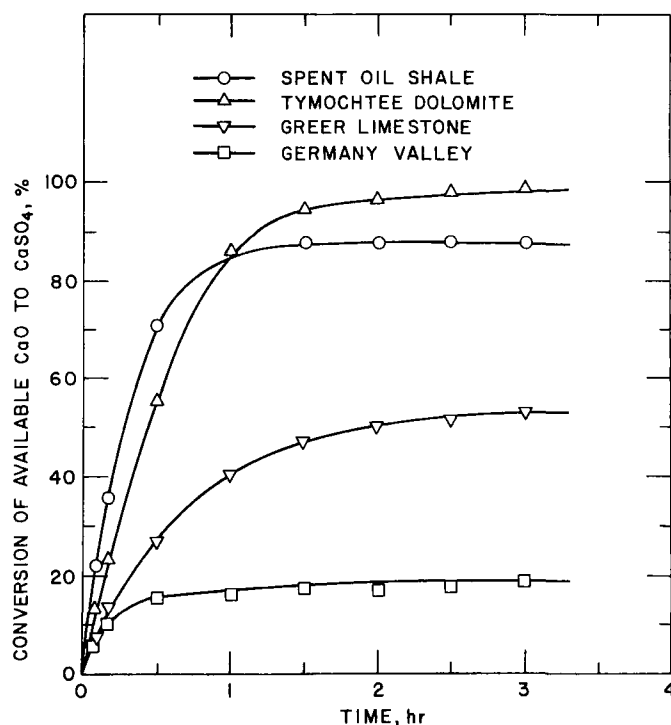


Fig. 13. Conversion (Measured with a TGA) of CaO to  $\text{CaSO}_4$  in Spent Oil Shale, Tymochtee Dolomite, Greer Limestone, and Germany Valley Limestone, Using 0.3%  $\text{SO}_2$ -5%  $\text{O}_2$  in  $\text{N}_2$  at 900 °C

d. Prediction of SO<sub>2</sub> Retention for Oil Shales

The reactivities of oil shale with SO<sub>2</sub> as determined with the TGA were used to predict calcium utilization by this sorbent and its SO<sub>2</sub> retention in an FBC pilot plant. The experimental kinetic data at 900°C were used to estimate the quantity of oil shale necessary to meet the SO<sub>2</sub>-emission standard of 0.5 g SO<sub>2</sub>/MJ (1.2 lb SO<sub>2</sub> emission/10<sup>6</sup> Btu) released in a combustor.

The SO<sub>2</sub> reactivity curves (Fig. 13) must be converted to curves for SO<sub>2</sub> retention vs. Ca/S ratio before the quantity of calcareous material necessary per unit of coal to meet the SO<sub>2</sub>-emission standard can be predicted. The predicted SO<sub>2</sub> retention for spent and virgin oil shale for a fluidized bed operated at 3.9 m/s with a bed height of 1.1 m is described in ANL/CEN/FE-78-3. Because the virgin oil shale has a lower SO<sub>2</sub> reactivity than spent shale at 900°C (Fig. 12) the virgin material requires a higher Ca/S ratio.

e. Evaluation of Oil Shale Sorbent for AFBC Sulfur-Removal System

The results, presented in ANL/CEN/FE-78-3 described above, were used to estimate the number of kilograms of oil shale necessary per kilogram of coal to meet the SO<sub>2</sub>-emission standard and were compared with previous results for limestone. The analysis was performed for 3% and 4.3% sulfur coals, both of which had a heating value of 28,319 kJ/kg (12,183 Btu/lb). The spent oil shale contained 33.5 wt % CaCO<sub>3</sub> and 0.66 wt % sulfur. The SO<sub>2</sub>-emission standard allows only 0.73 kg of sulfur to be emitted per 100 kg of such a coal.

The estimates of oil shale requirements were made for 3% and 4.3% sulfur coals combusted in a fluidized bed operated at 3.8 m/s with a bed height of 0.83 m; these estimates were then compared with similar requirements for Tymochtee dolomite, Greer limestone, and Germany Valley limestone.<sup>7</sup> The results are presented in Table 10. The Ca/S ratio of the virgin oil shale is similar to that of Greer limestone, a reactive stone used by Pope, Evans, and Robbins at their Rivesville FBC pilot plant. However, since the oil shale has a low CaCO<sub>3</sub> content in comparison with the limestones and dolomites (~30% vs. 50-98%) for both 3% and 4% sulfur coals, the requirements for shale are projected to be considerably larger than for the other stones.

It should be noted that these estimates are only for atmospheric FBCs operated at a high superficial gas velocity, not for pressurized FBCs. Decreasing the gas velocity and/or increasing the boiler pressure should decrease shale requirements substantially. Also, if Western low-sulfur coal (1-2% sulfur) is used in an FBC, the shale requirement will be reduced by a factor of approximately four.

f.. Evaluation of Oil Shale Use in a Fluidized-Bed Combustion Plant Employing a Carbon Burnup Cell

For an FBC system that employs a carbon burnup cell (CBC), CaSO<sub>4</sub> in the partially sulfated oil shale would decompose at the high operating temperature of the CBC (1000-1100°C) due to the reaction of CaSO<sub>4</sub> with SiO<sub>2</sub> to release SO<sub>2</sub> (as previously discussed). Thus, if oil shale is used in an FBC-CBC

Table 10. Requirements for Green River Oil Shale, Germany Valley Limestone, Greer Limestone, and Tymochtee Dolomite to Meet SO<sub>2</sub>-Emission Standard<sup>a</sup>

Calcium-Based Stone	Ca/S Ratio		kg of Stone/kg of Coal	
	3% S Coal	4.3% S Coal	3% S Coal	4.3% S Coal
Spent Oil Shale <sup>b</sup>	1.9	not possible	0.58	not possible
Virgin Oil Shale <sup>c</sup>	3.1	4.3	1.4	3.3
Germany Valley Limestone (ANL-9701)	3.8	7.5	0.36	1.0
Greer Limestone (ANL-8001)	3.1	3.8	0.36	0.6
Tymochtee Dolomite (ANL-5101)	1.0	1.5	0.18	0.4

<sup>a</sup>Basis: 28,319 kJ/kg coal; FBC operated at 3.8 m/s gas velocity and 0.83-m bed depth.

<sup>b</sup>Spent shale contains 0.66% S.

<sup>c</sup>Virgin shale has a heating value of 7020 kJ/kg and contains 0.9% sulfur.

system, the SO<sub>2</sub> in elutriated, partially sulfated oil shale might be released in the CBC, and, to meet the SO<sub>2</sub> emission standard, more SO<sub>2</sub> would have to be retained in the combustor. Assuming that only 5% of the bed material elutriates from the bed, it is estimated that SO<sub>2</sub> retention in the FBC would have to be increased to 95% to meet the SO<sub>2</sub>-emission standard for 4.3% sulfur coal. The results of this evaluation indicate that oil shales similar to Green River shale should not be used in a FBC-CBC system.

#### g. Attrition Results

The attrition tendencies of virgin Green River oil shale, Tymochtee dolomite, Greer limestone, and Germany Valley limestone as bed materials were determined. In the limestone and dolomite tests, simultaneous calcination and sulfation was conducted. From weight changes and chemical analyses of the original material, the final overhead, and final bed material, the percentage of the original material that remained in the bed was determined. The amount of attrition in the 2-h tests was taken to be the percentage of original material collected overhead.

In the tests of virgin oil shale, simultaneous kerogen combustion, calcination, and sulfation occurred. Again, chemical analyses and weight-change information were used to determine the percentage of original material collected overhead.

The extent of attrition of virgin oil shale was 22 wt %, whereas those for Tymochtee dolomite, Greer limestone, and Germany Valley limestone were 3%, 11%, and 38% respectively. These results suggest that the attrition rate of virgin oil shale is not unlike that of limestones and dolomites.

#### h. Conclusions

Laboratory analyses suggest that the calcium in oil shales has a high reactivity with  $\text{SO}_2$  and can be used in fluidized-bed coal combustors to reduce  $\text{SO}_2$  emissions. It is predicted that to meet the EPA  $\text{SO}_2$ -emission standard, more oil shale than limestone or dolomite would be required since the calcium content of shales is relatively low. Also, the Green River shale used in the tests contains approximately 1% sulfur, which may be released as  $\text{SO}_2$  in an FBC. The use of shales may be desirable if the FBC is operated at low superficial gas velocities (less than 3.2 m/s) or with low-sulfur coals (containing less than 3% sulfur). The oil shales should not be used in an FBC-CBC unless the shale elutriation rate is minimal, since at the temperature at which a CBC operates (1000-1100°C), the  $\text{CaSO}_4$  and the silicates in the elutriated shale would react to release  $\text{SO}_2$ .

The attrition rate of Green River oil shale was similar to that of limestones and a dolomite.

Only one oil shale, Green River oil shale, was used in this evaluation. Since the  $\text{SO}_2$  reactivity and attrition rates of limestones vary widely, a large variation is also expected for oil shales. Thus, these results are not necessarily applicable to all oil shales. The Green River oil shale was not tested in an experimental FBC, and its performance in such a unit might differ from the results reported. However, since all oil shales contain much less calcium than limestones contain, further investigation was not considered.

#### 5. Comparison of Limestone Calcium Utilization in an AFBC with TGA Projections (R. B. Snyder and W. I. Wilson)

Various investigators<sup>2,8-13</sup> have studied the reactivity of limestones with  $\text{SO}_2$ ; however, none has reported a method of accurately predicting the limestone reactivity with  $\text{SO}_2$  at specified fluidized-bed coal combustion conditions. When a high-sulfur (4% S) coal is used, approximately 85% of the  $\text{SO}_2$  generated must be retained in the bed material in order to meet EPA  $\text{SO}_2$ -emission standards. However, the percentage of sulfur that must be removed varies, depending on the sulfur content and heat content of a coal. Therefore, process R&D engineers, in reporting results of experimental combustion tests, usually give  $\text{SO}_2$  retention as a function of the molar ratio of calcium (in the limestone)/sulfur (in the coal) fed. The calcium utilization of the limestone can then be expressed as follows:

$$U = \frac{R}{\text{Ca/S}} \quad (2)$$

where

U = the fraction of the calcium converted to calcium sulfate  
 R = fraction of the sulfur dioxide retained in the combustor bed material  
 Ca/S = molar Ca/S feed ratio

The designer of a plant knows what value of R is required to meet the EPA SO<sub>2</sub>-emission standard for a designated coal but needs to know the Ca/S ratio required for the designated limestone(s) to meet this EPA standard. If the calcium utilization, U, for a given limestone can be predicted, the Ca/S ratio required to meet the EPA SO<sub>2</sub>-emission standard (R) can be determined from Eq. 2. However, the limestone calcium utilization, U, is also a function of the Ca/S ratio--for example, when a Ca/S ratio of 4 is used, the maximum calcium utilization is 0.25. Therefore, for a highly reactive limestone, the calcium utilization will be limited by the availability of SO<sub>2</sub> or the Ca/S ratio, whereas for a limestone having a low reactivity with SO<sub>2</sub>, the calcium utilization will be limited by the reactivity of the limestone. The value of R that is just large enough to meet the EPA SO<sub>2</sub> standard gives the minimum required Ca/S ratio.

This report presents an expression for U in terms of Ca/S which includes kinetic data obtainable from thermogravimetric analysis of the limestone in question, as well as values of specific fluidized-bed combustion operating parameters. A comparison is made between U calculated using this function and actual pilot-plant calcium utilization. The predictions presented below are for atmospheric fluidized-bed combustion (AFBC) only and cannot be directly used to predict pressurized fluidized-bed operating conditions.

Seven limestones which had been previously tested in pilot-scale FBCs\* were tested for reactivity with SO<sub>2</sub> and O<sub>2</sub> in the thermogravimetric analyzer (TGA). However, in these TGA studies, the particle size was -18 +30 mesh, and the results did not correlate well with actual pilot-plant calcium utilizations. In the results reported below, however, the particle size was smaller, -50 +70 mesh, and the correlation of TGA results and pilot-scale TGA results was good. All limestones, sized to -50 +70 mesh (250  $\mu$ m, median diameter), were precalcined in 20% CO<sub>2</sub> prior to reaction with the synthetic combustion gas. All sulfation reactions were performed at 900°C with a 0.3% SO<sub>2</sub>-5% O<sub>2</sub>-balance N<sub>2</sub> synthetic combustion gas.

The percent conversion of the calcium in the limestone to calcium sulfate was determined on the TGA and is given in Fig. 14 for the seven limestones. Reaction was rapid in the first hour, then became limited either by the gas-CaSO<sub>4</sub> solid diffusion process or by the decrease in the pore diffusion process or by the decrease in the pore diffusion coefficient of SO<sub>2</sub> due to pores becoming smaller.<sup>14</sup>

Predictions of calcium utilization in an AFBC were made, using the kinetic information obtained from the ANL TGA experiments (Fig. 14) and were

---

\*Pilot-scale FBCs are referred to in the report literature as process development units, test units, and fluidized-bed boilers.

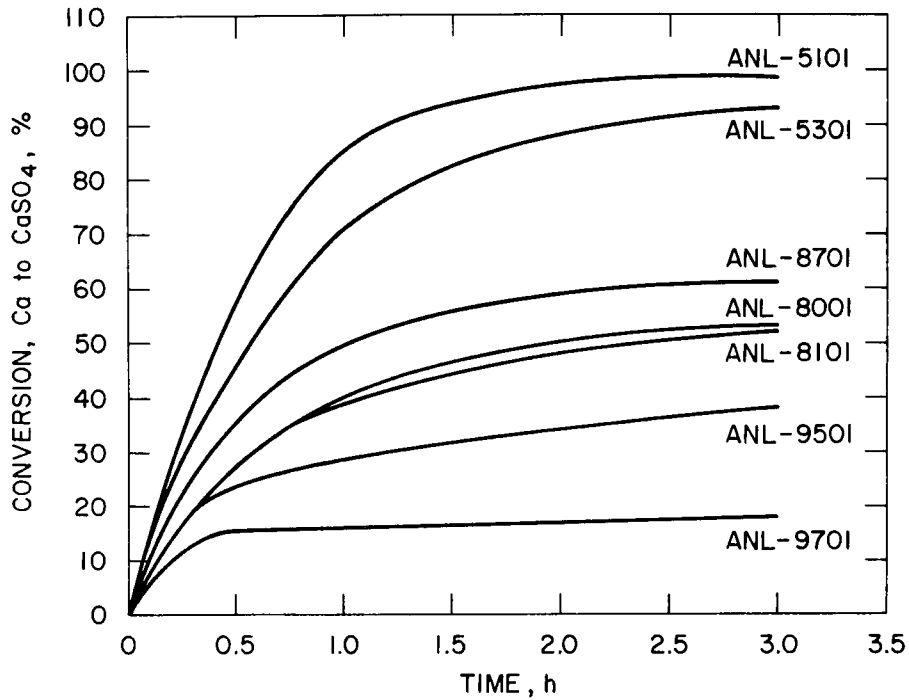


Fig. 14. Calcium Utilization in Seven Precalcined Limestones at 900°C as a Function of Time. Calcined at 900°C, 20% CO<sub>2</sub> (-50 +70 mesh)

compared with various pilot-plant experimental values of calcium utilization (Table 11). The pilot-plant data were from the following sources: Pope, Evans, and Robbins (PER)<sup>8</sup> determined the desulfurization behavior of Greer (ANL-8001), Germany Valley, (ANL-9701), and Chaney (ANL-8701), limestones; Argonne National Laboratory (ANL) studied limestones 1359 (ANL-9501), 1360 (ANL-8101), and 1337 (ANL-5301), and Tymochtee dolomite (ANL-5101); Consolidation Coal Co. (CCC) tested Tymochtee dolomite (ANL-5101); and Morgantown Energy Research Center (MERC) tested Greer limestone (ANL-8001).

The predicted  $U$  values shown in Table 11 were found using the TGA kinetic information along with a fluid-bed desulfurization equation (Eq. 3) developed by Keairns et al.<sup>2</sup> for the calculation of calcium utilization.

$$U = \frac{1}{Ca/S} \left[ 1 - \frac{V}{kH\epsilon} \left( 1 - e^{\frac{-kH\epsilon}{V}} \right) \right] \quad (3)$$

where

$U$  = calcium utilization, fraction

$Ca/S$  = calcium to sulfur mole ratio in the feed

Table 11. Comparison of Predicted and Pilot-Plant Calcium Utilization (U)

Organization	Limestone/ Dolomite	Ca/S	Pilot Plant		TGA-Predicted
			Particle Residence Time, h	Calcium Utili- zation, <sup>a</sup> %	Calcium Utili- zation, <sup>a</sup> %
PER	Germany Valley	4.9	2.6	16.0	13.3
PER	Germany Valley	2.8	2.6	25.0	16.0
PER	Chaney	3.7	2.6	21.6	24.3
PER	Greer	3.4	3	26.3	24.2
PER	Greer	3.1	2.6	26.6	26.2
PER	Greer	2.9	2.6	27.9	27.6
PER	Greer	2.4	2.6	28.0	31.7
MERC	Greer	5.76	-	13.6	16.9
MERC	Greer	2.17	-	40.6	40.9
ANL	1359	2.6	15	20	29.0
ANL	1359	2.4	15	22	29.6
ANL	1359	2.6	15	20	29.0
ANL	1359	2.3	15	36	29.7
ANL	1359	2.5	15	32	29.4
ANL	1359	2.5	15	34	29.4
ANL	1360	2.3	15	32	34.7
ANL	1337	2.2	15	37	42.8
ANL	Tymochtee	1.6	15	54	56.0
ANL	Tymochtee	1.5	15	53	59.2
CCC	Tymochtee	0.8	2.5	12.3	12.0
CCC	Tymochtee	0.4	5	23.3	23.7
CCC	Tymochtee	1.9	11	47.4	47.4
CCC	Tymochtee	1.5	13	62	57.0
CCC	Tymochtee	0.96	21	82	71.0

<sup>a</sup>The relative standard deviation between the observed and predicted calcium utilizations is +4.1%.

- $V$  = superficial gas velocity, m/s  
 $H$  = fluidized-bed height, m  
 $\epsilon$  = bed voidage, assumed to be 0.5  
 $k$  = average particle reaction rate constant,  $s^{-1}$

This fluid-bed desulfurization equation gives the calcium utilization as a function of the "average" reaction rate constant  $k$  of the particles in the bed, the Ca/S feed ratio, and the specified AFBC operating parameters.

The slopes of the curves in Fig. 14 give the instantaneous rate constants,  $k'$ , as a function of calcium utilization. The average limestone calcium utilization,  $U$ , is that value at which  $k$  and  $k'$  are equal (see Keairns et al.<sup>2</sup> for calculational details).

It should be noted that the pilot plant results in Table 11 represent a wide range of operating conditions. The PER combustion runs were done at 815 to 832°C. The ANL and MERC pilot plant runs were all performed at 871°C. The Consolidation Coal Co. runs with Tymochtee dolomite were performed at 982°C. In contrast, all TGA runs were performed at 900°C.

The superficial gas velocities ranged from 0.61 m/s in the MERC runs to 0.51 m/s used by PER. Pope, Evans, and Robbins used <0.6-cm (<1.4-in) limestone; 50% by weight of the material was smaller than 30 mesh (600- $\mu$ m dia). It would be expected that very little of the material smaller than 30 mesh remained in the bed for an appreciable time. In the ANL experimental runs, the average particle size was 540-630  $\mu$ m; Consolidation Coal Co. used -16 +28 mesh (1190-1000  $\mu$ m) material. The TGA-determined  $k$ 's and the actual Ca/S ratios and operating parameters of the pilot-plant runs were substituted into Eq. 3 to calculate the predicted  $U$ 's shown in Table 11.

The predicted calcium utilizations are plotted against actual pilot plant experimental values in Fig. 15. Agreement is within the experimental error for the pilot plants and thus is satisfactory. The relative standard deviation is  $\pm 4\%$ .

## 6. Prediction of Limestone Requirements for an FBC-CBC Combustor (R. B. Snyder and W. I. Wilson)

To reduce the size and cost of an AFBC, a high superficial gas velocity (3-4.6 m/s) is required. However, high gas velocities cause high loadings of dust (limestone and unburned coal) in the effluent gas stream. High gas velocities, therefore, result in low combustion efficiencies. Pope, Evans, and Robbins (PER)<sup>15</sup> reported combustion efficiencies of  $\sim 85\%$  at a fluidizing-gas velocity of 3.8 m/s in a process development unit (PDU) combustor. To increase overall combustion efficiency, PER incorporated into their process a carbon-burnup cell (CBC) which operates at a higher temperature than the combustor and at a lower fluidizing-gas velocity ( $\sim 1100^\circ\text{C}$ , 1.8 m/s). Unburned coal dust removed from the combustor effluent gas stream by cyclones was injected into a fluidized bed in a CBC where the unburned fuel was combusted to recover the heat values. Pope, Evans, and Robbins estimates that the overall combustion efficiency can be increased to approximately 99%.<sup>15</sup>



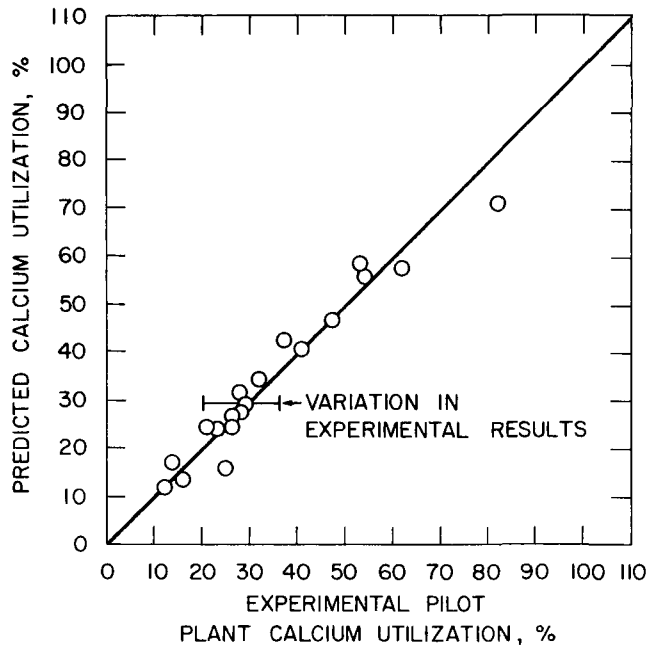


Fig. 15. Experimental and Calculated Calcium Utilizations.  
 -50 +70 mesh stone. 20% CO<sub>2</sub> in N<sub>2</sub> (precalcination)  
 0.3% SO<sub>2</sub>-5% O<sub>2</sub> in N<sub>2</sub> (sulfation) 900°C.

Due to the high operating temperature (1100°C) in the CBC, the SO<sub>2</sub> released in the CBC might not be captured by either partially sulfated limestones or fresh limestones injected into the CBC. As a result, 7% of the sulfur would bypass the sulfur-removal system of the combustor and be released as SO<sub>2</sub> from the CBC. Consequently, a greater percentage of the sulfur (released as SO<sub>2</sub>) would have to be captured in the combustor to meet the EPA SO<sub>2</sub>-emission standard (0.5 g SO<sub>2</sub>/MJ produced by the entire system). Because of this increased requirement for sulfur retention in the combustor, a greater overall Ca/S feed ratio would be required (at a higher sulfur retention, calcium utilization is lower). Thus, if it is assumed that no sulfur is retained in the CBC, much larger amounts of limestone would be required to meet the EPA SO<sub>2</sub>-emission standard.

Babcock and Wilcox<sup>16</sup> estimate that the weight ratio of unburned sulfur to carbon in the coal dust elutriated from the combustor is one-half that in the original coal. Thus, at a combustion efficiency of 85% in the combustor, approximately 93% of the sulfur in the coal is oxidized to SO<sub>2</sub> in the combustor; the other 7% is unburned and is elutriated from the combustor in the coal dust along with the partially sulfated limestone.

Conflicting results<sup>17,18</sup> have been reported by investigators as to the fate of the elutriated sulfur released as SO<sub>2</sub> in a CBC. The National Coal Board<sup>17</sup> and Argonne National Laboratory<sup>18</sup> found that above 870°C, the SO<sub>2</sub> reactivity of several limestones dramatically decreased. In contrast, PER<sup>15</sup> found that the addition of limestone 1359 (ANL-9501) to their CBC caused a two-thirds reduction in SO<sub>2</sub> emissions.

The TGA was utilized to determine the reactivity of three stones at the operating conditions of an FBC and a CBC. The results (reported previously in ANL/CEN/FE-77-11) showed that feeding fresh limestone or limestone that had been partially sulfated in the combustor to the CBC should reduce SO<sub>2</sub> emissions from the CBC by more than 60%. The quantity of limestone necessary to capture 60% of the SO<sub>2</sub> in a CBC depends largely upon the type of limestone tested and the CBC operating temperature. A typical range of limestone requirements for different stones is 0.36-1.2 kg of stone per kg of coal.

## 7. Estimation of Limestone Requirements for AFBC (R. B. Snyder and W. I. Wilson)

Using the TGA, projections of limestone requirements to meet the EPA SO<sub>2</sub>-emission standard for AFBCs were made. Sixty-one limestones\* were tested on the TGA for reactivity with SO<sub>2</sub> at 900°C using 0.3% SO<sub>2</sub>. Some results were previously reported (ANL/CEN/FE-78-4), and additional results are now available. There is a large variation in limestone-SO<sub>2</sub> reactivity and in the extent of conversion of calcium carbonate to calcium sulfate. For the high-calcium (>90% CaCO<sub>3</sub>) limestones tested, the conversion of CaCO<sub>3</sub> to CaSO<sub>4</sub> ranged from 19 to 66%, while for the dolomites (40-60% CaCO<sub>3</sub>) the range was 21 to 100%.

By use of limestone-SO<sub>2</sub> reactivity curves (not shown), estimates were made of the quantity of each limestone per unit weight of coal necessary to meet the Federal SO<sub>2</sub>-emission standards. These estimates were made for a fluidized-bed coal combustor operated with a 0.9-m bed depth and superficial gas velocities of 2.4 m/s (8 ft/s) and 3.6 m/s (12 ft/s) and using a coal containing 4.3% S and having a heating value of 28,300 kJ/kg (12,200 Btu/lb). In Table 12, the limestone/kg coal required for the reactor at the two different velocities are given for 57 of the 61 stones tested.

For a reactor operated at 2.4 m/s (8 ft/s), 54% of the total stones tested required less than 0.5 kg/kg of coal to meet the SO<sub>2</sub>-emission standard. This included 54% of the dolomites (with CaCO<sub>3</sub> concentrations of 48 to 60%) and 55% of the limestones (with CaCO<sub>3</sub> concentrations larger than 90%). All stones can meet the SO<sub>2</sub>-emission standard when the AFBC is operated at a superficial gas velocity of 2.4 m/s. At 3.6 m/s, only one stone is projected not to be able to reduce SO<sub>2</sub> emission sufficiently to meet the EPA standard.

These results indicate that a large percentage of the calcareous stones are highly reactive with SO<sub>2</sub>. Since limestones and dolomites are extremely plentiful throughout the United States, these results suggest that it is likely that there would be a high SO<sub>2</sub>-reactivity stone (which would minimize limestone requirements and limestone disposal cost) near a chosen combustor site. The highly reactive stones (54% of the stones tested) would require between 0.25 and 0.5 kg stone/kg coal to meet the present SO<sub>2</sub>-emission standard (combustor operated at 2.4 m/s).

It can be seen from Table 12 that increasing the superficial gas velocity from 2.4 m/s (8 ft/s) to 3.6 m/s increases the limestone requirements by approximately 90%. From the fluid-bed desulfurization equation developed by

---

\*The compositions and sources of the limestones used in these studies are given in Appendices A and B.

Table 12. Projected Limestone Requirements, kg Stone/kg of Coal,  
to Meet 0.5 g SO<sub>2</sub>/MJ Standard for AFBC

Limestone	Reactor A <sup>a</sup>	Reactor B <sup>b</sup>	Total Ca Utili- zation in TGA, <sup>c</sup> %
ANL-4801	0.30	0.40	100.0
ANL-4901	0.73	1.1	88.3
ANL-4902	0.30	0.43	86.2
ANL-4903	0.46	0.78	94.8
ANL-5001	0.40	0.48	100.0
ANL-5101 (Tymochtee)	0.27	0.37	99.2
ANL-5102	0.60	0.86	91.3
ANL-5201	0.48	0.92	93.7
ANL-5202	0.46	0.82	94.8
ANL-5203	0.45	0.82	93.1
ANL-5204	0.74	1.0	56.8
ANL-5205	0.59	0.9	85.0
ANL-5206	0.39	0.45	100.0
ANL-5207	1.2	2.4	75.8
ANL-5301 (1337)	0.34	0.53	96.8
ANL-5302	0.98	2.0	65.1
ANL-5303	0.83	1.3	68.9
ANL-5304	1.0	1.1	42.4
ANL-5401	0.33	0.36	97.7
ANL-5402	0.32	0.40	92.3
ANL-5403	0.39	0.59	97.2
ANL-5501	2.4	Std. not met	21.3
ANL-5601 (Dolowhite)	-	-	-
ANL-5602	0.89	1.2	44.8
ANL-5603	0.95	1.2	43.6
ANL-6101 (1351)	-	-	-
ANL-6301	0.37	0.49	79.7
ANL-6401	0.46	0.57	62.6
ANL-6501	0.49	0.93	77.0
ANL-6701	0.28	0.37	81.3
ANL-6702	-	-	13.1
ANL-7401	0.62	0.79	65.8
ANL-8001 (Greer)	0.48	0.73	53.2
ANL-8101 (1360)	0.47	0.51	53.6
ANL-8301	0.79	1.0	-
ANL-8701 (Chaney)	0.30	0.34	60.8
ANL-8901 (1343)	-	-	-
ANL-8902	0.52	0.8	44.0
ANL-8903	0.46	0.57	44.6
ANL-9201 (1336)	-	-	-
ANL-9401	0.35	0.44	52.5

(Cont'd.)

Table 12. (Cont'd.)

Limestone	Reactor A <sup>a</sup>	Reactor B <sup>b</sup>	Total Ca Utilization in TGA, <sup>c</sup> %
ANL-9402	1.5	2.0	26.5
ANL-9501 (Grove)	0.56	0.62	37.5
ANL-9502	0.43	0.71	55.6
ANL-9503	0.37	0.56	56.6
ANL-9504	0.44	0.51	43.9
ANL-9505	0.51	0.78	44.4
ANL-9601 (2203)	1.1	1.5	32
ANL-9602	0.45	0.61	51.7
ANL-9603	0.55	0.68	32.1
ANL-9701 (Germany Valley)	0.96	1.3	18.7
ANL-9702	0.52	0.61	31.0
ANL-9703	0.27	0.28	66.2
ANL-9704	0.36	0.42	41.7
ANL-9705	0.41	0.57	46.2
ANL-9706	0.34	0.41	49.2
ANL-9801	0.52	0.67	35.3
ANL-9802	0.32	0.52	61.8
ANL-9803	0.67	0.91	33.3
ANL-9901	0.39	0.43	39.6
ANL-9902	0.31	0.51	56.7
ANL-9903	0.51	0.80	56.7
Range	0.37-2.4	0.28-00	

<sup>a</sup>Reactor A is assumed to operate with a 0.9 m bed depth at 2.4 m/s. Calcium-SO<sub>2</sub> rate constant is 31.5 s<sup>-1</sup>.

<sup>b</sup>Reactor B is assumed to operate with a 0.9 m bed depth at 3.6 m/s. Calcium-SO<sub>2</sub> rate constant is 47 s<sup>-1</sup>.

<sup>c</sup>This column lists the percentages of calcium in the limestones (-50 +70 mesh) converted to CaSO<sub>4</sub> after the stone is first precalcined in 20% CO<sub>2</sub> at 900°C, then reacted at 900°C with a 0.3% SO<sub>2</sub>-5% O<sub>2</sub>-balance N<sub>2</sub> gas mixture for 3 h.

Westinghouse,<sup>12</sup> the rate constant for the calcium-SO<sub>2</sub> reaction can be calculated for the two sets of conditions studied. These reaction rate constant values are 31.5 and 47 s<sup>-1</sup>.

It should be noted that total calcium utilization in the TGA (Table 12) is not necessarily a good indicator of limestone performance in the combustor. Two examples are as follows: (1) In a comparison of Greer (ANL-8001) with ANL-7401, ANL-7401 has a greater calcium utilization on the TGA, but requires a greater amount of stone/kg coal than does Greer. (2) In a comparison of ANL-9902 with ANL-9901, 56.7% of the CaCO<sub>3</sub> in ANL-9902 is converted to CaSO<sub>4</sub>.

compared with 39.6% for ANL-9901. However, ANL-9901 requires less limestone than ANL-9902 at a superficial gas velocity of 3.6 m/s. Figure 16 shows the reactivity curves for the two stones. Sulfation of ANL-9901 is much faster than the sulfation of ANL-9902. Since the maximum  $\text{SO}_2$  residence time in a fluid bed with 0.9 m bed depth and 3.6 m/s gas velocity is approximately 0.25 s, the important factor in obtaining high  $\text{SO}_2$  retention is a high calcium- $\text{SO}_2$  reactivity, not total conversion of calcium to calcium sulfate. Thus, ANL-9901 is superior to ANL-9902.

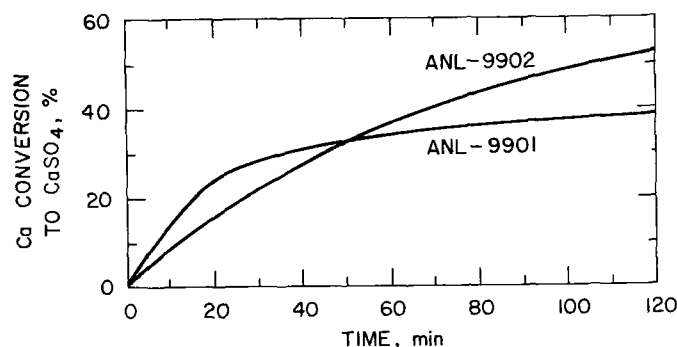


Fig. 16 TGA Reactivity Curves for ANL-9901 and ANL-9902 Limestones

The projections of limestone requirements given in Table 12 are sensitive to the rate of the calcium- $\text{SO}_2$  reaction or, in other words, to the slopes of the TGA curves of calcium conversion. Thus small changes in the rate of calcium conversion to  $\text{CaSO}_4$  can produce large changes in projected limestone requirements. The results given in Table 12 are more useful for comparing limestones than are absolute values. Finally, Table 12 results are given to two significant figures to allow comparison of limestones with each other; it is not suggested that the projected limestone requirements are accurate to two significant figures. Because the accuracy of the absolute numbers is not known, they should be used with caution.

It would be useful to be able to correlate limestone physical properties with limestone- $\text{SO}_2$  reactivity results. Since in general, the total calcium utilization of a limestone does reflect the reactivity of a stone with  $\text{SO}_2$ , investigators have attempted to correlate calcium utilization with limestone properties. From Fig. 17, we see that the chemical composition ( $\text{CaCO}_3$  concentration) of the stone does not correlate well with calcium utilization. It has been shown, however, that the average pore diameter of limestones that have been treated with agents that enhance reactivity with  $\text{SO}_2$  generally does correlate with calcium utilization. Therefore, the pore-size distributions of 23 untreated limestones and 21 untreated dolomites (after calcination at  $900^\circ\text{C}$  using a 20%  $\text{CO}_2$  in  $\text{N}_2$  gas mixture) were measured. The pore-size distributions were thus identical to those of calcined limestones that were reacted with  $\text{SO}_2$ . Figure 18 shows the calcium utilization as a function of average pore diameter. Although the correlation is poor, there is a general trend

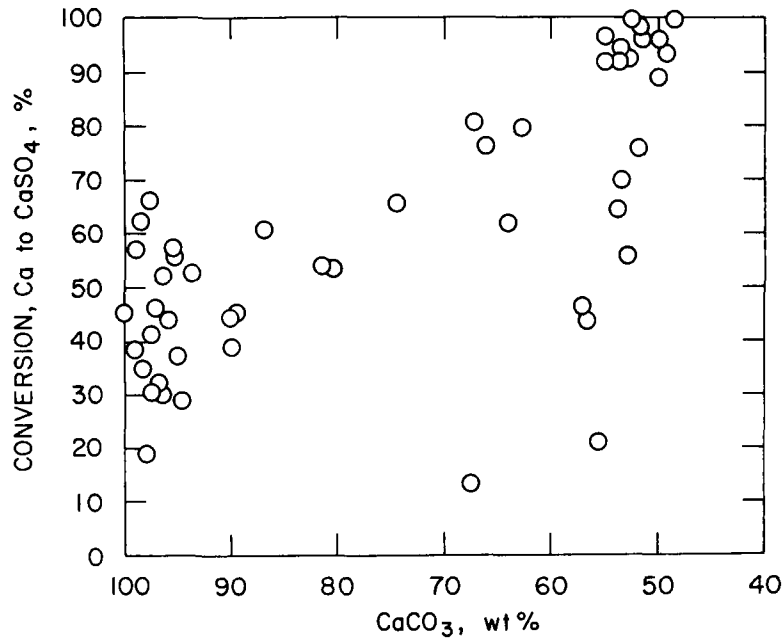


Fig. 17. Calcium Utilization of Limestones versus their  $\text{CaCO}_3$  Concentrations. Calcined at  $900^\circ\text{C}$ , 20%  $\text{CO}_2$  (-50 +70 mesh).

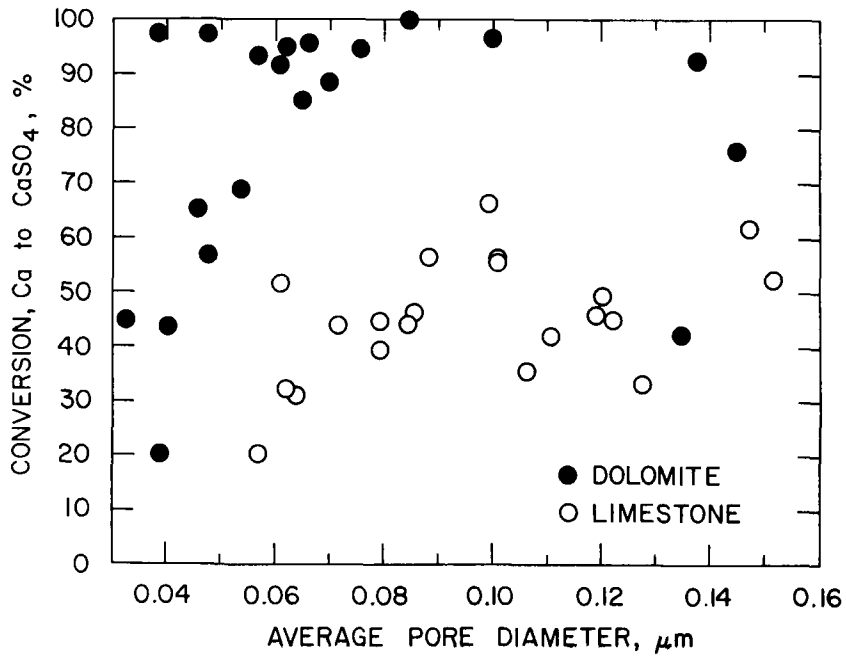


Fig. 18. Calcium Utilization as a Function of Pore Size for Calcined Stones

suggesting that other physical properties such as grain size may be important. Therefore, petrographic examinations of limestones were initiated to help understand limestone-SO<sub>2</sub> reactivity. This work is reported below.

8. Petrographic Examination of Limestones  
(R. B. Snyder, H. L. Fuchs, and W. I. Wilson)

As stated above, there is a large variation in calcium utilization for various limestones which have essentially the same chemical composition. It is believed that differences in SO<sub>2</sub> capacity of stones of similar composition are due to variations in the stone such as porosity, grain size, and grain defects. To investigate this, five stones (ANL-5402, ANL-5501, ANL-9802, ANL-9701, and ANL-5001) were selected for an initial petrographic study. The results were reported previously (ANL/CEN/FE-78-4) and are summarized here. Two dolomites were studied, one with high SO<sub>2</sub> reactivity and one with low SO<sub>2</sub> reactivity. The low SO<sub>2</sub> reactivity of one dolomite was due to its exceptionally large grain size (produced by metamorphism). Two limestones were also studied which had large differences in reactivity with SO<sub>2</sub>. Their reactivity differences could not be explained by petrographic properties. The fifth stone is a "popper"\* that is, it explodes upon calcination. Petrographic examination indicated that this popping might be due to inclusions of liquids, gases, or solid organics which form gases that rapidly expand upon heating. Another dolomite (ANL-5301) which also has a large number of inclusions is not a popper. This suggests that the type of inclusions, as well as their numbers, may affect whether popping occurs.

9. Effect of Water on SO<sub>2</sub> Reactivity  
(R. B. Snyder and W. I. Wilson)

The reactivity of limestones with SO<sub>2</sub> in the presence of excess oxygen has been investigated, using a TGA. In all of these experiments, a synthetic combustion gas composed of 0.3% SO<sub>2</sub>-5% O<sub>2</sub>-balance N<sub>2</sub> has been used. However, in a fluidized-bed combustor, the combustion gas also contains approximately 7% H<sub>2</sub>O. To determine any effect of water, three limestones were reacted with 0.3% SO<sub>2</sub>-5% O<sub>2</sub> gas having various concentrations of H<sub>2</sub>O. The presence of H<sub>2</sub>O in the reactant gas had essentially no effect on limestone-SO<sub>2</sub> reactivity. The results are also presented in a previous quarterly report (ANL/CEN/FE-78-4)

10. Limestone Attrition in a Fluidized-Bed  
(R. B. Snyder and W. I. Wilson)

The effects of certain variables on limestone attrition have been reported previously (ANL/CEN/FE-78-4) for ANL-8001, ANL-9601, and ANL-5101 stones. Several conclusions were drawn from these results and are summarized here:

---

\*"Poppers" are stones which, as the particles rupture or break up upon calcination, make a popping sound. Some stones actually explode into very fine particles. Of about 60 stones tested to date, approximately 20% are "poppers."

(1) An increase in temperature (20 to 870°C) increased the attrition rates of both limestones ANL-9601 and ANL-8001 but not that of ANL-5101. (These were 8-h batch tests with the stones fluidized by air.) More experiments with additional stones are needed to determine the effect of temperature on attrition.

(2) Calcination has no effect on attrition rate upon 8-h attrition at 870°C. The attrition rate of precalcined and virgin material was identical for all three stones. This conclusion does not apply to limestones or dolomites that are "poppers."

(3) Sulfation of a limestone may decrease its attrition rate. When sulfated, ANL-5101 and ANL-9601 stones had 30% and 40% as much attrition as when tested with all the conditions the same except that SO<sub>2</sub> was absent. ANL-8001 stone showed no attrition loss since this limestone in its natural form is very attrition-resistant.

(4) The extent of sulfation or rate of sulfation is important. Even though ANL-5101 stone is a softer stone than ANL-8001, simultaneous calcination and sulfation of ANL-5101 produced a stone that was more attrition-resistant than ANL-8001 stone. This is in agreement with results (ANL/CEN/FE-77-3) of previous attrition studies of ANL-8001 and ANL-5101 in the PDU pressurized combustor in which ANL-8001 and ANL-5101 losses due to attrition and elutriation were 20% and 16%, respectively.

(5) Limestones are not more attrition-resistant than are dolomites. For example, ANL-9601 (limestone 2203) which is very soft and has a high calcium content (96% CaCO<sub>3</sub>) is less attrition resistant than ANL-5101 (Tymochtee dolomite).

(6) Composition may be important (ANL/CEN/FE-77-3). Greater quantities of Al, Si, and Fe in a stone may produce more attrition-resistant stones. This can only be determined by examining a large number of limestones and dolomites.

(7) Other limestone physical properties such as grain size and grain defects are important. As shown previously (ANL/CEN/FE-77-3, p. 110), limestones with similar compositions can have widely different attrition rates.



TASK B. TURBINE-CORRODENT STUDIES  
(S. H. D. Lee)

In the prospective application of pressurized fluidized-bed combustion of coal to power generation, corrosion of turbine hardware due to attack by alkali-metal compounds present in the hot flue gas is a potential problem. This problem can be eliminated or alleviated by lowering the concentration of alkali-metal compounds in the hot flue gas to a level tolerable to the turbine. A direct method to accomplish this would be control of combustion so as to minimize evolution of alkali metal compounds. The mechanism of evolution of alkali-metal compounds during the combustion of coal at fluidized-bed combustion temperatures is not well understood. An alternative method of lowering the concentration of alkali metal compounds in the combustion gas is with a hot granular-bed filter upstream from the turbine.

Research work has been undertaken (1) to obtain a better understanding of the emission of alkali-metal compounds during the combustion of coal at the temperature range of fluidized-bed combustion, (2) to investigate the effectiveness of additives in controlling the emission of alkali-metal compounds during the combustion of coal, and (3) to develop an effective granular-bed filter sorbent material for the removal of alkali-metal compounds from hot combustion gas.

1. Emission of Alkali Metals during the Combustion of Coal

Work on this subject has continued. A simulated high-chlorine, high-sodium coal was investigated. This type of coal is of interest because of past observations that fouling and corrosion of the fireside of a boiler furnace is closely related to chlorine and sodium contents.<sup>19-21</sup> Simulated high-chlorine, high-sodium coals were made by impregnating coals with NaCl in a water solution.

This study was carried out using a laboratory-scale horizontal fixed-bed batch combustor system consisting of a preheating section which is preheated at startup, a combustion section where the sample is combusted, a filtration section containing a tubular alumina filter, and a cold-trap section containing a water-cooled metal cold trap. This combustor system was described in an earlier annual report in this series (ANL/ES-CEN-1016). Experimental results obtained from the combustion of Illinois Herrin No. 6 coal and activated coconut charcoal and part of results from the combustion of Glen-harold lignite (North Dakota) were reported in ANL/CEN/FE-77-3. Presented here are additional experimental results obtained from the combustion of Glen-harold lignite.

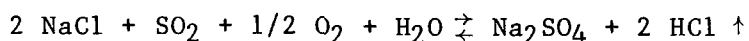
In the study of transport of alkali metals from the combustion of coal, it is important to understand the chemical form of the alkali metals present in the coal. In order to obtain information on this, 20-g samples of lignite were leached with distilled water at 95°C for 5 h and filtered, and the filter cake was leached with 5% HCl solution at 95°C for another 5 h. The water leachant was analyzed for Na<sup>+</sup>, K<sup>+</sup>, Cl<sup>-</sup>, and SO<sub>4</sub><sup>2-</sup>, and the acid leachant was analyzed for Na<sup>+</sup> and K<sup>+</sup>. Results showed that 44% of the sodium is present in compound forms that are soluble in water and 40% of the sodium is in a form soluble in 5% HCl solution. In contrast, potassium in lignite principally occurs in water-insoluble, acid-insoluble forms. A low concentration of Cl<sup>-</sup>

was observed in the water leachant indicating that the water-soluble sodium in lignite is apparently not present as the chloride. The sodium in lignite has been reported<sup>22</sup> to be present primarily as salts of humic acids.

The material balances for sodium in three series of combustion experiments with Glen-harold lignite were reported and discussed in the preceding annual report (ANL/CEN/FE-77-3) and for potassium in a quarterly report (Table 7, ANL/CEN/FE-77-8). Of the three series of experiments, one was with plain lignite, and the other two with 0.5 wt % NaCl-impregnated lignite. In all of these experiments, lignite was combusted in air at a flow rate of 3.5 L/min. Each series of experiments consisted of five batch combustion runs; in each run, 50 g of dry lignite was burned. Results indicated that the potassium in lignite behaves as if it is much more volatile than sodium. At 850°C, 38.1% of the potassium volatilized, whereas only 11.5% of the sodium volatilized; at 900°C, volatilization of potassium was 47.8% in comparison with 13.5% for sodium. Results also showed that the addition of NaCl to lignite significantly enhances the evolution of potassium during combustion. The potassium in the condensate collected from the cold-trap finger was identified by X-ray diffraction\* as KCl.

As shown by a leaching study potassium occurs in lignite as compound forms that mostly are not soluble in water. However, results obtained from the combustion of plain lignite indicated that significant amounts of potassium are converted into water-soluble compounds during combustion.

This phenomenon was previously observed for sodium. Results from the leaching of the combustion residue showed that during the combustion, not only is there physical vaporization of NaCl, but also NaCl undergoes the following chemical reaction to release chlorine and to form sodium sulfate in the residue:



## 2. Effect of Additives on the Retention of Alkali Metals in the Bed During the Combustion of Coal

The previous annual report (ANL/CEN/FE-77-3) showed that during the combustion of coals impregnated with 0.5 wt % NaCl, the greater the amount of mineral matter in the coal, the more the added NaCl is tied up in the ash and therefore the less NaCl is vaporized. Qualitatively, clay minerals and silica have been reported to be effective "getters" of alkali metals during the combustion of coal.<sup>23</sup> In order to quantitatively study the effectiveness of some additives (such as clay minerals, silica, and limestones, etc.) on the retention of alkali metals during combustion of coal, a series of experiments has been completed in which 0.5 wt % NaCl-impregnated activated coconut charcoal (in a mixture with additive) was burned. The same combustor as described in Section 1 above was used. In each experiment, 5 wt % additive was physically mixed with 20 g charcoal and the mixture was combusted at an air flow rate of 3.5 L/min, 900°C, and atmospheric pressure.

Experimental results obtained from this series of experiments were reported and discussed in detail in an earlier report (ANL/CEN/FE-77-8). Table 13 is a summary of the material balances of sodium and potassium. Fairly

\*Work done by B. Tani

Table 13. Material Balances of Sodium and Potassium  
from Combustion of 0.5 wt % NaCl-Impregnated  
Activated Coconut Charcoal Mixed with 5 wt %  
Additive

Experiment No. SL-10-	Additive	Total Amount, mg				% Alkali Fixed as Water Insoluble	
		Input		Output		Alkali	
		Na	K	Na	K	Na	K
1	None	50	188	49	125	12	5
2	Kaolinite No. 9	50	189	53	154	64	62
3	Montmorillonite No. 27	66	192	62	174	65	71
4	Greer Limestone	51	194	53	141	57	25
5	Dolowhite	50	188	47	154	22	10
6	Tymochtee Dolomite	50	194	48	150	46	22
7	Bauxite	50	188	51	165	64	61
8	Pure Alumina	52	188	45	157	10	14
9	Silica Gel	51	188	49	147	76	52
10	Al <sub>2</sub> O <sub>3</sub> Filter Powder	51	190	46	147	39	37

good material balances for sodium were obtained, except for the experiments in which pure alumina and Al<sub>2</sub>O<sub>3</sub> filter powder were the additives. For potassium, the total "Output" was more than 10% lower than the total "Input" in each experiment. Nonhomogeneity of the charcoal sample used, which could cause a great variation in the potassium content of the charcoal, is a possible source of the error since the material balance is very sensitive to the potassium content used in calculating the "Input" term. In contrast, error due to the variation in sodium content was not reflected in the sodium material balance because of the low sodium content of the charcoal. The large variation in the potassium content in the charcoal was previously observed (Table 30, ANL/CEN/FE-77-3).

In the two right-hand columns of Table 13 are the percentages of alkali fixed as water-insoluble alkali in the ash. This is a suitable basis for evaluating the effectiveness of an additive in retaining alkali metals because the alkali metals tied up in these forms are not easily vaporized into the combustion gas. As may be seen in Table 13 the retention effect of these additives, in general, was similar for sodium and potassium. Clay minerals (kaolinite and montmorillonite) tied up sodium in the ash very effectively. The SO<sub>2</sub> sorbents tested (Greer limestone, Tymochtee dolomite, and Dolowhite) were compared--the effectiveness of a sorbent for retaining sodium was found to be related to the amount of impurity (such as Al<sub>2</sub>O<sub>3</sub> and SiO<sub>2</sub>) in the sorbent. Greer limestone is an impure limestone (10% SiO<sub>2</sub> and 3% Al<sub>2</sub>O<sub>3</sub>) and showed some effectiveness in retaining sodium. In contrast, Dolowhite is a very pure dolomite and only a poor "getter." Bauxite is an aluminum ore and generally contains clay minerals. Its effectiveness was similar to that of kaolinite and montmorillonite. Pure alumina was inert. On the other hand, silica gel showed a substantial ability to tie up sodium. This is probably related to its large surface area. The results of this series of experiments clearly support the thought that clay minerals in the mineral matter of coal are responsible for the retention of alkali in the coal ash during the combustion of coal.

### 3. Removal of Gaseous Alkali Metal Compounds from the Hot Combustion Gas of Coal

Work is under way with a laboratory-scale, batch-type, fixed-bed combustor system (described in Section 1 above) to develop bed material for the granular-bed filter that will remove alkali metal compounds from the hot combustion gas of coal. In an experiment, a bed of candidate sorbent is placed between two perforated steel plates in a stainless steel tube. The tube, in the filtration section of the combustor, is fastened upstream from existing cold traps. A weighed pure alkali metal compound\* (such as NaCl or KCl) is heated and vaporized in the combustion section of the combustor, which is heated by induction heating. The vapor is carried by preheated flowing gas through the sorbent bed and finally is condensed on the cold traps and a backup filter (i.e., a glass wool filter). The candidate sorbent is tested at temperatures between 800 and 900°C and is evaluated for its effectiveness in removing the alkali metal compound from the alkali-metal-compound-bearing hot flowing gas.

The particle size range of each sorbent was carefully controlled by screening; all sorbents tested were -8 +10 mesh. Before a sorbent was tested, it was heat-treated in a muffle furnace at 900°C for 15 h in flowing air. The purpose of this treatment was to remove any possible alkali metal compounds present in the sorbent before the experiment which might be vaporized during the experiment.

It was found that a small fraction of the alkali metal compound vapor in the flowing gas was lost on the combustor wall upstream from the sorbent bed. Since substantial amounts of steel scale peel off the combustor wall at the

---

\*A.C.S. reagent

end of each test, it is believed that the loss of alkali compound was mainly due to reactions of alkali metal compound vapor with the hot stainless steel wall of the combustor. To obtain the amount of alkali metal compound vapor transported through the sorbent bed, the amount of alkali metal compound vapor vaporized during a test needs to be corrected for this loss. For the screening test experiments using the combustor system, the amount of loss was obtained using data from blank runs with the experimental conditions the same as in a regular experimental run except that the sorbent bed was absent. The candidate sorbents tested in screening tests were evaluated based on the material balance of alkali metal compound (obtained on a batch basis). In the rest of the experiments (parametric tests), each sorbent was evaluated based on the direct analysis of an alkali element in the sorbent that had been tested.

During this reporting period, several commercial products were screened (as described below) by measuring their effectiveness for removing NaCl, KCl, and K<sub>2</sub>SO<sub>4</sub> vapors. From the screening test results, the two most promising products, diatomaceous earth and activated bauxite were chosen for further parametric tests. Results from these screening and parametric tests were reported and discussed in detail in earlier quarterly reports (ANL/CEN/FE-77-11, -77-3, and -78-4). Presented here is a summary of these results, as well as additional results obtained since.

#### a. Screening Tests

NaCl Vapor Tests. Six commercial products (alundum, Celatom MP-91 diatomaceous earth, silica gel., Burgess No. 10 pigment, attapulugus clay, and activated bauxite) were first screened by measuring their effectiveness in removing NaCl vapor from hot NaCl-vapor-bearing flowing air. In each test, a 7.6-cm-thick sorbent bed was packed, and the bed was maintained at an average temperature of 870 °C under an air flow of 3.5 L/min. Under these conditions, the loading of NaCl vapor in the air was about 60 ppm, and the linear velocity of the air passing through the sorbent bed was 7.6 cm/s.

The NaCl material balances for these sorbent tests have already been reported (ANL/CEN/FE-77-11). The alundum, a high-purity  $\alpha$ -Al<sub>2</sub>O<sub>3</sub>, was inert. A good material balance obtained from the test with inert  $\alpha$ -Al<sub>2</sub>O<sub>3</sub> demonstrated that there was no physical condensation of NaCl vapor on the sorbent. Celatom MP-91 diatomaceous earth, Burgess No. 10 pigment, and activated bauxite effectively captured 74, 78, and 92% of the NaCl vapor, respectively. In other work in which silica gel was an additive to activated coconut charcoal which was combusted (Table 13), silica gel was effective in tying up sodium in the ash bed; however, when silica gel was used as a sorbent, it was only moderately effective in tying up NaCl vapor. This was due to the loss of porosity of the silica gel, as will be seen in the porosity-measurement study. Attapulugus clay showed fair effectiveness in capturing NaCl vapor; however, this clay, as well as Burgess No. 10 pigment, became fragile after the test. From a viewpoint of practical application, this behavior is not acceptable for a candidate sorbent because fine particles would be produced, increasing the load on the downstream particulate-removal facilities. In general, the activities of sorbents for NaCl-vapor capture were found to be related to their internal surface areas.

The results of an earlier water-leaching study of these sorbents indicated that for diatomaceous earth, Burgess No. 10 pigment, and attapulgus clay, the NaCl vapor was primarily retained via chemical reactions with the sorbents; for silica gel and activated bauxite, the NaCl vapor was retained by a physical adsorption process.

To investigate the capability of these sorbents at high gas velocity, Celatom MP-91 diatomaceous earth, Burgess No. 10 pigment, and activated bauxite were further tested at a flow velocity of 25 cm/s, using either air or a simulated flue gas. Average bed temperature was 880 C. The composition of the simulated flue gas was 3% O<sub>2</sub>, 16% CO<sub>2</sub>, 180 ppm H<sub>2</sub>O, 300 ppm SO<sub>2</sub>, 80 to 110 ppm NaCl vapor, and the balance N<sub>2</sub>. The material balances of NaCl for all of these tests showed that the capability of all three sorbents for NaCl vapor retention was substantially greater than at low gas velocities; 96, 85, and 98% NaCl captures were obtained by diatomaceous earth, Burgess No. 10 pigment, and activated bauxite, respectively. A possible explanation for this increase is that a higher linear velocity of the flue gas increases the mass transfer of NaCl vapor from the bulk of flue gas to the surface of the sorbent, thereby increasing sorption of NaCl vapor by the sorbent. Results obtained from the leaching of sorbents tested in this series of experiments again showed that the sodium removed by diatomaceous earth and Burgess No. 10 pigment was essentially present in chemical forms not soluble in water. In contrast, most of the sodium sorbed by activated bauxite was present in water-soluble form. The importance of this is that sodium adsorbed on activated bauxite can be easily removed by a simple leaching process, making it possible to regenerate activated bauxite for reuse. The regenerability of activated bauxite and the effect of regeneration on its sorption capability will be studied.

KCl-Vapor Tests. Except for low-rank Western coals, the potassium content of typical U.S. coal is higher than the sodium content--approximately two moles of potassium are present for each mole of sodium.<sup>24</sup> Potassium compounds and sodium compounds exist in coal in similar chemical forms. Potassium chloride and sodium chloride are present in saline groundwater permeating the rock and filling pores and cracks in the coal bed. Both potassium and sodium are also constituents of clay minerals in coal, such as illite and montmorillonite. Potassium chloride is known to have an appreciably higher vapor pressure at the fluidized-bed combustion temperature range than does sodium chloride (0.7 kPa at 900°C for KCl, as compared with 0.4 kPa for NaCl); therefore, its vapor is expected to be present in the flue gas of pressurized fluidized-bed combustors (PFBCs).

Thermodynamic calculations to identify the major species present at the operating conditions for a fluidized-bed combustor have been made by researchers at Westinghouse Research Laboratory.<sup>25</sup> Results of the calculations indicate that gaseous potassium chloride is the major potassium carrier. Based on these results, Celatom MP-91 diatomaceous earth, activated bauxite, and Burgess No. 10 pigment were further tested for their sorption capability for KCl vapor, under the same conditions used to test them with NaCl vapor at 25 cm/s linear gas velocity.

Material balances of KCl from tests of these sorbents for KCl-vapor capture indicated that diatomaceous earth and activated bauxite captured KCl vapor as effectively as they captured NaCl vapor. Ninety-eight and ninety-five

percent KCl vapor captures were obtained with diatomaceous earth and activated bauxite, respectively. In comparison with those two sorbents, Burgess No. 10 pigment was less effective for KCl vapor capture (74%), just as for NaCl vapor capture (shown above). The similar sorption activity of these sorbents toward both NaCl and KCl vapor is expected because of the similar chemical properties of NaCl and KCl.

K<sub>2</sub>SO<sub>4</sub>-Vapor Tests. In the flue gas from coal combustion, sodium and potassium are expected to be present as sulfates also. Sodium sulfate and potassium sulfate in liquid form are generally believed to be the precursors for metal sulfidation, the most common mode of hot corrosion occurring in gas turbines;<sup>26</sup> therefore, the ability of candidate sorbents to retain alkali metal sulfates must be demonstrated. Both sodium and potassium as sulfates have substantially lower vapor pressures than as chlorides. Because the maximum allowable operating temperature of the laboratory-scale fixed-bed combustor is 900°C, the sorption capability of the sorbents for alkali metal sulfates could not be determined using this combustor; therefore, a small-scale sorption-test rig that can be operated up to 1250°C was assembled. The apparatus is described in a previous report in this series (ANL/CEN/FE-78-4).

Two 24-h experimental runs were conducted, one each to test activated bauxite and diatomaceous earth for their abilities to retain potassium sulfate vapor in a simulated PFBC flue gas. Table 14 shows the experimental test conditions, and Table 15 shows the material balances of K<sub>2</sub>SO<sub>4</sub> from these two tests.

Table 14. Experimental Conditions for Testing  
Diatomaceous Earth and Activated Bauxite  
Sorbents for K<sub>2</sub>SO<sub>4</sub> Vapor Capture

Avg. Sorbent-Bed Temperature	850°C
System Pressure	100 kPa
Particle Size of Each Sorbent	8-10 mesh Tyler
Flow Gas Composition	2.3% O <sub>2</sub> 13.0% CO <sub>2</sub> 120 ppm H <sub>2</sub> O 110 ppm SO <sub>2</sub> 3 ppm K <sub>2</sub> SO <sub>4</sub> vapor Balance N <sub>2</sub>
Gas Flow Rate	8.85 L/min at room temperature
Linear Gas Velocity	27 cm/s at 850°C
Gas Hourly Space Velocity (GHSV)	62,000 h <sup>-1</sup> at 850°C
Duration of experiment	24 h

Table 15. Material Balances of  $K_2SO_4$  from Tests of  $K_2SO_4$  Vapor Capture by Diatomaceous Earth and Activated Bauxite

	$K_2SO_4$ , mg	
	Expt. KSO-4, Activated Bauxite	Expt. KSO-5, Diatomaceous Earth
<u>Input</u>		
(1) $K_2SO_4$ Vaporized	346	264
<u>Output</u>		
(2) $K_2SO_4$ Collected from		
(a) Combustion Tube	8	23
(b) Downstream Line and Condenser	2	3
(3) $K_2SO_4$ Captured by Sorbent <sup>a</sup>	<u>322</u>	<u>191</u>
Total	332	217
(4) $K_2SO_4$ Loss (by difference)	14	47
(5) % $K_2SO_4$ Capture [(3)/(1) x 100]	93.1	72.3

<sup>a</sup>Potassium concentration of the sorbent was obtained by dissolving two representative samples each of activated bauxite and diatomaceous earth in  $NH_4HF_2$  and a mixture  $H_2SO_4$ , HF, and  $HNO_3$ , respectively, and then analyzing the resulting solutions by atomic absorption. AA analyses were done by R. Bane.

As shown in Table 15,  $K_2SO_4$  vapor captures by activated bauxite and diatomaceous earth were 93.1 and 72.3%, respectively, during the 24-h experiments. The sorbents were tested at a fairly high gas hourly space velocity of  $62,000\text{ h}^{-1}$  (or a contact time of about 0.06 s) and at a fairly low  $K_2SO_4$  concentration in the flue gas as shown in Table 14. In a granular-bed filter operated with a PFBC, an increase in the percent  $K_2SO_4$  vapor capture by the sorbent can be expected to occur at longer contact times of  $K_2SO_4$  vapor with the sorbent bed and at the higher  $K_2SO_4$  vapor concentrations. The capabilities of these sorbents for removing  $K_2SO_4$  vapor from hot flue gas is comparable to their capabilities for removing alkali metal chloride vapors (demonstrated earlier). Since  $K_2SO_4$  and  $Na_2SO_4$  have similar chemical properties, one would expect that retention of  $Na_2SO_4$  vapor by these two sorbents would be similar to  $K_2SO_4$  vapor retention.



When activated bauxite and diatomaceous earth were tested with NaCl vapor, results obtained from water-leaching the sorbent indicated that NaCl vapor is adsorbed by activated bauxite in the form of NaCl and that the NaCl vapor reacts with diatomaceous earth to form products that are not soluble in water.

To gain an understanding of the reactions of  $K_2SO_4$  vapor with the two sorbents at the experimental conditions, after the  $K_2SO_4$  experiments, the two sorbents were each leached with distilled water using magnetic stirring at 95°C for 1 h. Table 16 shows the distribution of water-soluble and water-insoluble potassium species in both activated bauxite and diatomaceous earth sorbents.

Table 16. Distribution of Potassium Ion in the Sorbents

	$K^+$ , g-mol $\times 10^3$	
	Activated Bauxite	Diatomaceous Earth
Water-Soluble	0.61 (16.5%)	0.06 (2.7%)
Water-Insoluble <sup>a</sup>	<u>3.09</u> (83.5%)	<u>2.14</u> (97.3%)
Total <sup>b</sup>	3.70	2.20

<sup>a</sup>Obtained by the difference of total and water-soluble.

<sup>b</sup>Obtained by the analysis of  $K^+$  in the sorbent.

Table 16 indicates that in contrast to the water-soluble NaCl deposited on activated bauxite, products formed upon the reaction of  $K_2SO_4$  vapor with activated bauxite are only slightly soluble in water.

The products of the  $K_2SO_4$  vapor reactions with diatomaceous earth are essentially water-insoluble. At the end of the experiment, significant amounts of diatomaceous earth particles were observed to be coated with a layer of transparent, vitreous material, which was not observed on the activated bauxite sorbent. The X-ray diffraction analysis\* of the vitreous material showed that it was an amorphous substance and was not melted  $K_2SO_4$ . This indicates that during the experiments, the  $K_2SO_4$  melt in the sample did not creep and that apparently,  $K_2SO_4$  vapor reacted with diatomaceous earth to form glassy potassium silicates. The silicates so formed may be in chemical forms that dissolve very slowly in water or they may further combine with impurities such as oxides of aluminum, iron, calcium, and magnesium to form water-insoluble products.

---

\*Done by B. Tani

### b. Parametric Tests

The experimental results presented in the previous screening tests clearly indicate the effectiveness of both activated bauxite and diatomaceous earth sorbents in removing vapors of NaCl, KCl, and  $K_2SO_4$  from simulated PFBC flue gas. Consequently, systematic studies were initiated to investigate the effects of some operating variables in the sorption performance of these two materials. In this reporting period, the effect of sorbent-bed temperature, superficial gas velocity, and gas hourly space velocity (GHSV) of the flue gas were studied. Results of these studies are presented below.

Effect of Sorbent-Bed Temperature. Sorption capacities of diatomaceous earth and activated bauxite were measured at average bed temperatures of 800 and 880°C as a function of experiment duration. Tests were conducted at atmospheric pressure, using a simulated PFBC flue gas (3%  $O_2$ , 16%  $CO_2$ , 180 ppm  $H_2O$ , 300 ppm  $SO_2$  and the balance  $N_2$ ) containing 69 to 98 ppm NaCl vapor. The superficial gas velocity was 25 cm/s and the gas hourly space velocity was 67,000  $h^{-1}$ . The quantities of NaCl captured by sorbents and condensed on the cold traps were reported earlier (ANL/CEN/FE-78-4). Calculated sorption capacities (in mg NaCl/g sorbent) are plotted in Fig. 19.

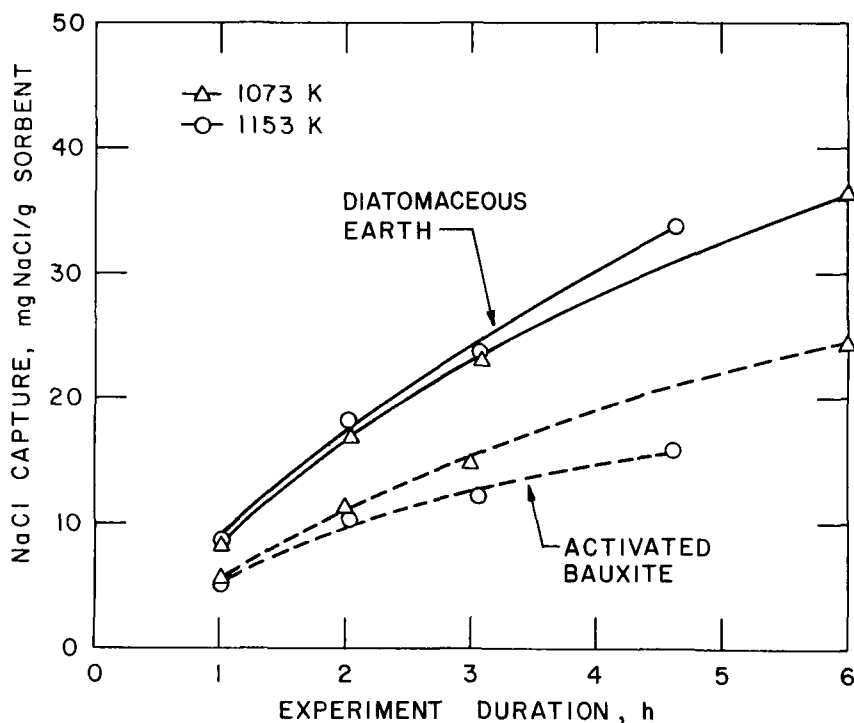


Fig. 19. Effect of Sorbent Bed Temperature on Sorption Capacity as a Function of Experiment Duration

As can be seen in Fig. 19, the sorption capacity of diatomaceous earth is substantially greater than that of activated bauxite on a weight basis (*i.e.*, mg NaCl/g sorbent). This is due to the activated bauxite being denser than diatomaceous earth. For all of these experiments, a 1.3-cm-thick bed was packed; therefore, on a volume basis (*i.e.*, mg NaCl/mL sorbent) the sorption capacity of activated bauxite is greater than that of diatomaceous earth.

Figure 19 also shows that the sorption capacity of diatomaceous earth increases with sorbent-bed temperature. This indicates that the reaction between NaCl vapor and diatomaceous earth is endothermic. In contrast to diatomaceous earth, the sorption capacities for activated bauxite decrease with increasing sorbent-bed temperature. Since a physical adsorption process is always exothermic, the amount of adsorbate sorbed on an adsorbent must always decrease with increasing temperature according to the principle of Le Chatelier; therefore, the present observation substantiates the conclusion (made above) that NaCl vapor is essentially captured by activated bauxite through a physical adsorption process. Figure 19 also shows that the sorption capacity of both diatomaceous earth and activated bauxite increase nonlinearly with time. This suggests that under the experimental conditions, neither the reaction rate between NaCl and diatomaceous earth nor the rate of adsorption of NaCl on activated bauxite is controlled by the rate of mass transfer of NaCl vapor from the bulk flue gas to the external surface of the sorbent.<sup>27</sup>

Effect of Superficial Gas Velocity of Flue Gas at Constant GHSV. In gas-solid reactions, as in the system considered in the present study, the effect of superficial gas velocity of flue gas passing through the sorbent bed on the sorption rate of NaCl vapor provides another means of measuring the role played by the mass transfer of NaCl vapor from the bulk flue gas to the external surface of the sorbent. For mass-transfer-controlled reactions, an increase in superficial gas velocity increases the mass transfer coefficient, thereby increasing the extent of reaction. The superficial gas velocity is also an important parameter for designing a sorber vessel because it determines the bed cross-sectional area for a given volumetric flow rate of flue gas to be treated.

Based on these reasons, a series of tests has been conducted to study the effect of superficial gas velocity on the sorption capacity of both diatomaceous earth and activated bauxite. In this series of experiments, -8 +10 mesh sorbent was tested at 800°C and atmospheric pressure in a simulated PFBC flue gas (3% O<sub>2</sub>, 16% CO<sub>2</sub>, 180 ppm H<sub>2</sub>O, 300 ppm SO<sub>2</sub>, and the balance N<sub>2</sub>) at superficial gas velocities of 25, 66, and 155 cm/s, and at a constant GHSV of 67,000 h<sup>-1</sup>. The NaCl vapor concentration in the flue gas ranged from 69 to 98 ppm. Increases in the superficial gas velocity of the flue gas at the sorbent bed were accomplished by reducing the cross section of the sorbent bed, but the amount of sorbent packed was kept constant to maintain a constant GHSV. For each superficial gas velocity, the sorbent was tested at durations of both 2 and 3 h as a double-check.

Tables 17 and 18 show NaCl vapor capture by diatomaceous earth and activated bauxite, respectively, as a function of superficial gas velocity. Calculated average rate of NaCl capture (in mg NaCl/g sorbent) [row (4) in both Tables 17 and 18 divided by experiment duration] are plotted as a function of superficial gas velocity in Fig. 20.

Table 17. Sodium Chloride Distributions from Tests of NaCl-Vapor Capture by Diatomaceous Earth as a Function of Superficial Gas Velocity of Flue Gas

Sorbent (15.0 g) was tested at 800°C and atmospheric pressure in a simulated PFBC dry flue gas at GHSV = 67,000 h<sup>-1</sup>

	Expt. HGC-23	Expt. HGC-24	Expt. HGC-37	Expt. HGC-38	Expt. HGC-42	Expt. HGC-41R
Duration of Experiment, h	2	3	2	3	2	3
Superficial Gas Velocity, cm/s	25	25	66	66	155	155
	NaCl, mg					
(1) NaCl Collected by						
(a) Cold Traps	42	56	29	52	29	82
(b) Glass-wool Filter	9	31	14	28	18	52
(2) NaCl Captured by Sorbent <sup>a</sup>	<u>251</u>	<u>343</u>	<u>328</u>	<u>422</u>	<u>332</u>	<u>397</u>
(3) Total	302	430	371	502	379	531
(4) Sorption Capacity, mg NaCl/g sorbent [(2)/15]	16.7	22.9	21.9 (17.8) <sup>b</sup>	28.1 (24.1) <sup>b</sup>	22.1 (17.6) <sup>b</sup>	26.5 (21.4) <sup>b</sup>

<sup>a</sup>Sodium concentration in the sorbent was obtained by dissolving representative samples of the sorbent in a mixture of H<sub>2</sub>SO<sub>4</sub>, HF, and HNO<sub>3</sub> and then analyzing the solution by flame emission spectrometry (FE). FE analyses were done by R. Bane.

<sup>b</sup>To allow comparison, these are values which would be obtained if the NaCl vapor were transported as in the 25 cm/s-series of experiments. For example, 17.8 was obtained from

$$302 \left( \frac{328}{371} \right) / 15.$$

Table 18. Sodium Chloride Distributions from Tests of NaCl-Vapor Capture by Activated Bauxite as a Function of Superficial Gas Velocity of Flue Gas

Sorbent (30.0 g) was tested at 800°C and atmospheric pressure in a simulated PFBC dry flue gas at GHSV = 67,000 h<sup>-1</sup>

	Expt. HGC-26	Expt. HGC-27	Expt. HGC-40	Expt. HGC-39	Expt. HGC-43R	Expt. HGC-44
Duration of Experiment, h	2	3	2	3	2	3
Superficial Gas Velocity, cm/s	25	25	66	66	155	155
	NaCl, mg					
(1) NaCl Collected by						
(a) Cold Traps	22	40	42	62	33	47
(b) Glass-wool Filter	10	22	25	33	20	27
(2) NaCl Captured by Sorbent <sup>a</sup>	<u>343</u>	<u>444</u>	<u>281</u>	<u>430</u>	<u>351</u>	<u>498</u>
(3) Total	375	506	348	525	404	582
(4) Sorption Capacity mg NaCl/g-sorbent [(2)/30]	11.4	14.8	9.4 (10.1) <sup>b</sup>	14.3 (13.8) <sup>b</sup>	11.7 (10.9) <sup>b</sup>	16.6 (14.4) <sup>b</sup>

<sup>a</sup>Sodium concentration in the sorbent was obtained by fusing representative samples of the sorbent with NH<sub>4</sub>HF<sub>2</sub>, dissolving the samples in distilled water, and then analyzing the solutions by flame emission spectrometry (FE). FE analyses were done by R. Bane.

<sup>b</sup>To allow comparison, these are the values which would be obtained if the NaCl vapor were transported as in the 25 cm/s-series of experiments. For example, 10.1 was obtained from  $375 \left( \frac{281}{348} \right) / 30$ .

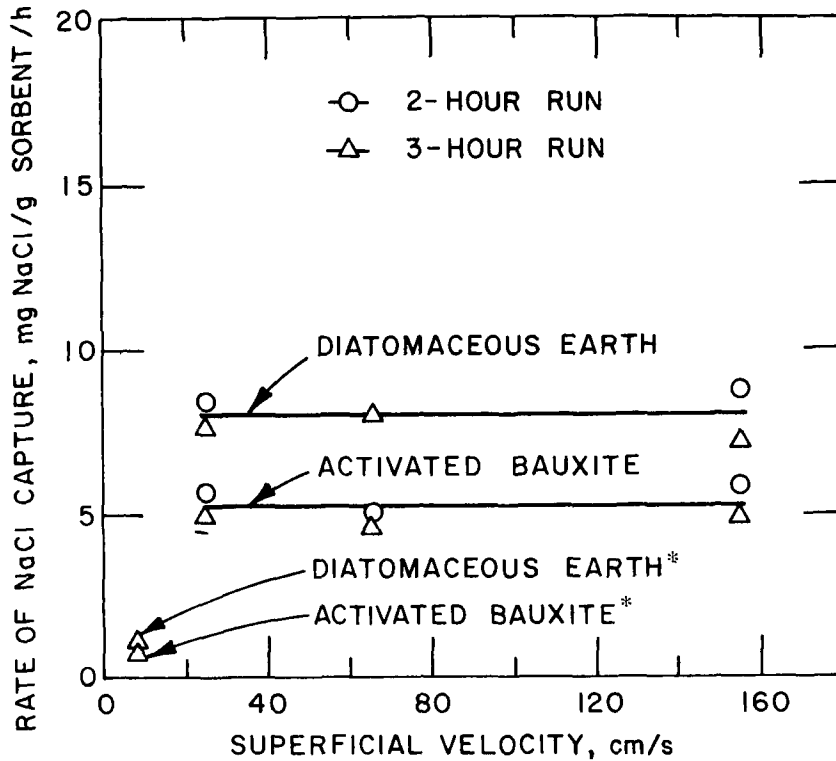


Fig. 20. Effect of Superficial Gas Velocity on Sorption Capacity at 800°C. \*Data were calculated from the results of a previous set of experiments (HGC-4 and HGC-8 in ANL/CEN/FE-77-11). These two values were revised to conform to the amounts of NaCl that would be transported in the 25 cm/s-series of experiments. In these two experiments, -8 +10 mesh sorbent was tested at 870°C and atmospheric pressure and in an air flow at GHSV = 3500 h<sup>-1</sup>.

Within the limits of experimental and analytical error, the sorption capacity is not affected by superficial gas velocity in any 2- or 3-h run, as shown in Fig. 20. These results verify that under the experimental conditions, the reaction between diatomaceous earth and NaCl vapor and the adsorption of NaCl vapor on activated bauxite are not controlled by the mass transfer of NaCl vapor from the bulk flue gas to the external surface of the sorbent. The sorption observed for these sorbents is controlled by the rate of diffusion of NaCl vapor through internal pores, the rate of adsorption of NaCl vapor on the active sites of the sorbent, or the chemical kinetics (in the case of diatomaceous earth).

Also included in Fig. 20 are the rates of NaCl capture for both of the sorbents, calculated from the results of a previous set of experiments (HGC-4 and HGC-8 in ANL/CEN/FE-77-11) revised to correspond to the amounts of NaCl vapor that would be transported in a 25 cm/s series of experiments.

In these two experiments, the two -8 +10 mesh sorbents were tested at 870°C and atmospheric pressure and with air flowing at a superficial gas velocity of 7.5 cm/s and GHSV = 3500. Because the sorbents were not tested under experimental conditions quantitatively comparable to those of high superficial gas velocity, the results are included in the figure for qualitative comparison only. It is seen that the rate is substantially smaller at a superficial gas velocity of 7.5 cm/s than at high superficial gas velocities. This indicates that at such a low superficial gas velocity, sorption of NaCl by these sorbents was probably mass-transfer controlled.

#### Effect of GHSV of Flue Gas at Constant Superficial Gas Velocity.

The GHSV is defined as the volumetric flow rate of flue gas in units of sorbent volumes per hour. The reciprocal of the GHSV, which is space time, is related to the contact time of flue gas with the sorbent bed. Thus, the GHSV determines the sorbent volume required for a given volumetric flow rate of flue gas to be treated.

A series of tests was conducted in which -8 +10 mesh sorbent was tested at 800°C and atmospheric pressure using a simulated PFBC flue gas (3% O<sub>2</sub>, 16% CO<sub>2</sub>, 180 ppm H<sub>2</sub>O, 300 ppm SO<sub>2</sub>, and balance N<sub>2</sub>) at a superficial gas velocity of 66 cm/s. The average concentration of the NaCl vapor in the flue gas was 80 ppm. The tests were each run for 2 h. All experiments were carried out at a constant flow rate of flue gas; therefore, GHSV was varied by varying the volume of the sorbent bed. Tables 19 and 20 show NaCl vapor capture by diatomaceous earth and activated bauxite, respectively, as a function of GHSV. Figure 21 is a plot of results given in Tables 19 and 20.

Figure 21 shows that, as expected, increased contact time of the flue gas with the sorbent increases the NaCl-vapor capture for both diatomaceous earth and activated bauxite sorbents. For Experiment HGC-37, the percent NaCl captured appears to be high. This experiment should be repeated to check this result. The results of this series of experiments indicate that at fairly short contact times of flue gas with the sorbent bed (about 0.2 s) and at 2-h times of experiments, 98.5% and 97% removal of NaCl vapor from hot flue gas can be achieved by activated bauxite and diatomaceous earth, respectively.

In addition to the sorbent-bed temperature, the superficial gas velocity, and the gas hourly space velocity of the flue gas, the sorption ability of a sorbent can be affected by several other variables. Among them are pressure, alkali metal compound vapor concentration, moisture content of the flue gas, and particle size of the sorbent. Studies on the effects of these variables on the sorption capability of activated bauxite and diatomaceous earth will be continued. The regenerability of activated bauxite by water leaching and desorption processes will also be explored. Finally, an economic evaluation will be done using these materials as granular-bed sorbents for removing alkali-metal compounds from PFBC hot combustion gas.

Table 19. Sodium Chloride Distributions from Tests of NaCl-Vapor Capture by Diatomaceous Earth as a Function of Gas Hourly Space Velocity (GHSV)

Sorbent was tested at 800°C and atmospheric pressure in a simulated PFBC dry flue gas at a superficial gas velocity of 66 cm/s. Duration of each experiment was 2 h.

	Expt. HGC-37	Expt. HGC-47	Expt. HGC-52R
GHSV, h <sup>-1</sup> (Contact Time, s)	67,000 (0.05)	33,500 (0.11)	18,600 (0.19)
	NaCl, mg		
(1) NaCl Collected by			
(a) Cold Traps	29	29	6
(b) Glass-Wool Filter	14	18	4
(2) NaCl Captured by Sorbent <sup>a</sup>	<u>328</u>	<u>292</u>	<u>318</u>
(3) Total	371	339	328
(4) % NaCl Capture by Sorbent, [(2)/(3)] x 100	88.4	86.1	97.0

<sup>a</sup>Sodium concentration in the sorbent was obtained by dissolving representative samples of the sorbent in a mixture of H<sub>2</sub>SO<sub>4</sub>, HF, and HNO<sub>3</sub>, and then analyzing the solution by flame emission spectrometry (FE). FE analyses were done by R. Bane.



Table 20. Sodium Chloride Distributions from Tests of NaCl-Vapor Capture by Activated Bauxite as a Function of Gas Hourly Space Velocity (GHSV)

Sorbent was tested at 800°C and atmospheric pressure in a simulated PFBC dry flue gas at a superficial gas velocity of 66 cm/s. Duration of each experiment was 2 h.

	Expt. HGC-40	Expt. HGC-50	Expt. HGC-51
GHSV, h <sup>-1</sup> (Contact Time, s)	67,000 (0.05)	33,500 (0.11)	18,600 (0.19)
	NaCl, mg		
(1) NaCl Collected by			
(a) Cold Traps	42	19	3
(b) Glass-Wool Filter	25	11	2
(2) NaCl Captured by Sorbent <sup>a</sup>	<u>281</u>	<u>348</u>	<u>330</u>
(3) Total	348	378	335
(4) % NaCl Capture by Sorbent, [(2)/(3)] x 100	80.7	92.1	98.5

<sup>a</sup>Sodium concentration in the sorbent was obtained by fusing representative samples of the sorbent with NH<sub>4</sub>HF<sub>2</sub>, dissolving the samples in slightly acidified distilled water, and then analyzing the solutions by flame emission spectrometry (FE). FE analyses were done by R. Bane.

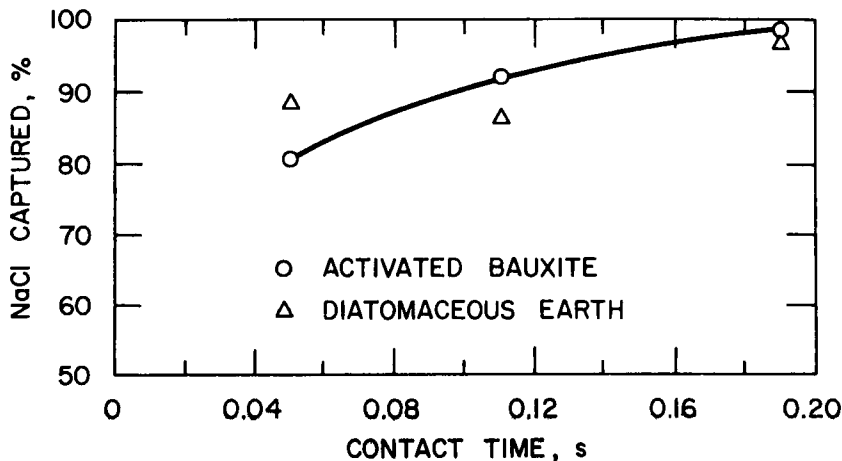


Fig. 21. Effect of the Contact Time of Flue Gas with Sorbent on NaCl Vapor Capture

## TASK C. TRACE-POLLUTANT CONTROL IN FBC

1. Trace-Element Behavior in Sorbent During Cyclic Utilization  
(W. M. Swift, G. W. Smith, and F. G. Teats)

Results obtained at Argonne National Laboratory and reported previously<sup>4,28,29</sup> indicated that smaller quantities of trace elements (such as Hg, F, and Br) would be emitted to the environment from fluidized-bed combustion than would be expected from a conventional coal-fired boiler. This conclusion was based on a comparison of (1) open mass balances made around the ANL 15.2-cm-dia pressurized fluidized-bed combustor with (2) similar mass balances reported<sup>30-32</sup> for conventional coal-fired boilers. The mass balances were open in that trace element concentrations were determined only for solid feed and effluent (and in the case of conventional boilers, liquid effluents) from the combustion processes. Trace-element emissions to the environment were assumed to be the percentages of the trace elements which had entered the combustion process but were not accounted for in the analyzed effluents.

The previous ANL study failed to consider, however, the potential influence of regeneration in a regenerative fluidized-bed combustion process on the release of trace elements to the environment. The regeneration reactor operates at temperatures as high as ~1100 °C, as compared with the ~900 °C operating temperature of the fluid-bed combustor. Thus, concern is justified that trace elements contained in the sulfated sorbent from the combustor might be released by volatilization during regeneration. A study was made, therefore, (1) to measure the levels of selected trace elements in the sorbent over several cycles of sulfation and regeneration, and determine the tendency for those elements to be enriched or depleted in the sorbent under these conditions, and (2) to make a material balance (based on solid samples only) for a single regeneration experiment, assessing changes in the trace element concentrations in the sorbent for evidence of trace element losses by volatilization. A summary of the experimental findings is presented here. A more detailed account of the work has been presented in a quarterly report (ANL/CEN/FE-78-3) issued during the past year.

a. Analytical

In a recently published proceedings of a workshop on the effects of trace contaminants from coal combustion, selected trace elements present in coal were classified in three broad categories of toxicity--i.e., high, medium, and low potential, for both terrestrial and aquatic life. The classification represents a "best estimate" based on the experience, knowledge, and intuition of the panel members.

In the previous trace-element investigation at ANL,<sup>4,28,29</sup> mass balances were made around the ANL 15.2-cm-dia PFBC for the following trace and minor elements: As, Be, Br, Co, Cr, F, Fe, Hg, K, La, Mn, Na, Pb, and Sc. In that investigation, the concentrations of Hg, Pb, Be, and F in particulate samples were determined by wet chemical techniques; concentrations of the remaining ten elements were determined by neutron activation analysis. Using the classification referenced above, of the fourteen elements studied previously, five (Be, Co, Cr, F, and Hg) are suspected of having a potentially high toxicity,

one (Pb) a potentially medium toxicity, two (As and Mn) a potentially low toxicity, and six (Br, Fe, K, La, Na, and Sc) are not listed.<sup>33</sup> Of the last six, the behavior of two elements (sodium and potassium) during PFBC is of interest in relation to the corrosion of hardware downstream from the combustor.

In the selection of the analytical approach for the current study, major consideration was given to selecting a method which would provide information on most elements assessed as having potentially high-toxicity and medium-toxicity effects on the environment. For this reason, spark-source mass spectroscopy (SSMS) was selected as the most suitable instrumental method of analysis.

The samples selected for analysis were sent to Oak Ridge National Laboratory, where they were analyzed for trace element impurities by SSMS. The results, except for twelve metals analyzed by stable isotope dilution, were obtained by a visual inspection and plate sensitivity technique. For the latter method, the reported results are considered accurate within a factor of two; isotope dilution results are considered accurate within  $\pm 20\%$  of the reported value. A duplicate of a sample analyzed by the Oak Ridge Analytical Chemistry Division was also sent to an independent commercial laboratory for SSMS analysis to allow comparison of the analyses.

#### b. Experimental

To assess the fate of trace elements during a regenerative FBC process, particulate samples of coal, ash, sorbent, and sulfated sorbent from the 10-cycle combustion-regeneration experiment with Tymochtee dolomite sorbent (ANL/CEN/FE-77-3, an earlier report in this series) were analyzed. This experiment was performed with no fresh makeup sorbent added after the first combustion half-cycle experiment. The nominal conditions for the combustion half-cycles, performed with Tymochtee dolomite and Arkwright coal, were a 900°C bed temperature, an 810-kPa system pressure, a 1.5 CaO/S mol ratio,  $\sim 17\%$  excess combustion air, a 0.9 m/s fluidizing-gas velocity, and a 0.9-m bed height. The regeneration half-cycles were performed using Triangle coal at a bed temperature of 1100°C, a system pressure of 158 kPa, and a fluidized-bed height of  $\sim 46$  cm. Table 21 lists and describes the samples analyzed.

#### c. Results

Verification of Analytical Results. Sample J-11270, sulfated Tymochtee dolomite, was submitted to both Oak Ridge National Laboratory (ORNL) and an independent commercial laboratory for comparative SSMS analyses of trace elements. Of the analyses for 43 elements by ORNL, 33 results were in agreement within stated analytical accuracies with the results reported by the commercial laboratory. Although not a conclusive demonstration of the quantitative accuracy of the ORNL results, this agreement is a good indication that the ORNL results are sufficiently reliable to make qualitative observations regarding the behavior of trace elements in a regenerative PFBC system. The ORNL results were used.

Table 21. Samples Analyzed in the Trace Element Study

Sample No.	Exp. No.	Sample Description
J-11270	REC-1K	Steady-state overflow sample of sulfated Tymochtee dolomite from first combustion cycle of 10-cycle combustion-regeneration experiment
J-11177	REC-1K	Same as for J-11270
J-11178	REC-10	Same as for J-11270 except that the dolomite is from the tenth combustion cycle
J-11179	CCS-10	Sulfated dolomite feed to the tenth regeneration cycle
J-11180	CCS-10	Steady-state sample of regenerated dolomite from the tenth regeneration cycle
J-11181	CCS-10	Steady-state sample of cyclone ash from the tenth regeneration cycle
J-11182	CCS-10	Sample of Triangle coal used in the tenth regeneration cycle
J-11183	CCS-10	Steady-state sample of ash that escaped from the cyclone and collected on a membrane filter during the tenth regeneration cycle

Trace Elements in Sulfated Tymochtee Dolomite Samples from the First and Tenth Combustion Cycles. Table 22 presents trace-element SSMS analyses for (1) samples of Tymochtee dolomite which had been sulfated only once and (2) samples which had been through nine sulfation-regeneration cycles and a tenth sulfation. Each of the samples in a pair (J-11270 and J-11177; J-11178 and J-11179) is expected to have similar compositions. The members of a pair are not, however, fractions of the same sample. The results for samples J-11178 and J-11179 are in excellent agreement. The agreement in results for samples J-11270 and J-11177 is less impressive, but is still considered quite good for nonduplicate samples.

The stability of trace elements in the sorbent during repeated utilization cycles was assessed by comparing the average concentrations of the elements in the samples of sulfated dolomite from the tenth combustion cycle with their average concentrations in the samples of sulfated dolomite from the first combustion cycle. In the comparisons, the average concentrations of the elements in the tenth-cycle-sulfated dolomite (Table 22) have each been

Table 22. Trace-Element Analyses for Tymochtee Dolomite Samples from the First and Tenth Combustion Cycles. (Concentrations are in ppm except where indicated otherwise.)<sup>a</sup>

Element	Sulfated Dolomite from First Combustion Cycle		Sulfated Dolomite From Tenth Combustion Cycle	
	Sample J-11270	Sample J-11177	Sample J-11178	Sample J-11179
<u>High-Toxicity</u>				
Be	≤ 5	<20	<20	<20
B	70	100	100	200
Cd	2 ± 0.4	4.5 ± 0.9	2.6 ± 0.6	1.8 ± 0.4
Co	<5	<10	20	20
Cr	20 ± 4	17 ± 3	100 ± 20	92 ± 18
Cu	30 ± 6	25 ± 5	33 ± 7	30 ± 6
F	100	---	---	---
Ni	100	240 ± 50	250 ± 50	350 ± 70
Tl	<1	0.1 ± 0.1	<1	1.3 ± 0.2
V	3	20	70	100
<u>Medium-Toxicity</u>				
Bi	<1	<1	<1	<1
Mo	<3	30 ± 6	40 ± 8	45 ± 9
Pb	4 ± 0.8	10 ± 2	10 ± 2	9 ± 2
Se	<10	<1	<1	<1
Ti	200	1000	1500	1500
Zn	25 ± 5	50 ± 10	110 ± 20	100 ± 20
<u>Low-Toxicity</u>				
As	10	2	7	10
Mn	60	70	70	100
<u>Toxicity Not Assessed</u>				
Al	2%	1%	2%	2%
Ba	50 ± 10	52 ± 10	180 ± 40	140 ± 30
Br	10	---	---	---
Ca	20%	20%	20%	20%
Cs	<1	---	---	---
Fe	5000 ± 1000	3600 ± 700	1.5 ± 0.3%	2 ± 0.4%
La	10	---	---	---
Ce	5	---	---	---
In	0.6 ± 0.1	0.5 ± 0.3	2 ± 0.4	1.5 ± 0.3
Pr	10	---	---	---
K	0.5%	0.6%	1%	0.6%
Li	2	---	---	---

(Cont'd.)

Table 22. (Cont'd.)

Element	Sulfated Dolomite from First Combustion Cycle		Sulfated Dolomite from Tenth Combustion Cycle	
	Sample J-11270	Sample J-11177	Sample J-11178	Sample J-11179
Toxicity Not Assessed (Cont'd.)				
Mg	10%	10%	10%	15%
Na	0.2%	0.5%	1%	1%
Nb	≤ 3	5	6	5
P	10	40	100	100
Nd	10	---	---	---
Sm	<5	---	---	---
Rb	20	30	20	25
S	10%	6%	7%	7%
Si	2%	≥2%	≥7%	≥7%
Sr	210 ± 40	190 ± 40	450 ± 90	450 ± 90
Th	<5	---	---	---
U	≤5	---	---	---
Y	2	---	---	---

<sup>a</sup>Factor-of-two accuracy except where indicated otherwise.

multiplied by 1.25 to adjust the concentrations of the ash-encrusted stone to the equivalent amount of virgin limestone in the once-sulfated stone. The sulfated dolomite from the tenth combustion cycle was encrusted with approximately 13 g of coal ash per 100 g of virgin dolomite sorbent.

Based on the analyses, it appears that the following elements were enriched in the ten combustion cycles: Cr, Tl, V, Mo, Zn, Ba, Fe, In, and Sr. The term "enriched" is applied here to an element which has a higher concentration in the sulfated dolomite from the tenth combustion cycle than in the sulfated dolomite from the first combustion cycle (consideration is given to the estimated accuracy of the analytical method for each element). The enrichment of these elements is undoubtedly related to the buildup of coal ash on the surface of the dolomite particles during repeated utilization cycles. Of the 31 elements for which samples from the first and tenth cycles were analyzed, none appeared to have been depleted during the ten cycles. Elements such as As, Cd, Cr, Pb, Ni, Se, Tl, and Zn, which have all exhibited a tendency to be volatile during coal combustion in conventional coal fired systems,<sup>34</sup> were either enriched or remained in the dolomite in approximately the same concentration during the ten combustion cycles.

Open Mass Balances Around the Regeneration Reactor During the Tenth Cycle Regeneration Step. Samples of the coal feed, the sulfated limestone feed to the regenerator, the regenerated sorbent, and the cyclone fly ash plus the fly ash that passed through the cyclones in the tenth cycle regeneration step were analyzed for trace elements to make mass balances. The material balances were open (the flue gas was not analyzed for volatile species) but can be used to indicate the distribution of trace elements in the various solids streams leaving the regenerator, as well as the potential loss of trace elements by volatilization.

Table 23 presents (1) the results reported by Oak Ridge for analysis of the samples by SSMS and (2) material balances based on those analyses and on the mass flow rates of the various solids streams.

Comparison of the concentration values in columns 3 and 4 of Table 23 (for the sulfated and regenerated sorbent) shows the stability of the 31 elements in the dolomite. Only the change in the concentration of nickel is greater than the estimated limits of analytical accuracy for the two samples; depletion of the nickel in the sorbent during regeneration is indicated. This result is not readily reconciled with the previous observation (based on Table 22 results), that concentrations of nickel in sorbent from the first and tenth combustion cycles were not significantly different, and may simply reflect analytical errors.

The open material balances for the 31 elements (Table 23) range from a low of ~39% for sulfur (does not include the SO<sub>2</sub> liberated during regeneration) to a high of ~130% for cadmium and manganese. The apparent depletion of nickel in the sorbent during regeneration resulted in a material balance for this element of only 48%. The low material balance for titanium (~57%) results from an unexplained loss of titanium in the system, as indicated by the low level of titanium in the ash from the cyclones and filter. The remaining material balances generally ranged from 70 to 130%. Due to the scatter, quantitative assessments of the behavior of the elements during regeneration are difficult. However, from the stability of the elements in the dolomite, it seems safe to conclude that the major influence of regeneration on trace-element emissions from an FBC system would result from the additional coal used as reductant in the regeneration step. Since this represents only a small fraction of the total coal requirement (~3%) of the FBC, the impact of regeneration on FBC emissions should be minor.

In conclusion, for the trace elements studied in the investigation, regeneration does not appear to result in the release of trace elements from the sorbent. A comparison of sulfated samples from the first and tenth combustion half-cycles actually indicated an increased concentration (in the dolomite) for 9 of the 31 elements studied. This is attributed to the buildup of coal ash on the sorbent over repeated utilization cycles. During a regeneration experiment, nickel was the only element which gave evidence of being depleted somewhat in the sorbent. However, analytical uncertainties prevent placing too much emphasis on this observation.

Table 23. Concentrations and Material Balances for Trace Elements in Steady-State Samples of Solids Entering and Leaving the Regeneration Reactor during the Tenth Regeneration Cycle

Element	Concentration <sup>a</sup> (in ppm except where noted otherwise)				Material Balance, %, (Out/In)x100
	Coal Feed	Sulfated Sorbent	Regenerated Sorbent	Cyclone Fly Ash + Filter Fly Ash	
<u>High-Toxicity</u>					
Be	<10	<20	<20	<20	--
B	10	200	200	200	91
Cd <sup>b</sup>	0.5	1.8	2.6	5.5	130
Co	7	20	20	20	87
Cr <sup>b</sup>	17	92	89	220	92
Cu <sup>b</sup>	80	30	30	110	73
Ni <sup>b</sup>	30	350	180	300	48
Tl <sup>b</sup>	0.2	1.3	1.7	1.4	120
V	30	100	120	40	100
<u>Medium-Toxicity</u>					
Bi	<1	<1	<1	<1	--
Mo <sup>b</sup>	6	45	40	28	78
Pb <sup>b</sup>	10	9	6	130	110
Se <sup>b</sup>	<1	<1	<1	<1	--
Ti	500	1500	1000	800	57
Zn <sup>b</sup>	35	100	130	170	110
<u>Low-Toxicity</u>					
As	0.5	10	10	5	88
Mn	5	100	150	30	130
<u>Toxicity Not Assessed</u>					
Al	2%	2%	1.5%	>2%	>60
Ba	94	140	130	350	83
Ca	0.2%	20%	22%	10%	98
Fe <sup>b</sup>	0.32%	2%	2.2%	1.6%	97
In <sup>b</sup>	0.2	1.5	1	1.1	60
K	1%	0.6%	1%	1.5%	120
Mg	0.05%	15%	15%	3%	88
Na	0.05%	1%	1%	1%	91
Nb	2	5	5	3	84
P	500	100	200	1000	120
Rb	10	25	30	50	110
S	0.1%	7%	3%	3%	39
Si	>2%	>7%	>4%	>5%	--
Sr <sup>b</sup>	150	450	400	450	81

<sup>a</sup>Accuracy estimated to be a factor of 2, except for elements for which other accuracy is indicated.

<sup>b</sup>Accuracy estimated to be +20% of stated value.



## TASK D. PARTICULATE CONTROL STUDIES

1. Evaluation of On-Line Light-Scattering Particle Analyzers  
(J. Montagna, G. W. Smith, and F. G. Teats)a. Introduction

In the development of pressurized fluidized-bed combustion (PFBC) systems, an on-line light-scattering particle analyzer for the flue gas could provide continuous particle size and loading analysis without disturbing the off-gas stream. These measurements would be used (1) in measuring the efficiency of upstream particulate-removing devices (cyclones and filters), (2) for establishing gas turbine performance at different particulate loadings, and (3) for protecting turbines or a test cascade in the event of a sudden system upset.

In a PFBC system, the flue gas will be at  $\sim 900^{\circ}\text{C}$  and  $\sim 1000$  kPa ( $\sim 10$  atm) between the boiler and the turbine. In the absence of an on-line particle analyzer, routine batch sampling of the hot off-gas (using inertial impactors) will be necessary. Batch sampling from a pressurized hot off-gas environment is difficult; another disadvantage is the long time lag between sampling and analysis of samples for this technique.

Two types of optical analyzers which have not yet been evaluated for fluidized-bed combustion applications were evaluated for characterizing the particles in a flue-gas stream that is representative of a stream that would be fed to a gas turbine. Both instruments use laser light beams. One is a single-particle analyzer (a particle morphokinometer, developed by Spectron Development Laboratory) which characterizes the scattered light from each particle (laser interferometer method), and the other is a Microtrac multi-particle analyzer developed by Leeds and Northrup, which characterizes the entire particle distribution in its optical path.

Single-Particle Analyzer. The principles of the Spectron single-particle analyzer are discussed by Farmer.<sup>35</sup> The experimental results obtained with this instrument and an evaluation of its performance were presented in the previous annual report (ANL/CEN/FE-77-3) and Reference 36.

Multiparticle Analyzer. The experimental results obtained using the multiparticle analyzer are reported here in summary form. Details of the study are available in another report in this series (ANL/CEN/FE-77-8) and in a topical report<sup>36</sup> published during the past year.

The Leeds and Northrup multiparticle analyzer used in this work utilizes a new measurement technique in which three measurements of the scattered light from a single laser beam directed into the off-gas duct are made. These measurements are used to determine the mean diameter and variance of the distribution for particles in the 1-50  $\mu\text{m}$  range. For particles with a unimodal size distribution, the size distribution can be obtained by examining the total scattering intensity as a function of scattering angle and laser beam polarization and by comparing the experimental data with theoretical calculations for assumed particle-size distributions.<sup>37</sup> One measured signal

is also proportional to the volume of the particles illuminated, making possible the calculation of the concentration of particles (loading) in the fluid stream.

#### b. System and Procedure for Flue-Gas Particle Measurements

The particle-size measurements were made in the flue-gas system of the ANL fluidized-bed combustion process development unit (PDU). Pairs of optical windows installed upstream from the primary cyclone and near the system outlet made it possible to size (1) the coarse entrained particles in the flue gas from the combustor, (2) the particles in the flue gas leaving the secondary cyclone, and (3) the very small particles in the flue gas leaving the sintered-metal filter assembly. The coarse particles leaving the combustor, previously determined to have a multimodal distribution, were not sized with the multiparticle analyzer, which is only suitable for unimodal distributions.

Particle-size measurements were obtained (1) using the on-line optical particle analyzer, (2) using an Andersen cascade impactor on gas samples extracted through sampling ports downstream from the optical window locations, and (3) using sieve and Coulter counter analysis of particulate samples obtained from cyclones and test filters. Particle-loading measurements were made by passing through glass fiber membrane filters the gas samples extracted through sampling ports.

The Coulter counter was calibrated with standard particles, and its measurements of particles in the flue gas agreed well with cascade-impactor measurements. Thus, it was assumed that these two measurements were representative of the true particle size distributions. The multiparticle analyzer was evaluated only by comparing its measurements with cascade impactor measurements.

#### c. Experimental Evaluation of the Multiparticle Analyzer

Measurement of Mean Particle Size. Table 24 lists the measured particle diameters and loadings for several experiments. Because less than 10% of the particles were smaller than  $1\text{ }\mu\text{m}$  (mass basis), the impactor distributions used for calculating the aerodynamic log-mean diameter, ( $\bar{D}_{AE}$ ) and loadings were not truncated to accommodate the range of the multiparticle analyzer ( $1\text{--}20\text{ }\mu\text{m}$  dia). When the loading (gravimetrically obtained) was relatively high ( $>0.1\text{ g/m}^3$  or  $>0.044\text{ grain/scf}$ ) in coal combustion experiments, the ( $\bar{D}_{AE}$ ) obtained with the impactor ranged from  $2$  to  $3.5\text{ }\mu\text{m}$  and the projected area mean diameter obtained with the multiparticle analyzer ( $\bar{D}_A$ ) ranged from  $2.2$  to  $3.4\text{ }\mu\text{m}$  for all suspended particle measurements. The volume mean diameters ( $\bar{D}_V$ ), also obtained with the multiparticle analyzer, ranged from  $2.9$  to  $5.5\text{ }\mu\text{m}$  for the same experiments.

In "cold" experiment LN-9-5, only elutriated virgin limestone particles were measured. The loading obtained with the Andersen impactor was also relatively high ( $>0.1\text{ g/m}^3$ );  $\bar{D}_A$  was  $2.7\text{ }\mu\text{m}$ , in comparison with  $1.5\text{ }\mu\text{m}$  for  $\bar{D}_{AE}$ . It had been expected that the measurements made with the various instruments on the suspended virgin limestone would agree better than those made on the mixture of particles during combustion experiments (LN-4, LN-5, LN-6). However, the agreement of  $\bar{D}_{AE}$  with  $\bar{D}_A$  for suspended particles from the combustion experiments was slightly better than for the measurements in the cold experiments under high-loading ( $>0.1\text{ g/m}^3$ ) conditions.

Table 24. Particle Sizes and Loadings Obtained with the Multiparticle Analyzer, the Andersen Impactor, and the Membrane Filter in Coal Combustion and Cold Elutriation Experiments.

FBC Combustor Conditions						
Pressure			308 kPa (3 atm)			
Temperature			855°C			
Fluidizing Gas Velocity			1 m/s			
Sorbent			Greer limestone			
Coal			Sewickley			
Exp.	Multiparticle Analyzer			Andersen Impactor		Membrane Filter
	$\bar{D}_V,^a$ $\mu\text{m}$	$\bar{D}_A,^b$ $\mu\text{m}$	Loading, $\text{g}/\text{m}^3$	$\bar{D}_{AE},^d$ $\mu\text{m}$	Loading, $\text{g}/\text{m}^3$	Loading, $\text{g}/\text{m}^3$
LN-4-1 <sup>e</sup>	5.1	2.8	0.43	2.2	0.33	0.64
LN-4-2 <sup>f</sup>	2.9	2.2	0.83	3.5	1.1	1.3
LN-5-1 <sup>e</sup>	5.5	3.4	0.18	6.0 <sup>g</sup>	0.21	0.41
LN-5-2 <sup>f</sup>	3.9	2.3	1.0	3.2	0.98	0.40
LN-6-1 <sup>e</sup>	4.4	2.8	0.46	3.0	0.12	0.54
LN-6-1 <sup>f</sup>	3.6	2.2	0.64	3.5	1.1	1.0
LN-10-3 <sup>f</sup>	3.8	2.2	1.5	2.0	0.56	-
LN-10-4 <sup>f</sup>	-	-	0.37	-	-	0.63
LN-11-1 <sup>e</sup>	11.9±0.3	5.5±0.11	0.12±0.01	1.9	0.01	0.009
LN-11-2 <sup>e</sup>	-	-	0.13±0.01	-	-	
LN-11-3 <sup>e</sup>	10.5±0.2	4.97±0.12	0.11±0.02	1.8	0.01	
LN-9-3 <sup>e,h</sup>	2.24±0.36	2.01±0.06	0.21±0.04	0.63	0.001	0.003
LN-9-2 <sup>e,h</sup>	-	-	0.10±0.02	-	-	
LN-9-5 <sup>f,h</sup>	3.77±0.23	2.72±0.07	1.20±0.06	1.5	0.115	0.110
LN-9-4 <sup>f,h</sup>	-	-	0.52±0.17	-	-	

<sup>a</sup>Volume mean diameter

<sup>b</sup>Projected particle area mean diameter

<sup>c</sup>1 g/m<sup>3</sup> = 0.437 grain/scf

<sup>d</sup>Aerodynamic mean diameter

<sup>e</sup>Downstream from sintered-metal filters

<sup>f</sup>Between secondary cyclone and filter

<sup>g</sup>Suspect. Possibly, unexpected particle reentrainment in the flue gas occurred.

<sup>h</sup>Cold elutriation experiments--only virgin limestone particles were fed

For particles leaving the cyclones (loadings  $\geq 0.1 \text{ g/m}^3$ ), there was better agreement between the mass log-mean diameter measurements made with the multiparticle analyzer and the impactor than between those made with the single-particle analyzer (only particles between 1.5 and 23.9  $\mu\text{m}$  were compared) and the Coulter counter. A loading of  $0.05 \text{ g/m}^3$  for particle diameters of 1-10  $\mu\text{m}$  is presently proposed as the approximate maximum tolerable loading for turbines. Because the particulate loading tolerances for turbines remain uncertain, it is desirable to have optical instruments capable of measuring particle loadings smaller than  $0.05 \text{ g/m}^3$ .

The agreement of  $\bar{D}_{AE}$  with  $\bar{D}_A$  was poorer for measurements made at lower loading conditions ( $< 0.01 \text{ g/m}^3$ ) in experiments LN-9 and LN-11 than in experiments at higher loadings. In these measurements at low loadings,  $\bar{D}_A$  was approximately three times as large as  $\bar{D}_{AE}$ . The aerodynamic mean diameter,  $\bar{D}_{AE}$ , ranged from 0.63 to 1.9  $\mu\text{m}$ , and  $\bar{D}_A$  ranged from 2.0 to 5.5  $\mu\text{m}$ . Since it was difficult to obtain accurate impactor measurements for the comparison, this agreement can be considered fair at this stage. Although, as previously reported<sup>36</sup>, particle size could be measured at low loadings with the multiparticle analyzer, no particle measurements could be made with the single particle analyzer at these low loadings because not enough particles passed through the sample space of that instrument.

Measurement of Particulate Loadings. In these experiments (Table 24), particulate loadings (as well as mean particle sizes) were determined with the multiparticle analyzer. Values obtained with the multiparticle analyzer were compared with values obtained by three backup methods. The amounts of particulate collected on a flue gas filter located downstream from the multiparticle analyzer windows and the sampling port provided one backup measurement. The other backup measurements utilized grab samples which consisted of (1) the particulate collected in the impactor, including a backup filter to the impactor, and (2) the material collected on a membrane filter.

For the measurements made during the combustion experiments (Table 24) in which the loadings were high ( $> 0.1 \text{ g/m}^3$ , gravimetrically obtained from impactor or membrane filter samples), the most disparate gravimetric loading value was one-fourth the loading measured with the multiparticle analyzer (Table 24). (The loadings from the multiparticle analyzer are proportional to the particulate density assumed, which in this work was  $1.0 \text{ g/cm}^3$ .) For many high loading measurements such as for LN-4-2, the gravimetric and multiparticle analyzer loadings were very similar.

Under low loading conditions ( $< 0.01 \text{ g/m}^3$ ), gravimetric loadings were one order of magnitude lower than the optical multiparticle analyzer loadings. The semicontinuous background loading signal from the multiparticle analyzer was compared with the background plus sample loading signal and was found to be only 4% greater than the background signal; this can account for the one-order-of-magnitude difference between the multiparticle analyzer loadings and the gravimetric loadings. These measurements at low loadings were made on suspended particles that had passed through sintered metal filters in the flue-gas system.

For the high-loading cold elutriation experiment (LN-9-4 and LN-9-5, Table 24), loadings determined gravimetrically were one order of magnitude smaller than those obtained in the high-loading hot experiments; for the low-loading cold elutriation experiments (LN-9-2 and LN-9-3), the measured

loadings were about two orders of magnitude smaller than in the low-loading hot experiments. The large difference between the gravimetric and optical data for experiment LN-9 may be due to an increase (over a period of one hour) in the multiparticle analyzer background signal during this cold experiment.

The average gas linear velocity in the flue-gas duct near the optical windows was  $\sim 30$  m/s during the cold experiments; during the hot combustion experiments, the linear gas velocity was only  $\sim 3$  m/s. A greater gas velocity creates more turbulence and a greater chance for particle buildup in the free space between the windows and the stream of flue gas and thus a higher background signal. The background signal was observed to decrease to normal after the flow of limestone-laden air was discontinued.

#### d. Conclusions

The multiparticle analyzer can characterize a distribution by providing the mean and a nongeometric variance of the distribution. However, only if the distribution is known and unimodal can the instrument describe the distribution of the particles. The distribution downstream from the cyclones of a PFBC system is expected to be log-normal, based on measurements in this and other studies. Therefore, particle distributions in this stream can be obtained from multiparticle analyzer measurements.

In measurements with the multiparticle analyzer at high loadings ( $>0.1$  g/m<sup>3</sup>), the projected particle area mean diameters were generally less than 25% smaller than the aerodynamic mass log-mean particle diameters determined with the impactor. At low loading conditions ( $<0.01$  g/m<sup>3</sup>), the mean diameters obtained with the multiparticle analyzer were approximately three times the log-mean diameters obtained with the impactor.

At high loadings, the most disparate gravimetric loading was one-fourth the loading measurement made with the multiparticle analyzer. However, many measurements made by these two techniques at these relatively high loadings were very similar. At low loadings ( $<0.01$  g/m<sup>3</sup>), the gravimetric loadings were one order of magnitude lower than the values obtained with the multiparticle analyzer. At these low loadings, the loading measurement signal of the multiparticle analyzer is only 4% greater than the background; this is a potential source of error. If the background signal can be reduced electronically or via cleaner windows and/or optical path, on-line measurements with this instrument to protect the gas turbines in PFBC systems will be very promising.

The multiparticle analyzer is at a stage of development allowing it to be used with little operator training. Compared to the single-particle analyzer previously tested, the multiparticle analyzer is a more advanced instrument and with some refinement can be useful now in the development of PFBC technology.

## 2. Particle Removal From Flue Gas

(W. Swift, G. Teats, A. R. Pumphrey, S. Smith, and J. Stockbar)

In pressurized fluidized-bed combustion, the hot flue gas from the combustor must be expanded through a gas turbine to recover energy and make the process economic. To prevent erosion of the turbine blades by particulate matter entrained in the flue gas, the particulate loading must be reduced to acceptably low levels.

Although the air-quality requirements for a gas turbine have yet to be experimentally demonstrated, estimates of what constitute "acceptably low levels" of particulate mass loading for a gas turbine generally range (depending on the particle size distribution from  $\sim 0.05$  to  $\sim 0.005$  g/m<sup>3</sup>).<sup>38</sup> If it is assumed that the loading in the flue gas as it leaves the combustor is of the order of 30 g/m<sup>3</sup>, the total particulate-removal efficiency required to meet the estimated turbine air quality requirements would be between 99.8 and 99.98%.

Existing devices readily adaptable to high-temperature, high-pressure particulate removal (e.g., conventional cyclones) are not very efficient in removing particulate matter with diameters smaller than  $\sim 10$   $\mu$ m. Achieving the "acceptable loading" necessary for PFBC requires, therefore, that highly efficient methods be developed for removing from flue gas the particulate solids having diameters between 2 and 10  $\mu$ m.

An experimental program is continuing at ANL to test and evaluate promising flue-gas cleaning methods in the off-gas system of the 15.2-cm-dia fluidized bed combustor. Techniques under investigation are granular-bed filtration, high-efficiency controlled-vortex cyclones, and acoustic agglomeration.

### a. Granular-Bed Filters

Granular-bed filters currently under development can be generally classified by the condition of the granular bed during filtration, i.e., fixed-bed, moving-bed, or fluidized-bed collectors. The concept of collection being investigated at ANL is the use of fresh or sulfated limestone or dolomite as granular-bed material in a fixed-bed collector with periodic bed replacement. Use of sorbent from the combustion process as the granular-bed material eliminates the need for "backflush" cleaning of the filter as in other fixed-bed concepts or for external cleaning and recycle of the granular bed as in moving-bed concepts. As is done with fixed granular beds that employ backflush cleaning, several granular-bed modules would be operated in parallel. Periodically, each module would be taken off line, and sorbent plus trapped particulate matter would be replaced with virgin bed material. The sorbent containing the trapped particulate matter could either be transferred to a regenerator (if sulfated sorbent from the combustor had been used as the filter medium) or disposed of.

To test the concept of using the sorbent material in a granular-bed filter, a small test-filter was assembled and installed in the flue-gas system of the ANL, 15.2-cm-dia fluidized-bed combustion PDU. The results of tests made using the test filter have been reported, as well as calculated

working ranges of parameters (ANL/CEN/FE-77-11 and ANL/CEN/FE-78-4). The following represents a summary of the previous reports.

Equipment and Experimental Procedure. The granular-bed test chamber is circular in cross section and can be modified to have an inside diameter of either 7.8 or 15.4 cm. The fixed, horizontal granular-bed filter is supported by a wire mesh screen. After the gas passes through the granular bed, the gas, now cleaned, exits through a port in the side of the granular-bed filter housing. Pressure taps located just above the top surface of the granular bed and below the support screen measure the pressure drop across the bed. A thermocouple just below the bed-support screen monitors the gas temperature during each test.

In a test of the granular-bed filter, a preweighed amount of bed material is charged into the granular-bed filter. While the fluidized-bed combustion system is brought to steady-state operating conditions, the flue gas (which has already passed through the primary and secondary cyclones), bypasses the granular-bed filter test loop. Once steady operating conditions are reached, the flow of flue gas is diverted through the granular-bed test loop. In the test loop, the flow of gas is either passed through the granular-bed filter or bypassed around the filter to a sample port where the flue gas is sampled using an Andersen cascade impactor and/or a membrane filter to determine particulate loading and/or size distribution.

During a granular-bed filtration cycle, the following quantities are recorded: (1) the initial pressure drop,  $\Delta P_i$ , across the granular-bed, (2) the pressure drop across the filter as a function of time, (3) the time for the pressure drop across the filter to equal  $\Delta P_i$  plus 6.9 kPa (1.0 psi), (4) the weight change of the granular bed during the filtration cycle, (5) the weight of material recovered on a sintered-metal filter downstream from the granular bed, and (6) the particulate sampler results.

Results. Experiments were performed to evaluate the effects of bed particle size, gas velocity, and bed depth on filtration efficiency of the granular bed. Virgin Tymochtee dolomite in two size ranges, -6 +14 mesh and -14 +30 mesh, were used in the experiments reported here. The mean particle diameters of the -6 +14 and -14 +30 mesh bed materials are  $\sim 2120$  and  $\sim 740$   $\mu\text{m}$ , respectively.

In experiments to measure the effect of bed depth on filtration efficiency for the -6 +14 mesh dolomite at a filtration velocity of 30 cm/s, filtration efficiency increased from  $\sim 91\%$  at a 5.1-cm bed depth to  $\sim 98\%$  at a 40.6-cm bed depth. In terms of filtration per unit depth, however, the filtration efficiency decreased from  $\sim 18\% / (\text{cm of bed})$  to  $\sim 2.4\% / (\text{cm of bed})$  when the bed depth was increased from 5.1 cm to 40.6 cm.

The effect of bed depth on filtration efficiency was also determined for the -14 +30 mesh dolomite. As with the -6 +14 mesh bed, a slight increase in filtration efficiency was indicated for a greater bed depth--from  $\sim 95\%$  at a 7.6-cm bed depth to  $\sim 97\%$  at a 30-cm bed depth. The small effect of bed depth on filtration efficiency for both the -14 +30 and -6 +14 mesh beds indicates that in both cases, filtration occurs at or near the bed surface.

A comparison of the results obtained for the two different mesh-size materials shows that at a filtration velocity of  $\sim 30$  cm/s, decreasing the mean bed-particle size from  $\sim 2120$   $\mu\text{m}$  to  $\sim 740$   $\mu\text{m}$  resulted in increased filtration efficiency over the range of bed depths used. Expressed in terms of percent penetration (100% - filtration efficiency), decreasing the particle size at the bed depths used reduced penetration by 35 to 40% (e.g., from 9% to 5%).

Tests designed to measure the effect of gas velocity on filtration efficiency have been inconclusive. Filtration tests were performed at gas velocities of 15, 30, and 60 cm/s. In addition to -6 +14 mesh and -14 +30 mesh beds of dolomite, sulfated limestone bed material obtained from the Pope, Evans, and Robbins atmospheric-bed test facility in Alexandria, West Virginia, was tested. Although this sulfated material had a mass mean particle diameter ( $\sim 700$   $\mu\text{m}$ ) approximately equal to that ( $\sim 740$   $\mu\text{m}$ ) of the -14 +30 mesh dolomite bed material, the sulfated limestone had a much broader particle size distribution (2 wt % on 6 mesh and 19 wt % smaller than 170 mesh).

For -6 +14 mesh virgin dolomite at a bed depth of 5.1 cm, no change in filtration efficiency was apparent over the range of velocities tested. However, for the -6 +14 mesh bed material at a bed depth of 20.4 cm and for the sulfated limestone at a bed depth of 5.1 cm, filtration efficiency apparently improved with decreasing gas velocity. The filtration efficiency for the sulfated bed material increased from 94% to 99% when the gas velocity was decreased from 60 cm/s to 15 cm/s, an 80% decrease in particle penetration through the bed. If this effect of velocity is real, it suggests that factors other than inertial impaction of the flue-gas particulate on the bed granules are important in governing particulate removal in the granular bed.

It is both interesting and encouraging to note that the best filtration results obtained in the tests reported here were obtained with the sulfated-limestone bed. This is considered to be the material most likely to be used in a practical application of the concept. The probable reason for its performance being superior to that of the sized bed materials is its broader particle-size distribution, and thus its lower bed porosity.

Particle loadings in the flue gas leaving the granular-bed filter generally ranged from 0.01 to 0.07 g/m<sup>3</sup>. These loadings fall in the higher end of the estimated range of acceptable particle loadings for gas-turbine operation, 0.05 to 0.005 g/m<sup>3</sup>.<sup>38</sup>

Because the particle loadings in the flue gas entering the granular-bed filter (which ranged from 0.3 to as high as 1.4 g/m<sup>3</sup>) could not be independently controlled, no attempt was made to correlate the particle loadings in the clean flue gas leaving the granular-bed filter with operating conditions.

Particle-size distributions of dust in the flue gas entering and leaving the granular-bed filter were also measured with the inertial impactor. Mass mean diameters of the dust, both entering and leaving the granular bed, were generally of the order of 2 to 4  $\mu\text{m}$ . Also, a comparison of inlet and outlet particle-size distributions revealed that filtration efficiency was constant over the range of dust particle sizes entering the filter, i.e., a 1- $\mu\text{m}$  dust particle entering the granular-bed filter was captured as efficiently



as was a 10- $\mu\text{m}$  dust particle entering the filter. This result was unexpected and may simply indicate that the sensitivity of the tests was insufficient to measure any effect.

It should be noted that dust leaving the filter generally contained between 10 and 25 wt % dust having particle diameters larger than 10  $\mu\text{m}$ . Thus, although the mass loadings in the flue gas leaving the granular-bed filter were within the range of the estimated requirements, the amount of >10- $\mu\text{m}$  particles in the effluent gas may prove to be too great to be acceptable. It should also be emphasized that the cascade impactor provides no information about particle sizes larger than 10  $\mu\text{m}$ . The distribution of large particles will have to be determined by other techniques.

The initial pressure drop across the clean bed at the beginning of a filtration cycle for gas velocities below 30 cm/s ranged from a low of  $\sim 1$  kPa (4 in. of  $\text{H}_2\text{O}$ ) for a 5.0-cm bed of the -6 +14 mesh bed material to a high of 15 kPa ( $\sim 60$  in. of  $\text{H}_2\text{O}$ ) for a 30-cm bed of -14 +30 mesh bed material. Although these pressure drops would be considered excessive in conventional particle-removal devices for atmospheric combustors, they are not unreasonable for PFBC applications.

The rate at which the pressure drop across the granular bed increased during a filtration experiment varied, depending on the efficiency of filtration; *i.e.*, the more efficiently the filter performed, the more rapidly the pressure drop across the filter increased. In one experiment in which the filtration efficiency was  $\sim 99\%$ , the initial pressure drop across the bed was  $\sim 7.7$  kPa (31 in. water gauge) and increased at a rate of  $\sim 17.6$  Pa/s (4.2 in. water gauge/min). At these conditions, the granular-bed filter would have to be regenerated quite frequently, perhaps every 0.5 h, to maintain an acceptable average pressure drop across the filter.

Assessment of PFBC Limestone Requirements and Granular-Bed Filter Design. A simple mass balance analysis was also performed to evaluate the compatibility of sorbent usage in a PFBC process with limestone requirements of the granular-bed filter. In the analysis, the rates of limestone usage and the gas volumetric flow for a 200-MWe electric PFBC were estimated and the permissible ranges of parameters such as bed thickness, gas velocity, and bed replacement rate for a granular-bed filter which would be compatible with the PFBC flows were assessed. The mass balance for the combustor (200 MWe) indicates that  $\sim 17.3$  Mg/h of solids overflow from the combustor would be available for use as filtration medium in the granular-bed filter. Based on a bulk density of  $1370 \text{ kg/m}^3$  for the sulfated sorbent,  $\sim 12.6 \text{ m}^3/\text{h}$  of the sulfated sorbent would be available for use in the granular-bed filter. Irrespective of the granular-bed filter design, a mass balance made on the filter indicates the maximum filter surface area as a function of granular-bed-filter thickness and frequency of filter regeneration, *i.e.*, the number of times the granular bed is changed per hour of operating time. The results of this analysis show that for a given bed thickness, the maximum total filter area which could be incorporated into the filter design decreases rapidly as the frequency of bed regeneration (cleaning) increases. At a bed thickness of 10 cm, for example, increasing the number of bed changes per hour from 0.5 to 3.0 decreases the maximum filter area possible from  $\sim 255 \text{ m}^2$  to  $\sim 42 \text{ m}^2$ .

The material balance around the combustor also provides the volumetric flow rate of the flue gas which would have to be filtered by the granular-bed filter. Thus, the linear velocity of the flue gas through the granular-bed filter can be calculated as a function of the filter surface area and the operating temperature and pressure.

The significant observation made from this analysis is that to maintain a relatively low gas velocity through the filter, *i.e.*, 0.1 to 0.2 m/s, a total filter surface area between  $\sim 160 \text{ m}^2$  and  $630 \text{ m}^2$  is required, depending on the system operating pressure. A granular-bed filter with an area of  $160 \text{ m}^2$  (the surface area necessary to handle  $227,000 \text{ m}^3$  of gas at  $815^\circ\text{C}$ , 2.02 MPa, and a gas velocity of 0.2 m/s) and with a filter thickness of 10 cm, would require bed replacement at intervals greater than one hour.

As indicated above, the pressure drop across the granular bed increased quite rapidly during those experiments in which high filtration efficiencies were obtained. In some experiments, the rate of pressure drop increase was as high as  $\sim 14.3 \text{ Pa/s}$  (1 psi every 8 min). Thus, with bed replacements at the rate of one per hour, the average pressure drop across the filter would be 30–35 kPa (4.5–5.0 psi). In order to reduce this very high value, the filter bed would have to be replaced more frequently, whereupon the limestone required for the filter would exceed that available from the PFBC process.

It should be emphasized, however, that the filtration experiment results presented above were obtained under conditions of high inlet particle loading, due to inefficient cyclones upstream from the granular-bed filter. Additional tests are planned (following the addition of a high-efficiency cyclone to the flue-gas system upstream from the granular-bed filter) to evaluate the granular bed with more realistic particle loadings and size distributions in the flue gas entering the granular-bed filter. Such additional tests will be necessary before filter performance can be evaluated along with the compatibility of sorbent usage in the PFBC process with material requirements of the granular-bed filter.

#### b. Acoustic Dust Conditioning

Acoustic dust conditioning is a technique used to enhance the natural tendency of polydispersed particulates to impact upon each other and agglomerate. Thus, the use of acoustics in controlling fine particle emissions is a process whereby the mean size of the effluent particles is significantly increased (and correspondingly their number is decreased) by exposure to high-intensity finite-amplitude acoustic fields. As described, acoustic dust conditioning is designed to increase the collection efficiency of downstream dust collectors.

Work is currently being carried out under subcontract at the University of Toronto to develop and fabricate a pulse-jet acoustic dust-conditioning system consisting of a pulse-jet sound generator, a resonant manifold, and an acoustic treatment section. A functional description of the various components in the system was given previously (ANL/CEN/FE-77-3). Reported here is the progress made at the University of Toronto toward completion of the fabricated pulse jet, acoustic dust-conditioning system which is to be installed in the flue-gas system of the ANL, 15.2-cm-dia combustor for testing and evaluation.

Pulse-Jet Development. Figure 22 is a photograph of a typical pulse jet used in the pulse-jet testing and development program. Pulse-jet development consisted of the fabrication of a number of pulse jets to test the effects of various geometrical configurations on the acoustic power and frequency range of the device. The objective, of course, was to achieve a high level of sound intensity, 155-160 dB, over a wide range of frequency. The geometrical parameters examined included:

1. The intake and exhaust-pipe geometry
2. Combustion-chamber length and diameter
3. Fuel-inlet nozzle geometry.

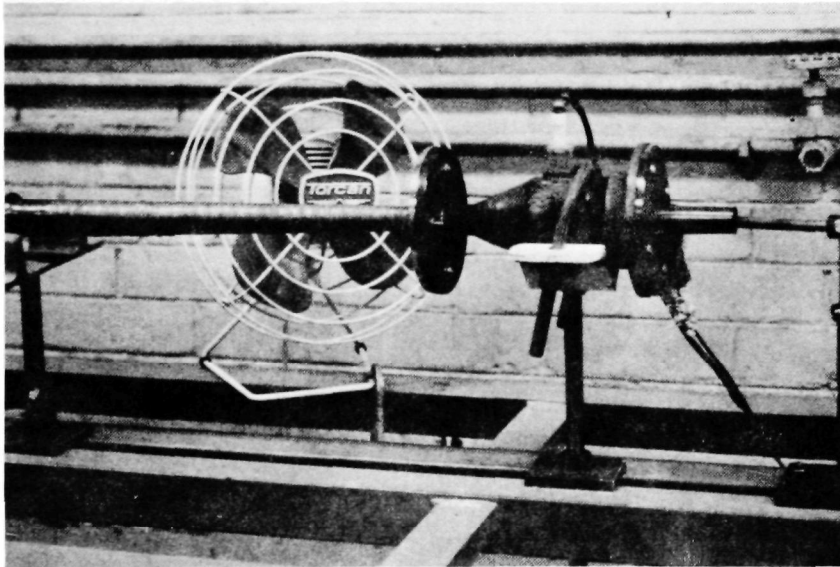


Fig. 22. Typical Pulse Jet Tested in the Pulse-Jet Development Program

Propane gas was used as fuel for the pulse jet. The unit was tested using six different combustion chambers of similar geometry but differing in length and diameter. Each combustion chamber was also tested with a variety of intake- and exhaust-pipe geometries. The following summarizes the state of development of the pulse jet:

1. A sound intensity of 155-160 dB has been obtained at a frequency of  $\sim 280$  Hz
2. Total thermal input to pulse jet is 40 to 45 kW
3. Combustion-chamber outer wall temperature can be maintained at  $370^{\circ}\text{C}$  ( $700^{\circ}\text{F}$ ), using forced-air-flow cooling
4. Tail-pipe inner surface temperature can be maintained below  $150^{\circ}\text{C}$  ( $300^{\circ}\text{F}$ ) by using forced-flow water cooling on its exterior surface
5. Cooling devices for the pulse jet remove  $\sim 12$  kW of the total thermal input of 40 to 45 kW.

All of the above results were obtained in testing at ambient pressure. Based on the unit which yielded the above results, a pulse-jet has been fabricated for subsequent testing at elevated pressures.

Resonant Manifold. The resonant manifold system (RMS), shown schematically in relationship to the pulse jet in Fig. 23, is also under development. As with the pulse jet, the manifold is being tested at ambient pressure prior to high-pressure testing. The RMS, in conjunction with the pulse jet, has been tuned at ambient pressure with a sliding piston, whose location can be adjusted through the downstream opening of the resonant manifold.

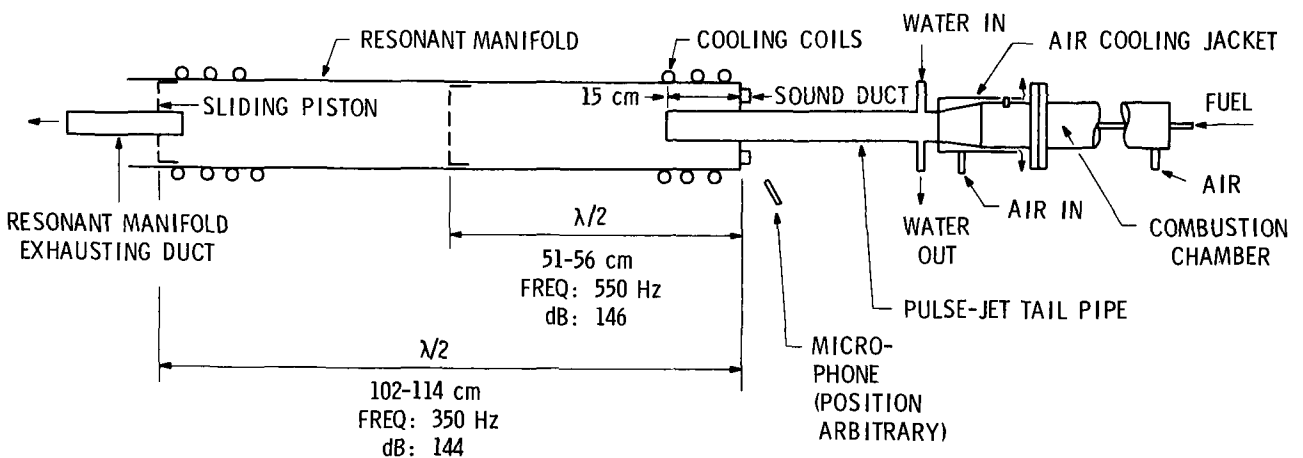


Fig. 23. Schematic of the Pulse Jet/Resonant Manifold System

Two locations of the resonant manifold and the corresponding half-wavelengths (as well as their respective frequencies) are also indicated in Fig. 23. They were determined by calculation and were confirmed by experimental measurement.

The entire length of the RMS is cooled by water flowing through a copper coil wound on the outside wall of the manifold. The outer wall temperature was maintained between 210 and 270°C. Approximately 16 kW of energy is removed by cooling of the manifold.

The variation in sound intensity between a tuned and untuned RM length can be as much as 10 dB. The RMS exhausting duct is not tuned with respect to the sliding piston to muffle the sound from the duct; the sound for the acoustic dust-conditioning system will be extracted from the opposing (upstream) sound duct(s) (see Fig. 23).

Fabrication of components for the high-pressure manifold has been completed. The design of the unit is basically that of the ambient-pressure unit illustrated in Fig. 23.

Pressure and Flow Controls. Installation of the pulse-jet/RMS as an integral part of the ANL FBC unit for testing requires that pressure and flow control between the two systems be controllable so that the two systems can be isolated from each other in case of emergency. The control system has been designed and is currently being set up at the University of Toronto for testing.

As soon as all three units (the pulse-jet, the resonant manifold, and the pressure and flow control system) have been operated satisfactorily as a unit at elevated pressure, the system will be transported to ANL for testing of its effectiveness in reducing particulate emissions from the ANL combustor.

c. High-Efficiency Cyclone

A high-efficiency, controlled-vortex cyclone (TAN-JET) has been obtained from the Donaldson Co. and has been installed in the flue gas system of the ANL combustor as a secondary cyclone. Experiments to evaluate the performance of the unit as a particulate-removal device are being initiated. In addition to testing of the cyclone's performance, the unit is intended to permit testing of the granular-bed filter under conditions of reduced loading from that previously used in granular-bed experiments. In addition, the cyclone will be extremely helpful in evaluating the capability of the pulse-jet acoustic agglomeration system for increasing the particle-removal efficiency of mechanical collectors.

## MISCELLANEOUS STUDIES

1. Pulsed L-Valve Tests  
(W. M. Swift)

a. Introduction

The L-valve is a type of a nonmechanical valve which can be used to control the flow of particulate solids into either dense-phase or lean-phase media, such as fluidized beds or pneumatic conveying lines. This valve, which uses a relatively small amount of aeration gas to control the flow of solids through the valve, has several advantages over mechanical valves: It is very inexpensive, has no moving parts subject to wear or seizure, and can be used in high-temperature and/or high-pressure environments.

In an L-valve, solids flow by gravity from the hopper into the top of the L-valve. By use of a timer and a solenoid valve, aeration gas is pulsed or supplied continuously at right angles to the solids downward flow. The gas transports the solids horizontally in dense-phase flow to the point where the solids are discharged into a pneumatic transport line or a fluidized-bed.

The L-valve has been used in various applications for a number of years. Only recently, however, were the effects of geometrical and particle parameters on the performance of an L-valve reported in the literature.<sup>39</sup> Specifically, the effects of pipe length and diameter, particle size and density, and the location of the aeration gas inlet on L-valve performance were reported.

ANL is interested in applying the L-valve to feed systems for fluidized-bed combustors. In particular, there is interest in adapting the L-valve to controlling solids feed rates for ANL's fluidized-bed combustion and sorbent-regeneration process development units. The process development units, however, require relatively low solids feed rates as compared with the high solids throughputs usually achieved with an L-valve. A 15.4-cm-dia atmospheric combustor, for example, requires feed rates of approximately 3.5 kg/h of coal and 1.1 kg/h of dolomite; in comparison, a feed rate as high as 9000 kg/h is reported in the literature<sup>39</sup> for a 7.6-cm ( $\sim 3$ -in.) L-valve with an aeration-gas flow rate of only 0.9 L/s ( $\sim 1.8$  ft<sup>3</sup>/min).

In an existing application of an L-valve at ANL for feeding sulfated sorbent to a regeneration reactor, the required feed rates are obtained by pulsing the L-valve aeration gas. By use of a 12.5-mm (3/8-in. pipe) L-valve, feed rates of 27 kg/h and less are obtained, using cycle times of  $>2$  s and an aeration period of  $\sim 0.5$  s/cycle. It is calculated that a feed rate of  $\sim 3.5$  kg/h would require a cycle time of  $\sim 16$  s. Thus, at low feed rates, feeding would be highly discontinuous.

A test program was performed to develop an L-valve feeder capable of operating at low solids feed rates and employing very short L-valve cycle times. The design performance requirements were that the valve be capable of feeding pulverized coal at the rate of 3.4 kg/h and of feeding dolomite at a rate of 1.1 kg/h. A minimum cycle rate of 1 cycle/s for coal feeding was specified to limit the coal feed increments to no greater than 5% of the burnout rate of 20 s assumed for the combustor. Cycle rates as low as 0.2 cycle/s were considered acceptable for dolomite feeding. L-valve aeration duty was to be held between 10 and 40% of the total cycle time. For coal feeding, a feed-rate variability of less than 2% between any two consecutive 100-s feed periods and less than 10% between any two 100-s periods greater than one hour apart were requirements for acceptable L-valve operation. The results of this study have been reported in detail in a recent quarterly report (ANL/CEN/FE-78-3). The following represents a summary of the significant findings.

#### b. Equipment and Procedure

The L-valve was a standard 9.52-mm (3/8 in.) stainless steel tubing cross fitting. The solids flowed from the bottom of the solids hopper in gravity flow down through a 25.4-mm (1-in.) downcomer line to the L-valve. The aeration gas entered the L-valve at right angles to the solids downward flow and transported the solids in dense-phase flow to a point where they again could fall under gravity flow into a pneumatic transport line. A rotameter in the aeration-gas line qualitatively indicated gas flow during the timed aeration pulses. The solenoid valve controlling the flow of L-valve aeration gas was operated by a timer which had a cycle-time capability of 0.1 to 9.9 s in 0.1-s increments; the solenoid-open capability ranged from 0.1 to 0.9 s in 0.1-s intervals.

A solid 9.52-mm rod was inserted into the L-valve through the downward-oriented leg of the cross fitting. The depth of penetration of the rod into the L-valve was adjustable, providing additional control of the solids flow rate.

Triangle coal ( $\sim 85$  wt % between 90 and 710  $\mu\text{m}$ ) and virgin Greer limestone ( $\sim 75$  wt % between 600 and 1400  $\mu\text{m}$ ) were used in the L-valve feeder tests. Tests to measure feeding rates were made using either the coal or a mixture of three parts by weight coal and one part by weight limestone.

### c. Test Results

Tests A1 to A3 represent three consecutive 100-s coal feeding tests using identical conditions--an aeration cycle time of 1.0 s and an aeration pulse of 0.2 s. The variance in feed rate between tests A2 and A1 was 2.0%; between tests A3 and A2, the variance was 3.3%.

In coal feeding tests B1 to B4, the conditions were identical to those for A1 to A3 except that the aeration-pulse duration was 0.1 s. The maximum variation in feed rate between any two consecutive feed intervals was 1.2%. The maximum deviation in feed rate of any feed period from the average feed rate was also 1.2%.

An examination of test results for series A and B illustrates the sensitivity of the feed rate to changes in aeration pulse time. Decreasing the aeration pulse from 0.2 s to 0.1 s at a total cycle time of 1.0 s decreased the feed rate by 25%--i.e., from 5.6 kg/h to 4.2 kg/h. To provide a finer control of feed rate, a timer capable of 0.01-s increments in both cycle and pulse duration time would be desirable.

Test series C and D (three experiments in each series) were done under conditions identical to those in series B except that the cycle time was 1.1 s in series C and 1.2 s in series D. Cycle times above 1.0 s exceed the specification originally set for each coal feed increment. At 1.2-s cycle time, however, the coal feed rate of 3.5 kg/h was very close to the design feed rate of 3.4 kg/h. Possibly, the same result could have been achieved at a 1.0-s cycle time if the timer had been capable of aeration pulses shorter than 0.1 s. It was noted that the feed rate (in terms of g/aeration pulse) decreased slightly with small increases in cycle time.

For test series E (2 tests), the rod was inserted into the bottom of the cross, extending to the centerline of the horizontal run of the L-valve. At the same test conditions as were used in the D-series runs (1.2-s cycle time; 0.1-s aeration pulse), the feed rate in E1 was approximately 20% lower with the rod inserted. In run E2, with a cycle time of 1.0 s and an aeration pulse of 0.1 s, the design feed rate of 3.4 kg/h was obtained.

The remaining experiments tested the premixing of coal and sorbent (mixtures contained 75 wt % coal) to achieve the design combined feed rate of 4.5 kg/h. No feed tests were made with dolomite alone, but feed rates near the 1.1 kg/h specified could very likely have been achieved by using the specified maximum cycle time of 5 s.

Tests F1 through F4 (with cycle times of 1.0 or 0.9 s and aeration pulse durations of 0.1 s) were the initial feed tests with the coal-limestone mixture. After test F1 with a cycle time of 1.0 s and a feed rate of 4.1 kg/h, the cycle time was reduced to 0.9 s and a feed rate of 4.4 kg/h was obtained. This feed rate is very close to the design feed conditions of

4.5 kg/h. The F-series test results also illustrate the sensitivity of the feeder to changes in cycle time. Decreasing the cycle time by 10% (from 1.0 to 0.9 s) increased the feed rate by ~8%.

Three H-series experiments, also performed with the coal-limestone mixture, a 0.9-s cycle time, and a 0.1-s aeration pulse, consisted of consecutive tests of 1200-s duration. The maximum variation in feed rate between any two tests was less than 1%. The results were also in good agreement with the results of tests performed at test durations of 100 s.

In the final set of tests, series J with 100-s duration, 1.0-s cycle time, and 0.1 or 0.2-s aeration pulse, the effect of decreasing the pressure drop across the solenoid valve was investigated. In the previous tests, the pressure in a surge tank in the aeration gas supply line was ~190 kPa (28 psia) with the L-valve feeding to ambient pressure. For the J-series experiments, the surge tank pressure was lowered to ~14 kPa. A comparison of experimental results shows that decreasing the pressure in the surge tank in one test decreased the feed rate ~10%--from 4.1 kg/h to 3.7 kg/h. By then increasing the aeration pulse from 0.1 to 0.2 s in three other tests, the feed rate was increased by ~25% to ~4.6 kg/h.

In conclusion, the test results demonstrate the potential of a pulsed L-valve feeder for providing low flow rates of solid materials. Problems of plugging in the L-valve were not encountered, even though the largest limestone particle fed, ~1400  $\mu\text{m}$ , was less than a factor of 6 smaller than the ID of the L-valve. Variations in solids feed rates at fixed test conditions were generally within the rigid specifications set forth in the test plan. With additional refinement of the L-valve timer to allow it to control the cycle time and pulse duration to 0.01-s intervals, the L-valve could be easily adapted to on-line control.



## APPENDIX A

## Compositions (wt %) of Limestones and Dolomites

Limestone	CaCO <sub>3</sub>	MgCO <sub>3</sub>	Fe <sub>2</sub> O <sub>3</sub>	Al <sub>2</sub> O <sub>3</sub>	SiO <sub>2</sub>	Na <sub>2</sub> O	K <sub>2</sub> O
ANL-4801	48.7	40.2	0.66	1.81	7.0	0.09	0.38
ANL-4901	49.9	43.0	1.69	0.93	1.69	0.05	0.12
ANL-4902	49.7	43.8	0.43	0.87	5.71	0.03	0.30
ANL-4903	49.2	44.6	0.52	0.90	8.77	0.05	0.50
ANL-5001	50.4	43.0	0.37	0.98	3.52	0.34	0.10
ANL-5101 (Tymochtee)	51.8	43.3	0.41	1.46	3.61	0.07	--
ANL-5102	51.2	43.4	0.62	0.43	1.2	0.05	0.19
ANL-5201	52.2	43.0	0.26	0.68	1.22	0.07	0.13
ANL-5202	52.7	42.0	0.34	0.87	1.60	0.11	0.15
ANL-5203	52.6	36.4	0.58	1.13	8.77	0.04	0.18
ANL-5204	52.9	45.8	0.25	0.04	0.54	0.04	0.01
ANL-5205	52.1	41.0	0.07	0.16	3.79	0.04	0.01
ANL-5206	52.7	42.2	0.13	0.25	1.14	0.05	0.02
ANL-5207	52.3	37.5	2.35	1.0	3.64	0.09	0.16
ANL-5301 (1337)	53.4	45.4	0.07	0.08	0.69	0.05	--
ANL-5302	53.9	44.9	0.16	0.43	1.35	0.03	0.07
ANL-5303	53.7	42.8	0.30	0.31	2.94	0.04	0.10
ANL-5304	53.5	3.7	2.33	0.73	36.12	0.16	0.41
ANL-5401	54.5	42.9	0.07	0.34	1.04	0.04	0.1
ANL-5402	54.9	27.3	2.73	1.10	10.14	0.08	0.43
ANL-5403	54.0	44.1	0.08	0.17	0.62	0.03	0.07
ANL-5501	55.6	43.3	0.23	0.18	2.97	0.03	0.03
ANL-5601 (Dolowhite)	56.8	45.6	0.09	0.01	0.18	0.02	--
ANL-5602	56.6	43.8	0.33	0.18	1.05	0.03	0.09
ANL-5603	56.3	41.7	0.46	0.60	1.08	0.2	0.22
ANL-5801	48.7	40.2	0.66	1.81	7.0	0.09	0.38
ANL-6101 (1351)	61.2	28.7	5.56	0.51	3.15	0.13	--
ANL-6301	63.2	32.6	0.39	0.28	2.54	0.04	0.05
ANL-6401	64.2	29.5	0.33	0.69	5.10	0.15	0.31
ANL-6501	65.9	31.5	0.38	0.28	2.08	0.04	0.05
ANL-6701	67.3	31.5	0.37	0.22	1.25	0.04	0.15
ANL-6702	67.5	0.91	0.08	0.18	30.22	0.08	0.13
ANL-7401	74.7	10.2	1.07	1.82	11.2	0.19	0.36
ANL-8001 (Greer)	80.4	3.5	1.24	3.18	10.34	0.23	--
ANL-8101 (1360)	81.6	11.6	0.86	0.19	1.86	0.10	--
ANL-8301	83.9	13.4	0.14	0.42	1.24	0.02	0.02
ANL-8701 (Chaney)	87.0	1.2	3.4	2.0	7.1	<0.1	--
ANL-8901 (1343)	89.8	2.2	0.66	1.04	4.0	--	--
ANL-8902	89.6	3.02	0.37	0.79	5.06	0.03	0.29
ANL-8903	89.3	1.21	0.98	0.83	5.5	0.12	0.22
ANL-9201 (1336)	92.6	5.3	0.2	0.42	1.26	0.10	--
ANL-9401	94.1	1.0	0.35	0.51	3.18	0.05	0.10
ANL-9402	94.7	0.87	0.14	0.23	0.63	0.02	0.02
ANL-9501 (Grove or 1359)	95.3	1.3	0.09	0.25	0.77	0.03	--

(Cont'd.)

## Appendix A (Cont'd.)

Limestone	CaCO <sub>3</sub>	MgCO <sub>3</sub>	Fe <sub>2</sub> O <sub>3</sub>	Al <sub>2</sub> O <sub>3</sub>	SiO <sub>2</sub>	Na <sub>2</sub> O	K <sub>2</sub> O
ANL-9502	95.6	3.36	0.05	0.11	0.42	0.02	0.04
ANL-9503	95.5	0.76	0.05	0.13	0.15	0.02	<0.01
ANL-9504	95.8	0.58	0.30	0.36	2.71	0.05	0.13
ANL-9505	95.1	3.47	0.90	0.29	0.70	0.04	0.03
ANL-9601 (2203)	96.5	3.3	0.17	<0.01	0.20	0.05	0.01
ANL-9602	96.2	0.43	0.12	0.21	1.19	0.03	0.01
ANL-9603	96.4	1.56	0.10	0.30	0.70	0.05	0.11
ANL-9701 (Germany Valley)	97.8	0.6	0.10	1.8	0.2	0.25	--
ANL-9702	97.5	0.68	0.05	0.05	0.21	0.01	0.01
ANL-9703	97.6	0.58	0.19	0.50	1.08	0.03	0.17
ANL-9704	97.8	0.34	0.30	0.05	0.15	0.04	0.02
ANL-9705	97.3	0.53	0.17	0.35	0.20	0.05	0.01
ANL-9706	97.3	0.98	0.08	0.06	0.23	0.03	0.01
ANL-9801	98.3	0.6	0.15	0.16	0.20	0.04	0.20
ANL-9802	98.2	0.47	0.18	0.10	0.29	0.04	0.01
ANL-9803	98.0	1.26	0.07	0.14	1.47	0.02	0.02
ANL-9901	99.1	0.60	0.05	0.06	0.17	<0.013	<0.01
ANL-9902	99.1	0.38	0.05	0.04	0.13	0.04	0.01
ANL-9903	99.8	0.53	0.02	0.16	0.24	0.20	0.01

## APPENDIX B

## Limestone Designations and Suppliers

Limestone	Limestone Supplier	Location
ANL-4801	Midwest Aggregates Corp.	Fort Wayne, IN
ANL-4901	--	
ANL-4902	Vulcan Materials	Monroe, WI
ANL-4903	Black Creek Limestone Co.	McCook Complex, IL
ANL-5001	Harris Limestone Co.	Piedmont, MO
ANL-5101 (Tymochtee)	E. F. Duff and Sons	Huntsville, OH
ANL-5102	Porter Limestone Co.	Rockton, IL
ANL-5201	Midwest Aggregates Corp.	Fort Wayne, IN
ANL-5202	Midwest Aggregates Corp.	Fort Wayne, IN
ANL-5203	Bullitt County Stone Co.	Shepardville, KY
ANL-5204	James River Limestone Co.	Buchanan, VA
ANL-5205	Mayville White Lime Works	Mayville, WI
ANL-5206	Mayville White Lime Works	Mayville, WI
ANL-5207	Quapaw Co.	Drumwright, OK
ANL-5303 (1337)	Chas Pfizer Co.	Gibonsville, OH
ANL-5302	Vulcan Materials Co.	Birmingham, AL
ANL-5303	May Stone and Sand	Fort Wayne, IN
ANL-5304	Vulcan Materials Co.	Parsons, TN
ANL-5401	Delta Mining Co.	Mill Creek, OK
ANL-5402	Raid Quarries (Medusa Aggregates)	Burlington, IA
ANL-5403	U.S. Steel Corp.	Chicago, IL
ANL-5501	Lime Products Corp.	Union, ME
ANL-5601 (Dolowhite)	Kaiser Refractories	Salinas, CA
ANL-5602	G. & W. H. Corson, Inc.	Plymouth Meeting, PA
ANL-5603	York Stone Co.	York, PA
ANL-6101 (1351)	Jeffery Limestone Co.	Parma, MI
ANL-6301	Meshberger Stone, Inc.	Columbus, IN
ANL-6401	G. & W. H. Corson, Inc.	Plymouth Meeting, PA
ANL-6501	Meshberger Stone, Inc.	Columbus, IN
ANL-6701	Osmundson Bros.	Adams, MN
ANL-6702	Vulcan Materials Co.	Parsons, TN

(Cont'd.)

## APPENDIX B (Cont'd.)

Limestone	Limestone Supplier	Location
ANL-7401	Fort Calhoun Limestone Co.	Fort Calhoun, NE
ANL-8001 (Greer)	Greer Limestone Co.	Morgantown, WV
ANL-8101 (1360)	Monmouth Stone Co.	Monmouth, IL
ANL-8301	Vulcan Materials Co.	Birmingham, AL
ANL-8701 (Chaney)	--	--
ANL-8901 (1343)	Hooper Brothers Quarry	Weeping Water, NE
ANL-8902	Vulcan Materials Co.	Parsons, TN
ANL-8903	Civil Bend Bethany Falls	Bethany, MO
ANL-9201 (1336)	Georgia Marble Co.	Tate, GA
ANL-9401	Pete Lien and Sons	Rapid City, SD
ANL-9402	Lime Products Corp.	Union, ME
ANL-9501 (Grove or 1359)	Grove Lime Co.	Stephens City, VA
ANL-9502	American Aggregates	Indianapolis, IN
ANL-9503	Southern Materials	Ocala, FL
ANL-9504	Rose Equipment, Inc.	Weeping Water, NE
ANL-9505	Midwest Minerals	Pittsburgh, KS
ANL-9601 (2203)	Columbia Quarry Co.	Valmeyer, IL
ANL-9602	Delta Mining Corp.	Mill Creek, OK
ANL-9603	G. & W. H. Corson, Inc.	Plymouth Meeting, PA
ANL-9701 (Germany Valley)	Greer Limestone Co.	Morgantown, WV
ANL-9702	Hemphill Brothers	Seattle, WA
ANL-9703	Austin White Lime Co.	McNeil, TX
ANL-9704	Midwest Limestone Co.	Gilmore, City, IA
ANL-9705	Western Materials Co.	Orleans, IL
ANL-9706	U.S. Steel Corp.	Chicago, IL
ANL-9801	Iowa Limestone Co.	Alden, IA
ANL-9802	Chem. Lime Inc.	Clifton, TX
ANL-9803	Rigsby and Barnard Quarry	Cave In Rock, IL
ANL-9901	Western Materials Co.	Orleans, IN
ANL-9902	Southern Materials	Ocala, FL
ANL-9903	Calcium Carbonate Co.	Fort Dodge, IA

## REFERENCES

1. J. A. Shearer, I. Johnson, and C. B. Turner, The Effect of Sodium Chloride on the Reaction of SO<sub>2</sub>/O<sub>2</sub> Mixtures with Limestones and Dolomites, Argonne National Laboratory Report ANL/CEN/FE-78-8 (July 1978).
2. D. L. Keairns et al., Fluidized-Bed Combustion Process Evaluation, Phase II, Pressurized Fluidized-Bed Coal Combustion Development, Report EPA-650/2-75-027-C, Westinghouse Research Laboratory, Pittsburgh, Pennsylvania (Sept. 1975)
- 2a. D. A. Wenz, I. Johnson, and R. D. Wolson, J. Chem. Eng. Data 14(2), 250-252 (1969).
3. G. J. Vogel et al., Regeneration of Sulfated Limestone from FBCs and Corrosive Effects of Sulfation Accelerators in FBCs, Annual Report, July 1977-September 1978, Argonne National Laboratory Report ANL/CEN/FE-78-13.
4. G. J. Vogel et al., A Development Program on Pressurized Fluidized-Bed Combustion. Annual Report July 1, 1974-June 30, 1975, Argonne National Laboratory Report ANL/ES-CEN-1011.
5. T. A. Hendrickson, Synthetic Fuels Data Handbook, Cameron Engineers, Inc., Denver, p. 7 (1975).
6. R. B. Snyder, W. I. Wilson, Irving Johnson, and A. A. Jonke, Synthetic Sorbents for Removal of Sulfur Dioxide in Fluidized-Bed Combustion, Argonne National Laboratory Report ANL/CEN/FE-77-1.
7. R. B. Snyder, W. Ira Wilson, and Irving Johnson, The Prediction of Limestone Requirements for SO<sub>2</sub> Emission Control in Atmospheric Fluidized Bed Combustion, presented at the 5th International Conference on Fluidized-Bed Combustion, Washington, DC, December 1977.
8. John E. Mesko, Multicell Fluidized-Bed Boiler Design, Construction, and Test Program, ERDA Report FE-1237-Q76-3 (Mar. 1976).
9. S. S. Strom et al., Preliminary Evaluation of Atmospheric Pressure Fluidized-Bed Combustion Applied to Electric Utility Large Steam Generators, EPRI Report RP 412-1, interim report, Alliance, Ohio (Feb. 1976).
10. Robert L. Gall, Joseph S. Mei, and John S. Wilson, Fluidized-Bed Combustion Test of Low-Quality Fuels--1. Anthracite Refuse, Morgantown Energy Research Center, Morgantown, West Virginia (May 1977).
11. R. C. Hoke et al., Studies of the Pressurized Fluidized-Bed Coal Combustion Process, Report EPA-600/7-76-011, Exxon Research and Engineering Company, Linden, New Jersey (Sept. 1976).
12. Neil H. Coates (Ed.), Fluidized-Bed Combustion, Mitre Corporation, McLean, Virginia (May 1976).
13. E. P. O'Neil, D. L. Keairns, and W. F. Kittle, Thermochem. Acta 14, 209 (1976).

14. M. Hartman and R. Coughlin, A.I.C.h.E. J. 22, 490 (1976).
15. E. B. Robinson, R. D. Glenn, S. Ehrlich, J. W. Bishop, and J. S. Gordin, Study of Characterization and Control of Air Pollutants from a Fluidized-Bed Combustion Unit - The Carbon Burnup Cell, EPA Contract CPA 70-10, Pope, Evans, and Robbins (Feb. 1972).
16. H. B. Lange and C. L. Chen, SO<sub>2</sub> Absorption in Fluidized Bed Combustion of Coal--Effect of Limestone Particle Size, EPRI Project No. RP 719-1, The Babcock and Wilcox Co., Alliance, Ohio (Mar. 1977).
17. Reduction of Atmospheric Pollution, National Coal Board, London England, Reference No. DHB 060971 (Sept. 1971).
18. A. A. Jonke et al., Reduction of Atmospheric Pollution by the Application of Fluidized-Bed Combustion, Argonne National Laboratory Report ANL/ES-CEN-1004 (June 1971).
19. W. T. Reid, External Corrosion and Deposits-Boilers and Gas Turbines, American Elsevier Publishing Company, New York, p. 140 (1971).
20. P. H. Tufle and W. Beckering, A Proposed Mechanism for Ash Fouling Burning Northern Great Plains Lignite, J. Eng. Power, Trans. ASME, 407 (1975).
21. G. H. Gronhovd, W. Beckering, and P. H. Tufle, Study of Factors Affecting Ash Deposition from Lignite and Other Coals, ASME Winter Annual Meeting, Los Angeles, Calif. Nov. 16-20, 1969. p. 9.
22. L. E. Paulson and W. W. Fowkes, Changes in Ash Composition of North Dakota Lignite Treated by Ion Exchange, U.S. Bureau of Mines RI 7176, p. 18 (1968).
23. K. E. Phillips, Energy Conversion from Coal Utilization CPU-400 Technology, Annual Report for July 1974 - June 1975, Combustion Power Co., Inc., Report FE-1536-A1.
24. R. R. Ruch, H. J. Gluskoter, and N. F. Shimp, Occurrence and Distribution of Potentially Volatile Trace Elements in Coal, Final Report, Illinois State Geological Survey, No. 72 (Aug. 1974).
25. An Investigation of Hot Corrosion and Erosion Occurring in a Fluid Bed Combustion-Gas Turbine Cycle Using Coal as Fuel, FE/1536-2, Westinghouse Research Laboratory (May 1977).
26. H. E. Lunt, Hot Corrosion in Gas Turbine, preprint, presented at the Winter Annual Meeting of ASME, Atlanta, Georgia, Nov. 27-Dec. 2, 1977.
27. J. Szekely, J. W. Evans, and H. T. Sohn, Gas-Solid Reactions, Academic Press, Inc., New York, Chap. 2 (1976).

28. W. M. Swift, G. J. Vogel, A. F. Panek, Potential of Fluidized-Bed Combustion for Reducing Trace-Element Emissions, Paper No. 75-46.3, presented at the 68th Annual Meeting of the Air Pollution Control Association, Boston, Mass., June 15-20, 1975.
29. W. M. Swift, G. J. Vogel, A. F. Panek, and A. A. Jonke, Trace-Element Mass Balances around a Bench-Scale Combustor, Proceedings of the Fourth International Conference on Fluidized-Bed Combustion, the MITRE Corporation, McLean, Virginia (1976).
30. J. W. Kaakinen, R. M. Jordan, M. H. Lawasani, and R. E. West, Trace Element Behavior in Coal-Fired Power Plant, Environ. Sci. Technol. 9(9), 862 (1975).
31. D. H. Klein, A. W. Andren, J. A. Carter, J. F. Emery, C. Feldman, W. Fulkerson, W. S. Lyon, J. C. Ogle, Y. Talmi, R. I. Van Hook, and N. Bolton, Pathways of Thirty-Seven Trace Elements through Coal-Fired Power Plants, Environ. Sci. Technol. 9(10), 973 (1975).
32. C. E. Billings, A. M. Sacco, W. R. Matson, R. M. Griffin, W. R. Coniglio, and R. A. Handley, Mercury Balance on a Large Pulverized Coal-Fired Furnace, J. Air Pollut. Control Assoc. 23(9), 773 (1973).
33. Effects of Trace Contaminants from Combustion, Proceedings of a Workshop, Aug. 2-6, 1976 (Report ERDA 77-64, available from NTIS, Springfield, Virginia).
34. D. F. S. Natusch, J. R. Wallace, and C. A. Evans, Jr., Toxic Trace Elements: Preferential Concentration in Respirable Particles, Science 183 (4121), 292 (1974).
35. W. M. Farmer, Measurements of Particle Size, Number Density, and Velocity Using a Laser Interferometer, Appl. Optics 10, 2603 (1972).
36. J. C. Montagna, G. W. Smith, F. G. Teats, G. J. Vogel, and A. A. Jonke, Evaluation of On-Line Light-Scattering Particle Size Analyzers for Measurements at High Temperature and Pressure, Argonne National Laboratory Report ANL/CEN/FE-77-7 (Feb. 1978).
37. E. L. Weiss and H. N. Frock, Rapid Analysis of Particle Size Distribution by Laser Light Scattering, Powder Technol. 14, 287 (1976).
38. D. L. Keairns et al., Fluidized-Bed Combustion Process Evaluation, EPA-650/2-75-027-C, Environmental Protection Agency (1975).
39. T. M. Knowlton and I. Hirsan, L-Valves Characterized for Solids Flow, Hydrocarbon Process. 57, 149 (Mar. 1978).

**TECHNICAL REPORT DATA**  
(Please read Instructions on the reverse before completing)

1. REPORT NO. <b>EPA-600/7-79-203</b>		2.		3. RECIPIENT'S ACCESSION NO.	
4. TITLE AND SUBTITLE <b>Support Studies in Fluidized-bed Combustion-- 1978 Annual Report</b>				5. REPORT DATE <b>August 1979</b>	
				6. PERFORMING ORGANIZATION CODE	
7. AUTHOR(S) <b>I. Johnson, G. J. Vogel, S. H. D. Lee, D. S. Moulton, F. F. Nunes, J. A. Shearer, G. W. Smith, E. B. Smyk, R. B. Snyder, W. M. Swift, F. G. Teats (cont block 15)</b>				8. PERFORMING ORGANIZATION REPORT NO. <b>ANL/CEN/FE-78-10</b>	
9. PERFORMING ORGANIZATION NAME AND ADDRESS <b>Argonne National Laboratory 9700 South Cass Avenue Argonne, Illinois 60439</b>				10. PROGRAM ELEMENT NO. <b>INE825</b>	
				11. CONTRACT/GRANT NO. <b>IAG-D5-E681 (EPA) and W31-109-Eng-38 (DoE)</b>	
12. SPONSORING AGENCY NAME AND ADDRESS <b>EPA, Office of Research and Development * Industrial Environmental Research Laboratory Research Triangle Park, NC 27711</b>				13. TYPE OF REPORT AND PERIOD COVERED <b>Annual; 7/77 - 9/78</b>	
				14. SPONSORING AGENCY CODE <b>EPA/600/13</b>	
15. SUPPLEMENTARY NOTES (*) DoE is cosponsor. Project officers: D. A. Kirchgessner (EPA); John Geffken (DoE). EPA-600/7-76-019, -77-138, and -79-157 are related reports. (Cont. fm block 7: C. B. Turner, W. I. Wilson, and A. A. Jonke.)					
16. ABSTRACT The report gives results of laboratory- and process-scale EPA studies supporting the national development of atmospheric and pressurized fluidized-bed combustion (PFBC) of coal. Program objectives are: (1) to develop basic information needed to optimize the use of limestone for SO <sub>2</sub> emission control from FBC; and (2) to develop information on processes to treat high-temperature high-pressure gases from PFBC, enabling them to be used to operate gas turbines. Limestone sulfation enhancement experiments showed CaCl <sub>2</sub> and MgCl <sub>2</sub> to be more effective than NaCl in increasing the pore size and hence the sulfation capability of calcined limestones. Experiments to evaluate coal-pyrolysis char as a feedstock for FBC were conducted on Wyoming subbituminous coal pyrolyzed at about 650 C. Char combustion efficiencies were 94-99%. The use of oil shale for SO <sub>2</sub> emission control in FBC was evaluated. Considerably larger quantities of shale (than limestone or dolomite) would be required because of shale's lower CaO content. Studies are being conducted to assist in preventing hot-corrosion of turbine blades by alkali-metal compounds from PFBC. Results of one set of experiments show that various mineral additives are highly effective in retaining Na and K in the bed: 90-95% of the elements can be retained.					
17. KEY WORDS AND DOCUMENT ANALYSIS					
a. DESCRIPTORS		b. IDENTIFIERS/OPEN ENDED TERMS		c. COSATI Field/Group	
Pollution		Pollution Control		13B 08G	
Fluidized Bed Processing		Stationary Sources		13H, 07A	
Combustion		Char		21B	
Coal		Trace Elements		21D 13G	
Calcium Carbonates				07B 11M	
Sulfur Oxides				07D	
Oil Shale					
Charcoal					
Gas Turbines					
Corrosion					
Chemical Analysis					
18. DISTRIBUTION STATEMENT <b>Release to Public</b>		19. SECURITY CLASS (This Report) <b>Unclassified</b>		21. NO. OF PAGES <b>110</b>	
		20. SECURITY CLASS (This page) <b>Unclassified</b>		22. PRICE	